Traversable Wormholes and Regenesis

Traversable Wormholes and Regenesis

A dissertation presented

by

Ping Gao

to

The Department of Physics

in partial fulfillment of the requirements

for the degree of

Doctor of Philosophy

in the subject of

Physics

Harvard University

Cambridge, Massachusetts

April 2019

Dissertation Advisor: Daniel Louis Jafferis Ping Gao

Traversable Wormholes and Regenesis

Abstract

In this dissertation we study a novel solution of traversable wormholes in the context of AdS/CFT. This type of traversable wormhole is the first such solution that has been shown to be embeddable in a UV complete theory of gravity. We discuss its property from points of view of both semiclassical gravity and general chaotic system.

On gravity side, after turning on an interaction that couples the two boundaries of an eternal BTZ black hole, in chapter 2 we find a quantum matter stress tensor with negative average null energy, whose gravitational backreaction renders the Einstein-Rosen bridge traversable. Such a traversable wormhole has an interesting interpretation in the context of ER=EPR, which we suggest might be related to quantum teleportation. However, it cannot be used to violate causality. We also discuss the implications for the energy and holographic entropy in the dual CFT description.

The gravity solution of this traversable wormhole indicates that in holographic systems signals generated by a source could reappear long after they have dissipated, with the need of only performing some simple operations. In chapter 3, we argue the phenomenon, to which we refer as "regenesis", is universal in general quantum chaotic many-body systems, and elucidate its underlying physics. The essential elements behind the phenomenon are: (i) scrambling which in a chaotic system makes out-of-time-ordered correlation functions (OTOCs) vanish at large times; (ii) the entanglement structure of the state of the system. The latter aspect also implies that the regenesis phenomenon requires fine tuning of the initial state. Compared to other manifestations of quantum chaos such as the initial growth of OTOCs which deals with early times, and a random matrix-type energy spectrum which reflects very large time behavior, regenesis concerns with intermediate times, of order the scrambling time of a system. We also study the phenomenon in detail in general two-dimensional conformal field theories in the large central charge limit, and highlight some interesting features including a resonant enhancement of regenesis signals near the scrambling time and their oscillations in coupling. Finally, we discuss gravity implications of the phenomenon for systems with a gravity dual, arguing that there exist regimes for which traversability of a wormhole is quantum in nature, i.e. cannot be associated with a semi-classical spacetime causal structure.

Contents

Citations to previously published work

Most of this thesis has appeared in print elsewhere. Details for particular chapters are given below.

Chapter 2

- Gao, Ping, Daniel Louis Jafferis, and Aron C. Wall. "Traversable wormholes via a double trace deformation." Journal of High Energy Physics 2017.12 (2017): 151. `arXiv:1608.05687`

Chapter 3

- Gao, Ping, and Hong Liu. "Regenesis and quantum traversable wormholes." `arXiv:1810.01444`

Electronic preprints (shown in `typewriter font`) are available on the Internet at the following URL:

`http://arXiv.org`

Acknowledgments

Six-year PhD student life in Harvard is a memorable time, in which I got to know the frontier of physics, started to build up my own research, and had wonderful experiences with many great people, to whom I would like to say "Thank you!"

I am deeply grateful to my advisor Prof. Daniel Louis Jafferis. In past six years, he taught me how to think about problems with clear physical intuition. He is brilliant and always has special insight on many seemingly well understood problems. I was often amazed by his ability to capture the essence of problems, which might take me quite a long time of computation to obtain, within just a few lines of simple calculations or some elegant physical argument. Working with him inspired me to try thinking problems in various angles. I believe his insight, taste and enthusiasm towards physics will continue to affect my research in the future. He is a very supportive advisor that he was always optimistic and encouraging me to find a way out whenever I fell into the swamp of complicated calculation and felt frustrated. I specially thank Daniel for guiding me to the project on traversable wormholes, which is the main topic of this thesis. It raises my strong and long-term interest in the interface between quantum gravity, quantum many-body system and quantum information.

I would also like to express my gratitude to Prof. Hong Liu. I was impressed by his clear and pedagogically excellent lecture on holographic duality, which helped me understanding this grand topic in a short time. Besides the help in class, I am also grateful for his guidance, stimulating discussions and insightful comments in our collaborations on effective field theory of hydrodynamics and regenesis. He has a strong intuition in finding an elegant and simple physical interpretation behind complicated calculation, which affects my way of thinking on physics.

Thanks to my committee members: Prof. Andy Strominger and Prof. Melissa Franklin. They gave me useful feedback on my research process. In particular, I want to single out Andy for his excellent course on black holes that is very beneficial to my understanding on quantum gravity.

Moreover, I must express my gratitude to many other professors who taught a course I took or sat in. I have taken Prof. Xi Yin's super well-organzied courses on string theory and CFT, that built up my foundamental knowledge in these areas. I have enjoyed many mathematical courses by Hiro Lee Tanaka, Hector Pasten, Jonathan Mboyo Esole and Prof. Curt McMullen. I am quite impressed by the elegance of mathematics, though it still requires more time for me to gain applicable insight from it.

Thanks to Logan McCarty, Louis Deslauriers, Prof. Daniel Louis Jafferis and Prof. Gerald Gabrielse for giving me opportunities working as a TF in their courses. It was a very interesting experience teaching in Harvard. I specially thank Louis Deslauriers for our discussions on teaching skills and many other interesting topics beyond physics. I thank all students in my sections as they helped me improving my teaching skills.

During my whole PhD years, I have benefited from discussions with many professors, postdocs and peer PhDs: incluing Prof. Cumrun Vafa, Prof. Daniel Harlow, Prof. Juan Maldecena, Prof. Leonard Susskind, Prof. Washington Taylor, Prof. Xiao-Liang Qi, Douglas Stanford, Biao Lian, Xun Gao, Zhen Bi, Alex Lupsasca, Daliang Li, Huajia Wang, Temple He, Dan Kapec, Wenbo Fu, Yingfei Gu, Ziwen Liu, Zhehao Dai, Wenjie Ji, Linda Ye, Junru Li, Liujun Zou, Zhenbin Yang, Baurzhan Mukhametzhanov, Patrick Jefferson, Monica Pate, Scott Collier, David Kolchmeyer, Victor Rodriguez, Bruno Balthazar, Monica Kang, Jing Shi, Li Zeng, Agmon Nathan and Douglas Mendoza. Especially, I learnt a lot from my collaborators Aron Wall and Paolo Glorioso. I thank all of them for making me a better physicist. Thanks to my friends Chenglong Yu and Boyu Zhang from math department for their patient explanations on my (sometimes dumb) questions on math.

Outside of physics, there are so many wonderful friends to thank. Without them, my graduate life would be much gloomier and more monotonous. I thank Wei Chen, Yuan Yang, Yu Wang, Zhaoheng Gong, Haoxin Li, Jin Sun, Xiawei Wang, Zheng Cui, Fang Li, Yingqun Cui, Yunfei Li and my roommates Patrick Tung, Ziliang Che, Koji Shimizu, Xing Chen, Jiwei Wu, Qian Di and He Yang for our chitchats throughout the years.

I would like to specially thank three organizations and all my friends therein. I thank Prof. Claire Conceison, Xiang Li, Lin Qi, Ruby Xie, Run Chen, Tianlin Zheng, Dadi Gao, Yu Xia, Ruiyang Shi, Amy Liu, Guangya Zeng, Yuning Su, Yuehan Wang and Abby Li for organizing MIT Wuming theater club together and producing amazing shows. It opened a new dimension of my life about theater art. I thank Yang Song, Bing Wang, Xiaodan Zhuang, Jeffrey Wang, David Chu, Mengmeng Xu, Jialing Lv, Yangxiaolu Cao, Heng Gao, Qiong Zhang, Tao Gao, Mengyun Zhang for helping building up our THAA and ACE dragonboat teams and winning medals. I was so much encouraged as fighting with all my teammates, especially when I felt frustrated on research. I thank Master Anlin Wang and Li Zeng for teaching me Taichi and cofounding Harvard GSAS Anlin Taichi Wudao Association. They taught me how to relax my body and mind in the stressful PhD years.

Last but not least, I want to sincerely thank my mother Guiying Tang, my father Liusheng Gao and my beloved wife Xiaoqi Wu. Their constant love and support have offered me the confidence to pursue my dream to be a great physicist.

In dedication to my mother 唐桂英, *my father* 高柳生 *and my wife* 吴小琪.

Chapter 1

Introduction and Summary

Interstellar travel is a long-time dream of human beings. In particular, in many science fictions, like "Interstellar", people in the future are imagined to master the ability to utilize traversable wormholes in the universe to travel to some remote galaxies [57].

Nevertheless, as the authors in [58] pointed out that such configurations require "exotic matter" that violates the null energy condition (NEC), which roughly means that the matter should have negative rest mass. This is believed to be physically impossible in classical theories. Fortunately, in quantum field theory, the null energy condition is false. One example is Casimir effect, and another is free field theory in a squeezed state. However, in many situations there are other no-go theorems that rule out traversable wormholes.

Violation of the averaged null energy condition (ANEC) is a prerequisite for all traversable wormholes [58, 79, 80, 38]. It states that there must be infinite null geodesics passing through the wormhole, with tangent vector k^μ and affine parameter λ, along which

$$\int_{-\infty}^{+\infty} T_{\mu\nu} k^\mu k^\nu d\lambda < 0. \tag{1.1}$$

The physical picture is that by Raychaudhuri's equation for null geodesic congruence, light rays will defocus only when ANEC is violated. In that case, the light rays will focus when entering one end of the wormhole and defocus when going out the other end.

There are reasonable arguments that the ANEC is always obeyed along infinite achronal geodesics in various cases [32, 46, 47, 44, 82, 84, 24]. Here, "achronal" is a crucial condition which means that any two points on the geodesics cannot be connected by another timelike line, otherwise it is called chronal. It follows that in achronal spacetime, light ray goes along fastest path. This is sufficient to rule out traversable wormholes joining two otherwise

disconnected regions of spacetime [32]. On the other hand, for geometry like a cylinder, it is chronal and one can easily see that Casimir energy violates ANEC.

In our solution of traversable wormhole, we start with an eternal AdS black hole [55], whose Penrose diagram has two black holes connected by an Einstein-Rosen bridge (see Fig. 2.1a). In this geometry, the two AdS boundaries are spacelike separated and the Einstein-Rosen bridge is non-traversable. In particular, the geodesics on event horizon are null and achronal. In our configuration, we will directly couple the two boundaries, and signals from early times on the horizon can intersect it again at late times, exactly via the coupling on the boundaries. The causal structure of the manifold is modified as a result that the original horizon is no longer achronal. It turns out that we can choose the coupling to generate some negative energy matter on future horizon and violate ANEC. This negative energy is similar to the Casimir effect, since the interaction between the boundaries implies that the radial direction is effectively a compact circle.

Another problematic aspect of traversable wormholes is that they have the potential to lead to causal inconsistencies. For example, by applying a boost to one end of a wormhole one could attempt to create a configuration with closed time-like curves [58]. The direct interaction of the boundaries that we require implies that no such paradoxes may arise. Indeed, the relative boost between two boundaries will change their relative time identification, which is completely fixed in prior by our local coupling on them. Moreover, our traversable wormhole will always be a longer path than going along boundary, which is required by causality. This means that our traversable wormhole is not appropriate as a shortcut for interstellar trip.

The geometry of eternal AdS black hole is dual to two identical CFTs living on each boundary in a highly entangled state, thermofield double state (TFD):

$$|TFD\rangle = \frac{1}{Z}\sum_n e^{-\beta E_n/2}\,|n_L\rangle\,|n_R\rangle \tag{1.2}$$

where $|n_{L,R}\rangle$ is the energy eigenstate with energy E_n in each CFT. In either left or right system, the state looks like a thermal density matrix with inverse temperature β. In order to study the effect of coupling, we will deform the system by turning on a relevant double trace deformation [1]

$$\delta S = \int dt\; d^{d-1}x\; h(t,x)\mathcal{O}_R(t,x)\mathcal{O}_L(-t,x), \tag{1.3}$$

where $\mathcal{O}$ is a scalar operator of dimension less than $d/2$, dual to a scalar field φ. This connects the boundaries with the same physical time orientation, since the t coordinate

runs in opposite directions in two wedges (see Fig. 2.1a). The small deformation $h(t, x)$ has support only after some turn-on time t_0. By the AdS/CFT correspondence, we can be certain that this relevant deformation corresponds to a consistent configuration in quantum gravity. Because of this, the traversable wormhole we find is the first such solution that has been shown to be embeddable in a UV complete theory of gravity. In Chapter 2, we show a specific example in Schwarzschild BTZ black holes.

The process of a particle traveling through the wormhole can be described in three steps. First, we shoot this particle to left black hole at some early time. Second, after the particle falls into this black hole, we turn on the interaction between two boundaries around t_0. This perturbation will produce some negative energy matter on the future horizons of both black holes. Third, because these two black holes are connected via Einstein-Rosen bridge, the particle will scatter with the negative energy matter and escape from the right black hole. See the magenta curve in Fig. 2.4 as an illustration of the geodesics of the traversing particle.

The traversable wormhole we found has an interesting interpretation in the context of ER=EPR [53]. Maldacena and Susskind conjectured that any pair of entangled quantum systems are connected by an Einstein-Rosen bridge (the non-traversable wormhole). Our example thus provides a way to operationally verify a salient feature of ER=EPR that observers from opposite sides of an entangled pair of systems may meet in the connected interior. Since in [53] any such meeting is trapped behind the horizon, it is not obvious how its occurrence could be confirmed by exterior or CFT measurements. What we found is that if, after the observers jump into their respective black holes, a boundary-boundary coupling is activated, then the Einstein-Rosen can be rendered traversable, and the meeting inside may be seen from the boundary. In other words, our traversable wormhole configuration offers an efficient way to probe the region behind horizon.

Relations to quantum information

In the viewpoint of quantum information, we propose that the traversable wormhole is dual to a dynamical description of quantum teleportation. We could image that the particle passing through the traversable wormhole carries a qubit, Q, and the whole traversing process has a clear feature of transmission of quantum information from one part to the other part in an entangled system (recall thermofield double state (1.2) is a highly entangled state). The qubit, Q, through the wormhole is that it appears to be sent "via the entanglement", rather than directly by the inter-boundary coupling. One obvious reason

is that at the time the interaction is activated, Q is in fact spacelike separated from the boundary in the bulk picture, so in the bulk approximation Q and $\mathcal{O}$ are independent quantum variables. From the CFT perspective, this is because Q has thermalized into the left system before the $\mathcal{O}_L\mathcal{O}_R$ interaction is turned on, so no quantum information about Q appears to be accessible to the operator $\mathcal{O}$. Of course, the boundary coupling is nevertheless crucial for the existence of the traversable wormhole. In section 2.5, we show that the operation in quantum teleportation could be written exactly as a coupling between two systems. In [75], the authors constructed a protocol of teleportation sharing some similarity with our traversable wormhole setting. However, the complexity of their operation is much larger than our simple coupling. How to precisely construct the traversable wormhole as a dynamical quantum teleportation remains as an open question.

Another possible interpretation of our result is to relate it to the recovery of information described in [36]. Assuming that black hole evaporation is unitary and black hole itself is a fast scrambler, it is in principle possible to eventually recover a qubit which falls into a black hole, from a quantum computation acting on the Hawking radiation. Assume that you have access to an auxiliary system maximally entangled with the black hole (for example the auxiliary system could be all past Hawking radiation before Hawking-Page time collected from the black hole and fully controlled by your quantum computer). The information Q sent into the black hole will be fast scrambled and it seems extremely hard to get it back. However, it turns out that you only need a small (order unity) additional quantity of Hawking radiation to reconstruct Q using your quantum computer. In our system, the coupling between the two systems could be heuristically understood as collecting a few more Hawking quanta from one side and triggers the appropriate quantum computation on the other side to make the qubit reappear again. In [86], the authors proposed an efficient algorithm to reconstruct Q. However, their algorithm requires a large number of Grover-like iteration, whereas in our traversable wormhole we only need to apply a momentary coupling. This simple "holographic algorithm" must reply on some special property of scrambling evolution, which requires further investigation.

Regenesis in many-body chaotic systems

Before having a precise understanding in quantum information, it is very beneficial to discus the boundary dual picture of traversable wormholes in a field theory setting. Based on AdS/CFT, a black hole is dual to a dissipative system with finite temperature. When we excite a signal in a dissipative system, it will decay away exponentially. However,

the traversable wormhole picture seems to indicate that the signal could re-appear in the other system if they are in a highly entangled state. In chapter 3, We studied this new phenomenon which we call "regenesis", where the signal can re-appear with the need of only performing some simple operations. It looks quite mysterious how information will be restored, although travelling through a traversable wormhole seems a very natural picture in the bulk.

Consider two identical uncoupled quantum field theory systems, to which we will refer as L, R systems, prepared in thermofield double state (1.2) at $t = 0$. Consider at some time $t = -t_s < 0$ turning on an external source φ^R for some few-body Hermitian operator J^R for a short interval. In the R system there is an induced expectation value $\langle J^R(t)\rangle$, which will dissipate after φ^R is turned off. But there is no response in the L system as by definition $[J^L, J^R] = 0$. If we couple the two systems at $t = 0$ just like the (1.3) for some few-body operator $\mathcal{O}(x)$, we surprisingly find that the signal reappears as the expectation value of left operator $\langle J^L(t)\rangle_g$ [1] becomes nonzero if both $t,\ t_s$ are of order of scrambling time t_*.[2] Such phenomenon in AdS_2 is discussed in [52] using gravitational scattering amplitude. Note that here $\mathcal{O}$ and J are generic few-body operators which do not need to have any common degrees of freedom between them.

Indeed, this phenomenon, to which we refer as "regenesis," is universal for generic quantum chaotic systems. A general result we obtain is that in a generic chaotic system for $t, t_s \gg t_*$: (i) $\langle J^L(t)\rangle_g$ is supported only for $t \approx t_s$ when g is nonzero; (ii) as a function of t_s, $\langle J^L(t = t_s, \vec{x})\rangle_g$ has the following behavior

$$\langle J^L(t_s, \vec{x})\rangle_g \approx C(g)\, \varphi^R(-t_s, \vec{x}), \qquad t_s \gg t_* \tag{1.4}$$

where $C(g)$ is an $O(1)$ constant depending on g. We thus find that the "input signal" φ^R from the R system at $t = -t_s$ regroups at $t = t_s$ in the L system long after it has dissipated! From (i) we can infer that the signals which are input earlier in the R systems appear later in the L system, so in fact what one finds is the time reversed form of the input signal. The result (1.4) is insensitive to the specific form of L-R interaction (1.3). The behavior for $t_s \sim t_*$ is more complicated. To make a concrete example, in Chapter 3, we study

[1] In Chapter 3 we use a different convention by replacing h in (1.3) by g, where subscript g means expectation value with deformed Hamiltonian, and that the signal is generated in R system and transmitted to L system.

[2] Scrambling time is defined here as the time scale when $\langle [V(t), W(0)]^2\rangle$ between generic few-body operators V, W become $O(1)$.

the regenesis phenomenon in two-dimensional conformal field theories (CFT) in the large central charge limit which is known to be chaotic [64].

The essential elements behind the regenesis behavior (1.4) are: (i) scrambling in a chaotic system makes out-of-time-ordered correlation functions (OTOCs) vanish for $t \gg t_*$ [68, 51], and (ii) the entanglement structure of (1.2) which strongly correlates an operator inserted at $(-t, \vec{x})$ with an operator at $(t, \vec{x})$. Compared to other manifestations of quantum chaos such as the initial growth of OTOCs which deals with early times, and a random matrix-type energy spectrum which reflects very large time behavior, the regenesis phenomenon concerns with intermediate times, of order the scrambling time of a system.

The most mysterious aspect of regenesis phenomenon is that the signal will be regrouped in L system after dissipation in R system. It sounds like a melodramatic story in which a "cat" is brought back to life in L system long after her death in R system and her body being scrambled into the environment. Indeed, there are two essential points behind this story. First, regenesis requires an extremely fine tuning as we must require the entanglement structure at the time when we turn on the coupling to be exactly thermofield double state, and meanwhile the signal is generated at least t_* ago. If the system is macroscopic, the scrambling time t_* could also be macroscopic, which makes the tuning extremely hard. Second, as we shown in Section 3.2.4, at least for $t, t_s \gg t_*$, the signal reappeared in L system is quantum in nature and its fluctuation cannot be suppressed by any macroscopic measurement. This means that the regenesis effect does not hold for macroscopic matter like a real cat in the regime of (1.4). Exactly due to its quantum nature, we argue that (1.4) is an interference effect which does not have any semi-classical spacetime structure interpretation. We would like to heuristically propose the existence of "quantum traversable wormhole" to include this feature, though we do not have a precise way to characterize it.

Chapter 2

Traversable Wormholes via a Double Trace Deformation

This thesis chapter originally appeared in the literature as
Gao, P., Jafferis, D.L. and Wall, A.C., *2017. Traversable wormholes via a double trace deformation. Journal of High Energy Physics, 2017(12), p.151.*

2.1 Introduction

Traversable wormholes have long been a source of fascination as a method of long distance transportation [57]. However, such configurations require matter that violates the null energy condition, which is believed to apply in physically reasonable classical theories. In quantum field theory, the null energy condition is false, but in many situations there are other no-go theorems that rule out traversable wormholes.

In this work we find that adding certain interactions that couple the two boundaries of eternal AdS-Schwarzschild results in a quantum matter stress tensor with negative average null energy, rendering the wormhole traversable after gravitational backreaction. The coupling we turn on has the effect of modifying the boundary conditions of a scalar field in the bulk, which changes the metric at 1-loop order.

Violation of the averaged null energy condition (ANEC) is a prerequisite for all traversable wormholes [58, 79, 80, 38]. It states that there must be infinite null geodesics

passing through the wormhole, with tangent vector k^μ and affine parameter λ, along which

$$\int_{-\infty}^{+\infty} T_{\mu\nu} k^\mu k^\nu d\lambda < 0. \tag{2.1}$$

The physical picture is that by Raychaudhuri's equation for null geodesic congruence, light rays will defocus only when ANEC is violated. In that case, the light rays that focus in one end of the wormhole can defocus when going out the other end.

There are reasonable arguments that the ANEC is always obeyed along infinite achronal geodesics [32, 46, 47, 44, 82].[1] This is sufficient to rule out traversable wormholes joining two otherwise disconnected regions of spacetime [32]. Furthermore, the generalized second law (GSL) of causal horizons also rules out traversable wormholes connecting two disconnected (asymptotically flat or AdS) regions, due to the fact that the future horizon of a lightray crossing through the wormhole has divergent area at very early times, which contradicts the increase of generalized entropy along the future horizon [84].

For small semiclassical perturbations to a stationary causal horizon, both the GSL and the ANEC follow from lightfront quantization methods that are valid for free or superrenormalizable field theories [83]. (There is also evidence that these results extend to more general field theories [24, 40, 39, 45, 16]).

In our configuration, signals from early times on the horizon can intersect it again at late times, by passing through the directly coupled boundaries. The causal structure of the manifold is modified as a result, changing the commutation relations along null geodesics through the wormhole and making them no longer achronal. For the same reason, a causal horizon extending through the wormhole intersects itself, removing the piece with divergent area. Hence the above impossibility results do not apply. The negative energy matter in our configuration is similar to the Casimir effect, since the interaction between the boundaries implies that the radial direction is effectively a compact circle.

Another problematic aspect of traversable wormholes is that they have the potential to lead to causal inconsistencies. For example, by applying a boost to one end of a wormhole one could attempt to create a configuration with closed time-like curves [58]. The direct interaction of the boundaries that we require implies that no such paradoxes may arise (for a more detailed discussion, see section 4).

The traversable wormhole we find is the first such solution that has been shown to

[1] A set of points is achronal if no two of the points can be connected by a timelike curve; otherwise it is chronal.

be embeddable in a UV complete theory of gravity. A phenomenological model of a static BTZ wormhole that becomes traversable as a result of nonperturbative effects in a $1/c$ expansion was proposed in [69] (c being the central charge), however it was not shown that the metric obeys any field equations. A traversable wormhole solution of five dimensional Einstein-Gauss-Bonnet gravity was found in [11, 77, 3], however that low energy effective theory appears to lack a UV completion [18]. Another example was found [8] in a theory with a conformally coupled scalar, in a regime in which the effective Newton's constant becomes negative. This suggests that this solution also cannot arise in a UV complete model. The important fact that the boundary CFT dual of a traversable wormhole must involve interactions between the two CFTs was noted in [69, 3].

The eternal black hole with two asymptotically AdS regions is the simplest setting to investigate these questions [55]. We will deform the system by turning on a relevant double trace deformation [1]

$$\delta S = \int dt\ d^{d-1}x\ h(t,x)\mathcal{O}_R(t,x)\mathcal{O}_L(-t,x), \tag{2.2}$$

where $\mathcal{O}$ is a scalar operator of dimension less than $d/2$, dual to a scalar field φ. This connects the boundaries with the same time orientation, since the t coordinate runs in opposite directions in two wedges (see Fig. 2.1a). The small deformation $h(t,x)$ has support only after some turn-on time t_0. By the AdS/CFT correspondence, we can be certain that this relevant deformation corresponds to a consistent configuration in quantum gravity.

The eternal black hole has a Killing symmetry which is time-like outside the horizon. Null rays along the horizon $V = 0$ pass through the bifurcation surface of the Killing vector, and asymptote to $t \to -\infty$ on the left boundary and $t \to +\infty$ on the right boundary (see Fig. 2.1b). Denote the affine parameter along this ray as U. In the linearized analysis around this solution, the throat will become marginally traversable if $\int dU\ T_{UU} < 0$, where the integral is over the whole U coordinate.

It is instructive to see explicitly in this case that a small spherically symmetric perturbation of the stress tensor $T_{\mu\nu} \sim O(\epsilon)$ results in a traversable wormhole exactly when the ANEC is violated, by solving the linearized Einstein equation for $h_{\mu\nu} = \delta g_{\mu\nu} \sim O(\epsilon)$. Using Kruskal coordinates for the background metric, we find that at $V = 0$,

$$\frac{(d-2)}{4}\left[\left((d-3)r_h^{-2} + (d-1)\ell^{-2}\right)\left(h_{UU} + \partial_U(U h_{UU})\right) - 2r_h^{-2}\partial_U^2 h_{\phi\phi}\right] = 8\pi G_N\, T_{UU} \tag{2.3}$$

where ϕ is the azimuthal angle, r_h is the horizon radius of the black hole and the cosmological constant is $\Lambda = -\frac{(d-2)(d-1)}{2l^2} < 0$.

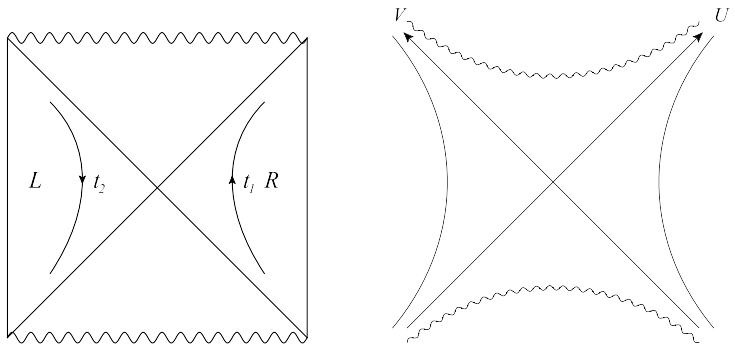

Figure 2.1: (a) is the Penrose diagram and (b) shows the Kruskal coordinates of the eternal black hole

Since the deformation of the Hamiltonian is small, after the scrambling time, the fields ought to approach a stationary state with respect to an asymptotic Killing symmetry $U\partial U$. Hence T_{UU} must decay faster than U^{-2}, as does each term in LHS of (2.3) after imposing a suitable gauge at past and future infinity. Therefore, if we integrate (2.3) over U the total derivative terms drop out and we obtain

$$8\pi G_N \int dU T_{UU} = \frac{(d-2)}{4}\left((d-3)r_h^{-2} + (d-1)\ell^{-2}\right)\int dU h_{UU} \tag{2.4}$$

Linearized diffeomorphisms around the stationary black hole background act on $h_{\mu\nu}$, but when the AdS asymptotic conditions are imposed the quantity $\int_{-\infty}^{+\infty} dU\ h_{UU}$ is gauge invariant. Note that the null ray originating on the past horizon is given in coordinates by

$$V(U) = -(2g_{UV}(0))^{-1}\int_{-\infty}^{U} dU h_{UU} \tag{2.5}$$

after including the perturbation to linear order, where $g_{UV}(0) < 0$ is the UV component of the original metric on the $V = 0$ slice. If the ANEC is violated, $V(+\infty) < 0$, and a light ray from left boundary will hit the right boundary after finite time.

Note that if there existed any state in which the wormhole was traversable in the system defined by the decoupled Hamiltonian, $H_L + H_R$, then it would contradict the AdS/CFT duality. This is because in the decoupled system, no operator on the left can influence the right, which implies that no signal can be transmitted between the boundaries through the bulk.

At the linearized level, if one modifies the state as $|\text{tfd}\rangle \to e^{i\epsilon A}|\text{tfd}\rangle$ for small ϵ, the average null energy becomes $\langle \int dU T_{UU}\rangle = i\epsilon\langle[\int dU T_{UU}, A]\rangle$. If this were non-vanishing for

any operator A, then by adjusting the sign of ϵ, the throat could be made traversable. It is easy to check that the expectation value of this commutator indeed vanishes.

In fact, $|\text{tfd}\rangle$ is invariant under $H_R - H_L$, which corresponds to the bulk Killing symmetry $i\partial_t$ (note the directions are opposite in left and right wedges). On the horizon $V = 0$, one can show $\partial_t = U\partial_U$ in Kruskal coordinates, which is just a dilation of the U direction. Note that under the $U \to \lambda U$ scaling, $T_{UU} \to \lambda^{-2} T_{UU}$ and $dU \to \lambda dU$, which implies $[H_R - H_L, \int dU T_{UU}] = -i \int dU T_{UU}$. Therefore

$$(H_R - H_L) \int dU T_{UU} |\text{tfd}\rangle = [H_R - H_L, \int dU T_{UU}] |\text{tfd}\rangle + \int dU T_{UU} (H_R - H_L) |\text{tfd}\rangle = -i \int dU T_{UU} |\text{tfd}\rangle. \tag{2.6}$$

This implies that $\int dU T_{UU} |\text{tfd}\rangle$ is either an eigenvector of $H_R - H_L$ with eigenvalue $-i$, or identically zero. Since $H_R - H_L$ is a Hermitian operator, whose eigenvalues must be real, it follows that $\int dU T_{UU} |\text{tfd}\rangle = 0$. In other words, T_{UU} in the modified state along $U > 0$ will exactly cancel that along $U < 0$. Beyond the linearized level, one can show that the backreaction always causes the throat to lengthen [53, 67], so that it cannot be traversed in any state of the decoupled system, as expected.

We will consider a deformation of the Hamiltonian that turns on at some time t_0 in (2.2).[2] At the linearized level, this has the same effect as changing the state to the future of t_0. Now there is no reason for the above cancellation to occur since T_{UU} along $U < 0$ is unchanged. Therefore, one expects that generically by an appropriate choice of sign one will render the Einstein-Rosen bridge traversable, as long as the deformation couples the two boundaries.[3]

The simplest option in the large N limit is a double trace deformation. This has the effect of modifying the boundary conditions for the dual scalar field, such that some amplitude of a wave hitting one boundary will be transmitted to the opposite one. This does not change the eternal black hole solution classically, but results in a quantum correction to the matter stress tensor.

In order to be sure that the configuration is an allowed one, we choose the deformation to be relevant. Then it will be a renormalizable deformation of the CFT, and the

[2] We do not consider the case of a time-independent interaction, in order to prevent the quantum state from becoming non-regular on the past horizon.

[3] A deformation of only H_R has the same effect on the ANE as a change in the state, by bulk causality, since the past causal cone of the deformation does not intersect the $V = 0$ null sheet. This again agrees with the fact that when the boundaries are decoupled, no traversable wormhole can exist.

dual geometry will not be modified by backreaction in an uncontrolled way at the AdS boundaries. Also, heuristically, the effect of such a deformation coupling the two CFT's should be strong in the IR, which suggests that it renders the deep interior traversable.

Recall that the conformal weight of a scalar operator $\mathcal{O}_i$ is given by $\Delta = \frac{d}{2} \pm \sqrt{(\frac{d}{2})^2 + M^2}$, where M is the mass of the bulk field, and the plus or minus sign depends on the choice of asymptotic boundary conditions. In the case $M^2 > 0$, only the plus sign leads to normalizable modes. However, unitarity in AdS space [15] allows a slightly tachyonic bulk field: $M^2 > -(\frac{d}{2})^2$, in which modes of both signs are normalizable and we are free to choose either one. To have a relevant deformation, we start with the alternative boundary condition, associated with the minus sign.

A brief overview of this chapter is as follows. In section 2.2, we calculate the bulk two-point function with the modified Hamiltonian at linear order in h. In section 2.3, we use the point-splitting method to calculate T_{UU} on the $V = 0$ slice. Numerical result shows that T_{UU} is rendered negative by our boundary interaction. We find an analytic expression for $\int dU T_{UU}$, which is negative for all $0 < \Delta < 1$. In section 2.4 we calculate the energy and entropy of the resulting CFT state, and describe their holographic bulk duals. In section 2.5, we discuss the properties of this traversable wormhole and propose a quantum teleportation interpretation in the ER=EPR context. The appendix is a detailed calculation of $\int dU T_{UU}$.

Throughout we use units where $c = \hbar = 1$.

2.2 Modified bulk two-point function

For simplicity, we consider the eternal BTZ black hole [6, 5] (for a review, see [19]), whose metric is

$$ds^2 = -\frac{r^2 - r_h^2}{\ell^2} dt^2 + \frac{\ell^2}{r^2 - r_h^2} dr^2 + r^2 d\phi^2 \tag{2.7}$$

The inverse temperature of the BTZ black hole is determined by its horizon radius r_h as $\beta = 2\pi\ell^2/r_h$. Here and below we set AdS length ℓ to 1. Without any deformation of the Hamiltonian, the bulk free field two-point function in the BTZ background with $r^{-\Delta}$ fall-off was first derived by the mode sum method in [42].

In right wedge, it is

$$\langle \varphi_R(x) \varphi_R(x') \rangle_0 = \frac{1}{2^{3-\Delta}\pi} (G_+ + G_-)(G_+^{-1} + G_-^{-1})^{1-2\Delta} \tag{2.8}$$

where

$$G_{\pm} \equiv \left(\frac{rr'}{r_h^2} \cosh r_h \Delta\phi \pm 1 - \frac{(r^2 - r_h^2)^{1/2}(r'^2 - r_h^2)^{1/2}}{r_h^2} \cosh r_h \Delta t \right)^{-1/2} . \tag{2.9}$$

The bulk field operator $\varphi_R(x)$ in the eternal black hole background can be understood as a non-local CFT operator [61]. In particular, $\varphi_R(x)$ can be expanded in terms of the right boundary dual operator as

$$\varphi_R(t, r, \phi) = \int_{\omega>0} d\omega\, dm \left(f_{\omega m}(r) e^{-i\omega t + im\phi} \mathcal{O}_{\omega m} + f^*_{\omega m}(r) e^{i\omega t - im\phi} \mathcal{O}^\dagger_{\omega m} \right) \tag{2.10}$$

where $f_{\omega m}(r)e^{-i\omega t+im\phi}$ are bulk positive frequency normalizable modes approaching $r^{-\Delta}$ when $r \to \infty$ and $\mathcal{O}_{\omega m}$ is the boundary annihilation operator defined by

$$\mathcal{O}(t, \phi) = \int d\omega\, dm \left(e^{-i\omega t + im\phi} \mathcal{O}_{\omega m} + e^{i\omega t - im\phi} \mathcal{O}^\dagger_{\omega m} \right) . \tag{2.11}$$

Therefore, the bulk to boundary correlation function is given by

$$\begin{aligned} K_\Delta(r, t, \phi) &\equiv \langle \varphi_R(t, r, \phi) \mathcal{O}(0, 0) \rangle = \lim_{r' \to \infty} r'^\Delta \langle \varphi_R(t, r, \phi) \varphi_R(0, r', 0) \rangle_0 \\ &= \frac{r_h^\Delta}{2^{\Delta+1}\pi} \left(-\frac{(r^2 - r_h^2)^{1/2}}{r_h} \cosh r_h t + \frac{r}{r_h} \cosh r_h \phi \right)^{-\Delta} , \end{aligned} \tag{2.12}$$

where we used translation symmetry in t and ϕ to move (t', ϕ') to the boundary origin. This expression is real only when (r, t, ϕ) is space-like separated from the boundary origin. For time-like separation, general analytic properties of Wightman functions imply that one should change t to $t - i\epsilon$, which assigns a phase of $e^{-i\pi\Delta}$ when $t > 0$ and of $e^{i\pi\Delta}$ when $t < 0$.

Now we consider the time dependent modified Hamiltonian of (2.2):

$$\delta H(t) = -\int d\phi\, h(t, \phi) \mathcal{O}_R(t, \phi) \mathcal{O}_L(-t, \phi), \tag{2.13}$$

where $h(t, \phi) = 0$ when $t < t_0$. Using evolution operator $U(t, t_0) = \mathcal{T} e^{-i\int_{t_0}^t dt \delta H(t)}$ in interaction picture, the bulk two-point function is

$$\left\langle \varphi_R^H(t, r, \phi) \varphi_R^H(t', r', \phi') \right\rangle = \left\langle U^{-1}(t, t_0) \varphi_R^I(t, r, \phi) U(t, t_0) U^{-1}(t', t_0) \varphi_R^I(t', r, \phi) U(t', t_0) \right\rangle \tag{2.14}$$

where superscripts H and I represent Heisenberg and interaction picture respectively. To leading order in h, (2.14) is (suppressing r and ϕ coordinates and omitting I)

$$G_h \equiv -i \int_{t_0}^{t} dt_1 h(t_1) \langle [\mathcal{O}_L(-t_1)\mathcal{O}_R(t_1), \varphi_R(t)] \varphi_R(t') \rangle - i \int_{t_0}^{t'} dt_1 h(t_1) \langle \varphi_R(t) [\mathcal{O}_L(-t_1)\mathcal{O}_R(t_1), \varphi_R(t')] \rangle$$

$$\begin{aligned}
&\simeq -i\int_{t_0}^{t} dt_1 h(t_1)\,\langle\varphi_R(t')\mathcal{O}_L(-t_1)\rangle\,\langle[\mathcal{O}_R(t_1),\varphi_R(t)]\rangle + (t\leftrightarrow t')\\
&= i\int_{t_0}^{t} dt_1 h(t_1) K_\Delta(t'+t_1-i\beta/2)\left[K_\Delta(t-t_1-i\epsilon)-K_\Delta(t-t_1+i\epsilon)\right] + (t\leftrightarrow t')\\
&= 2\sin\pi\Delta\int dt_1 h(t_1) K_\Delta(t'+t_1-i\beta/2) K^r_\Delta(t-t_1) + (t\leftrightarrow t')
\end{aligned} \tag{2.15}$$

where in the second line we used large N factorization and causality, in that $\mathcal{O}_L$ commutes with any φ_R, in the third line we used the KMS condition [34]

$$\langle\mathcal{O}_R(t)\mathcal{O}_L(t')\rangle_{tfd} = \langle\mathcal{O}_R(t)\mathcal{O}_R(t'+i\beta/2)\rangle_{tfd} \tag{2.16}$$

and in the last line K^r_Δ is the retarded correlation function

$$K^r_\Delta(t,r,\phi) = |K_\Delta(t,r,\phi)|\;\theta(t)\;\theta\left(\frac{(r^2-r_h^2)^{1/2}}{r_h}\cosh r_h t - \frac{r}{r_h}\cosh r_h\phi\right) \tag{2.17}$$

One can also derive (2.15) using the bulk mode sum method with modified boundary conditions. This approach would allow one to compute the stress tensor for finite h, not just perturbatively. According to Lorentzian AdS/CFT, the double trace deformation [85, 10], from the point of view of the right wedge, is equivalent to a source term $h(t,\phi)\mathcal{O}_L(-t,\phi)$, for $\mathcal{O}_R(t)$, activating the initially frozen fall-off component of the bulk field. The same applies to the left wedge. Therefore the asymptotic behavior of a global bulk mode φ living in the entire eternal black hole should satisfy

$$\varphi(r\to\infty_R)\to\alpha_R(t,\phi)r^{-\Delta}+\beta_R(t,\phi)r^{-2+\Delta},\;\; \beta_L(t,\phi)=h(-t,\phi)\alpha_R(-t,\phi) \tag{2.18}$$

$$\varphi(r\to\infty_L)\to\alpha_L(t,\phi)r^{-\Delta}+\beta_L(t,\phi)r^{-2+\Delta},\;\; \beta_R(t,\phi)=h(t,\phi)\alpha_L(-t,\phi) \tag{2.19}$$

where the subscript 1 is for right wedge and 2 is for left wedge.

The thermofield double state of the eternal black hole is the vacuum state in the Kruskal patch [43]. This is analogous to the relation between the Minkowski vacuum and the Rindler thermofield double state [78]. Choosing the appropriate global bulk modes $H^{(\pm)}_{\omega m}$[4] and applying the method of [43], we can construct φ as

$$\varphi(x) = \int_{\omega>0} d\omega\, dm (H^{(+)}_{\omega m}(x) b^{(+)}_{\omega m} + H^{(-)}_{\omega m}(x) b^{(-)\dagger}_{\omega m} + h.c.) \tag{2.20}$$

[4]This step is very tricky because at order h, the $r^{-\Delta}$ component is not constrained by the deformation. The only requirement is that the modified two point function must be regular on horizon. We were able to find a choice to reproduce (2.15) up to normalization.

where $b^{(\pm)}_{\omega m}$ are annihilation operators used to define the vacuum. We find the two-point function in this vacuum is the same as (2.15) up to normalization. Since the calculation is quite involved, we do not include it in this paper.

2.3 1-loop stress tensor

The stress tensor is given by variation of action with respect to $g^{\mu\nu}$,

$$T_{\mu\nu} = \partial_\mu\varphi\partial_\nu\varphi - \frac{1}{2}g_{\mu\nu}g^{\rho\sigma}\partial_\rho\varphi\partial_\sigma\varphi - \frac{1}{2}g_{\mu\nu}M^2\varphi^2 \tag{2.21}$$

The 1-loop expectation value can be calculated by point splitting,

$$\langle T_{\mu\nu}\rangle = \lim_{x\to x'}\partial_\mu\partial'_\nu G(x,x') - \frac{1}{2}g_{\mu\nu}g^{\rho\sigma}\partial_\rho\partial'_\sigma G(x,x') - \frac{1}{2}g_{\mu\nu}M^2G(x,x') \tag{2.22}$$

where $G(x,x')$ is 2-point function. In this formula, one must renormalize the stress tensor by subtracting the coincident point singularities from the 2-point function, which are given by the Hadamard conditions [62]. Since these are determined by the short distance dynamics, this subtraction is unchanged when we modify the boundary conditions, and it has no effect on the order h correction that we are interested in.

At leading order, as we reviewed in the Introduction, $\int dUT_{UU}$ is zero on the horizon $V=0$. Indeed, the leading order two point function in the BTZ black hole is (2.8) where ϕ has periodicity 2π and all $\Delta\phi + 2\pi n$ images are summed. The only coincident point pole comes from the $n=0$ component. Summing over the other n components, one finds that in Kruskal coordinates the leading order stress tensor $T_{UU}\sim O(V^2)$ in the $V\to 0$ limit, so that $T_{UU}=0$ along the horizon.

The subleading 2-point function is given by (2.15). Note that $h(t,\phi)$ is dimensionful and its dimension is $2-2\Delta$ because in (2.13) $\mathcal{O}$ has dimension Δ[5]. Moreover, since $h(t,\phi)$ is a boundary CFT smearing function, it should not depend on any bulk length scale (e.g. r_h and ℓ) explicitly but only on the inverse temperature β. Let us assume that $h(t,\phi)$ is uniform over ϕ:

$$h(t,\phi) = \begin{cases} h(2\pi/\beta)^{2-2\Delta} & t\geq t_0 \\ 0 & t<t_0 \end{cases} \tag{2.23}$$

[5]Here we implicitly defined the unit length angular coordinate $x\equiv\phi\ell$. Taking the limit $r\to\infty$ in BTZ metric (2.7), the boundary metric is flat $ds_b^2 = -dt^2+dx^2$.

where h is a dimensionless constant. In Kruskal coordinates

$$e^{2r_h t} = -\frac{U}{V}, \ \frac{r}{r_h} = \frac{1-UV}{1+UV} \tag{2.24}$$

the change in the 2-point function is

$$\begin{aligned} G_h =& C_0 \left(\frac{2\pi}{\beta}\right)^{2\Delta-2} r_h \int \frac{dU_1}{U_1} d\phi_1 h(U_1,\phi_1) \left(\frac{1+UV}{U/U_1 - VU_1 - (1-UV)\cosh r_h(\phi-\phi_1)}\right)^{\Delta} \\ &\times \left(\frac{1+U'V'}{U'U_1 - V'/U_1 + (1-U'V')\cosh r_h(\phi'-\phi_1)}\right)^{\Delta} + (U,V,\phi \leftrightarrow U'V',\phi') \end{aligned} \tag{2.25}$$

where $C_0 = \frac{r_h^{2\Delta-2}\sin\Delta\pi}{2(2^\Delta\pi)^2}\left(\frac{2\pi}{\beta}\right)^{2-2\Delta}$ and we transformed the integral over t_1 to Kruskal coordinates in which the boundary is $U_1V_1 = -1$. Note that this result applies to both the black hole and black brane cases because the integration of ϕ_1 over 0 to 2π and summing over n with modification $\phi_1 \to \phi + 2\pi n$ is equivalent to the integration of ϕ_1 over the whole real axis. Since we only focus on T_{UU} component on the horizon $V = 0$ and the derivative on U and U' in (2.22) has nothing to do with the value of V and V', we can take both points to the horizon first, namely $V = V' = 0$. Similarly, we can take $\phi = \phi'$ first for simplicity. Since $h(t_1,\phi_1)$ is uniform in ϕ_1, ∂_ϕ is still a Killing vector of the system and therefore G_h should not depends on ϕ. Defining $y = \cosh r_h(\phi_1 - \phi)$, on horizon we have

$$G_h = hC_0 \int_{U_0}^{U} \frac{dU_1}{U_1} \int_1^{\frac{U}{U_1}} \frac{2dy}{\sqrt{y^2-1}} \left(\frac{U_1}{U-U_1 y}\right)^{\Delta} \left(\frac{1}{U'U_1+y}\right)^{\Delta} + (U \leftrightarrow U') \equiv F(U,U') + F(U',U) \tag{2.26}$$

where $U_0 = e^{r_h t_0}$. The integral range of (2.26) is given by the step function in (2.17), which ensures that $U - U_1 y \geq 0$. Note that the integral in (2.26) is dimensionless. Since G_h has dimension 1 (φ_R has dimension $\frac{1}{2}$ in 3-dimension spacetime), if we restore ℓ in (2.26), we find the total length scale dependence of G_h is ℓ^{-1}.

Note that $g_{UU} = 0$ in the original BTZ geometry. By (2.22), T_{UU} on horizon is

$$T_{UU} = \lim_{U'\to U} \partial_U \partial_{U'} (F(U,U') + F(U',U)) = 2 \lim_{U'\to U} \partial_U \partial_{U'} F(U,U') \tag{2.27}$$

where we should note the dimension of T_{UU} is the same as G_h because U is dimensionless. Since the integration ranges are only functions of U, we can take the U' derivative before evaluating the integral

$$T_{UU} = -4h\Delta C_0 \lim_{U'\to U} \partial_U \int_{U_0}^{U} dU_1 \int_1^{\frac{U}{U_1}} \frac{dy}{\sqrt{y^2-1}} \frac{U_1^\Delta}{(U-U_1 y)^\Delta (U'U_1+y)^{\Delta+1}} \tag{2.28}$$

Defining a new variable $x = \frac{y-1}{U/U_1-1}$ and integrating over x we get

$$T_{UU} = -\frac{4h\Delta C_0\Gamma(\frac{1}{2})\Gamma(1-\Delta)}{\sqrt{2}\Gamma(\frac{3}{2}-\Delta)}\lim_{U'\to U}\partial_U\int_{U_0}^{U}dU_1\frac{F_1(\frac{1}{2};\frac{1}{2},\Delta+1;\frac{3}{2}-\Delta;\frac{U_1-U}{2U_1},\frac{U_1-U}{U_1(1+U'U_1)})}{U_1^{-\Delta+1/2}(U-U_1)^{\Delta-1/2}(1+U'U_1)^{\Delta+1}} \tag{2.29}$$

where we used the integral representation of Appell hypergeometric function. The integral over U_1 is finite as long as $\Delta - 1/2 < 1$, namely $\Delta < 3/2$, because in the integrated region, the only potentially divergent point is around $U_1 \to U$ from below since F_1 is a complete function when $\Delta < 3/2$. In particular, when $U_1 \sim U$, $F_1 \to 1$, which implies $\Delta < 3/2$ is the sufficient and necessary condition for integrability. Defining a new variable $z = \frac{U_1-U_0}{U-U_0}$, the domain of integration in (2.29) becomes 0 to 1 and therefore we can exchange the order of ∂_U and $\int dz$. After differentiating w.r.t. U, and restoring the variable U_1, we get

$$T_{UU} = -\frac{2h\Delta C_0\Gamma(\frac{1}{2})\Gamma(1-\Delta)}{\Gamma(\frac{3}{2}-\Delta)}\int_{U_0}^{U}\frac{dU_1U_1^{2\Delta}(f_1+f_2+f_3)}{(U-U_0)(U-U_1)^{\Delta-1/2}(1+U_1^2)^{\Delta+1}U^{\Delta+1}(U+U_1)^{1/2}} \tag{2.30}$$

where

$$f_1 = \frac{-2\Delta(UU_1^2+U_0)+3UU_0U_1+U_0+2U_1}{1+UU_1}F_1(1-\Delta,\frac{1}{2},1+\Delta,\frac{3}{2}-\Delta,u,v) \tag{2.31}$$

$$f_2 = \frac{2(1+\Delta)(U-U_1)(U_0+2UU_0U_1-UU_1^2)}{(2\Delta-3)U(1+U_1^2)(1+UU_1)}F_1(1-\Delta,\frac{1}{2},2+\Delta,\frac{5}{2}-\Delta,u,v) \tag{2.32}$$

$$f_3 = \frac{U_0(U-U_1)}{(2\Delta-3)(U+U_1)}F_1(1-\Delta,\frac{3}{2},1+\Delta,\frac{5}{2}-\Delta,u,v) \tag{2.33}$$

$$u = \frac{U-U_1}{U+U_1}, \qquad v = \frac{U-U_1}{U(1+U_1^2)} \tag{2.34}$$

Performing the final integral numerically, we plot the result in Fig. 2.2a.

In the figure, we see that the null energy is negative after we turn on the insertion at $U_0 = 1$ if we take positive h. Physically, this means the light-like ray $V = 0$ becomes time-like after U_0 and a spaceship that enters early enough may escape the black hole!

One may note that when $\Delta < 1/2$, T_{UU} is finite but when $\Delta > 1/2$, T_{UU} is singular near insertion time U_0. However, this singularity is not essential because it is integrable, as we will see later when we calculate $\int dUT_{UU}$ along the horizon $V = 0$. Indeed, the classical solution of Einstein equations for a shockwave insertion in the bulk in Kruskal coordinates contains a delta function, which is also an integrable singularity [67]. One might also worry that the derivative of g_{UU} and the Riemann curvature are singular at the turn-on and

turn-off times, although T_{UU} and $\int dU T_{UU}$ are not. However, this is simply due to the fact that we turned the insertion on and off as a step function. If this process were taken to be smooth enough, there would be no singularity.

To see the late time behavior, we can use the z variable to rewrite (2.30) in the large U limit. In this limit, f_1 dominates among all f_i's in (2.30). Using the identity $F_1(a;b,b';c;z,0) = {}_2F_1(a,b;c;z)$ we obtain

$$T_{UU} \to \frac{4h\Delta^2 C_0 \Gamma(\frac{1}{2})\Gamma(1-\Delta)}{\Gamma(\frac{3}{2}-\Delta)U^{2\Delta+2}} \int_0^1 \frac{dz\, z^{2\Delta+1}{}_2F_1(1-\Delta,\frac{1}{2},\frac{3}{2}-\Delta,\frac{1-z}{1+z})}{((z+\epsilon)^2+\epsilon)^{\Delta+1}(1-z)^{\Delta-1/2}(1+z)^{1/2}} \to 0_+ \tag{2.35}$$

where ϵ is a small number of order U^{-1} and which implies that T_{UU} becomes positive and decays to zero at late times.

If we turn off the interaction at some finite time U_f, when $U > U_f$, we can safely pass ∂_U into the U_1 integral, which leads to

$$T_{UU} = -\frac{4h\Delta C_0 \Gamma(\frac{1}{2})\Gamma(1-\Delta)}{\Gamma(\frac{1}{2}-\Delta)} \int_{U_0}^{U_f} dU_1 \frac{U_1^{2\Delta+1} F_1(-\Delta;\frac{1}{2},\Delta+1;\frac{1}{2}-\Delta;\frac{U-U_1}{U+U_1},\frac{U-U_1}{U(1+U_1^2)})}{(U-U_1)^{\Delta+1/2}(U+U_1)^{1/2}U^{\Delta+1}(1+U_1^2)^{\Delta+1}} \tag{2.36}$$

In deriving (2.36), we used a property of the derivative of the Appell hypergeometric function and equation (7a) in [66]. The numerical result is plotted in Fig. 2.2b.

In this figure, we see that after turning off the interaction, T_{UU} has a jump and becomes positive at late times. In particular, when $\Delta > 1/2$, T_{UU} becomes divergent again right after U_f. Fortunately, it is again an integrable divergence which should not cause any physical problem. By the identity [63]:

$$F_1(a;b,b';c;x,y) = \sum_{m\geq 0} \frac{(a)_m (b)_m}{m!(c)_m} x^m {}_2F_1(a+m,b';c+m;y) \tag{2.37}$$

the late time behavior can be analyzed by taking the $U \to \infty$ limit in (2.36):

$$T_{UU} \sim \frac{4h\Delta^2 C_0}{U^{2\Delta+2}} \log U \log \frac{U_f}{U_0} \to 0_+$$

Again, we find T_{UU} becomes positive after some time and decays to zero. In both late time analyses, T_{UU} decays like $U^{-2\Delta-2}$, which validates the assumption that $U h_{UU}$ and $\partial_U h_{\phi\phi}$ vanish when $U \to \infty$ in (2.3).

In the above discussion, we see that at some finite time T_{UU} becomes positive whether or not we turn off the insertion, which might appear dangerous for the fate of the worm

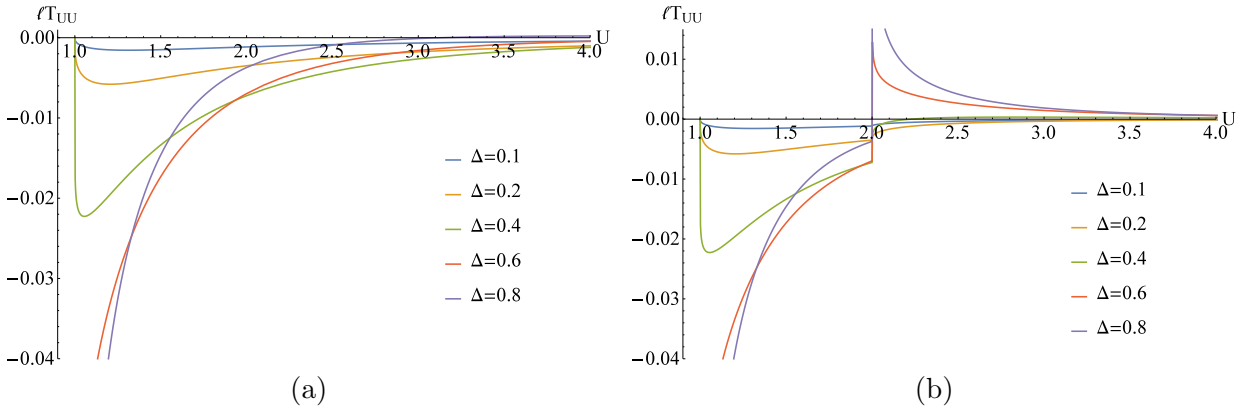

Figure 2.2: (a) shows the null energy along the horizon when the interaction is turned on at $U = U_0 = 1$ and never shut off, with our choice for the sign of the coupling h; (b) shows the case where it is turned on at $U = U_0 = 1$ and turned off at $U = U_f = 2$. In both cases, $h = 1$. We see clearly in both (a) and (b) that T_{UU} becomes negative after turn-on; in (b) T_{UU} becomes positive after turn-off. Blue is for $\Delta = 0.1$; yellow is for $\Delta = 0.2$; green is for $\Delta = 0.4$; pink is for $\Delta = 0.6$; purple is for $\Delta = 0.8$

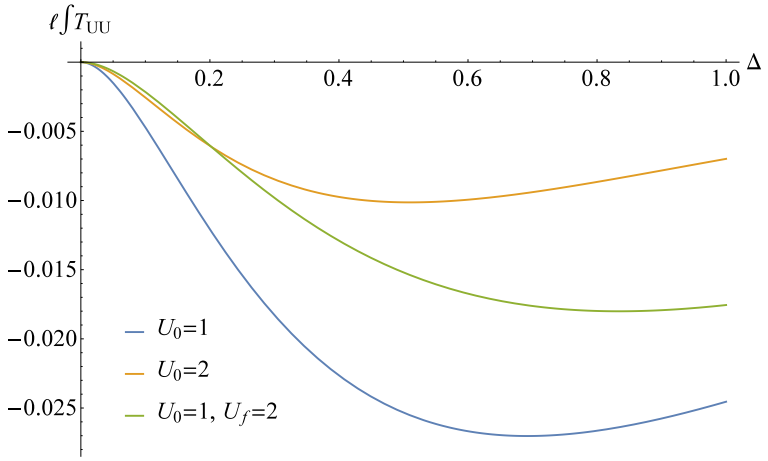

Figure 2.3: $\int dU T_{UU}$ as a function of Δ; blue is for $U_0 = 1$; yellow is for $U_0 = 2$; green is for $U_0 = 1$ and $U_f = 2$

hole. The crucial diagnostic is the sign of the integral of T_{UU} over the whole $V = 0$ slice. This is what determines whether a light ray on horizon eventually reaches the boundary at spatial infinity.

It looks horrible to integrate U in (2.30) from U_0 to infinity. Interestingly and surprisingly, by some tricks, we can get a closed form for it (see Appendix 2.A):

$$\int_{U_0}^{\infty} dU T_{UU} = -\frac{h\Gamma(2\Delta+1)^2}{2^{4\Delta}(2\Delta+1)\Gamma(\Delta)^2\Gamma(\Delta+1)^2\ell} \frac{{}_2F_1(\frac{1}{2}+\Delta, \frac{1}{2}-\Delta; \frac{3}{2}+\Delta; \frac{1}{1+U_0^2})}{(1+U_0^2)^{\Delta+1/2}} \tag{2.38}$$

If we turn off the interaction at U_f, the integral is just the difference between $\int_{U_0}^{\infty} dU T_{UU}$ and $\int_{U_f}^{\infty} dU T_{UU}$. We plot the result as a function of Δ in Fig. 2.3.

In this figure, we see that for all Δ values from 0 to 1, the integral of T_{UU} is always negative, which demonstrates the existence of a traversable wormhole. Furthermore, the earlier we turn on the insertion, the larger the effect is. In particular, even if T_{UU} becomes positive in late times, the wormhole still exists since the integral of T_{UU} remains negative. Note that $\Delta = 0$ is a special case where $\int dU T_{UU} = 0$. Indeed, the only $\Delta = 0$ operator in CFT is the identity and of course adding the product of identity operators to Hamiltonian has no effect on the system.

2.4 Holographic Energy and Entropy

In this section we will consider the implications of a traversable wormhole for the holographic entanglement entropy conjecture, which in this context relates the entanglement entropy between the two boundary CFT's to the area/entropy of certain extremal surfaces in the bulk theory [65, 41, 9, 25, 23].

As a preliminary, we discuss the change of energy of the CFT state. Long after the interaction is shut off, the system returns to thermal equilibrium. Thus the final horizon area can be determined from the energy of the system, measured on the left or the right. It is straightforward to check that, in our state, the energy decreases at linear order in h with the sign choice that rendered the wormhole traversable:

After deforming the Hamiltonian ($t > t_0$), the state in Schrödinger picture is

$$|\Psi(t)\rangle = e^{-iH_0(t-t_0)} U(t, t_0) \, |\text{tdf}\rangle \, . \tag{2.39}$$

Expanding $U(t, t_0)$ to leading order in $h(t)$ given by (2.23), we find that the change in the

energy on the right is

$$\begin{aligned}\delta E_R &= i\int_{t_0}^{t} dt_1 h(t_1)\,\langle \text{tdf}|\,[\delta H(t_1), H_R]\,|\text{tdf}\rangle \\ &= \int_{t_0}^{t} dt_1 d\phi h(t_1)\,\langle \text{tdf}|\,\partial_t \mathcal{O}_R(t_1,\phi)\mathcal{O}_L(-t_1,\phi)\,|\text{tdf}\rangle \\ &= \frac{h r_h^2}{2^{\Delta+1}\ell^3}\sum_n\left(\frac{1}{(\cosh 2r_h t + \cosh 2\pi r_h n)^\Delta} - \frac{1}{(\cosh 2r_h t_0 + \cosh 2\pi r_h n)^\Delta}\right)\end{aligned} \tag{2.40}$$

where in the second line we used the Heisenberg equation and in last line the boundary two-point function is obtained by taking limit $r \to \infty$ in (2.8) where ϕ has period 2π, and all of its images are summed over in the global BTZ black hole.[6] If the interaction shuts off at t_f, the energy obviously becomes constant for $t > t_f$, and t in (2.40) is replaced by t_f. Therefore, the effect of the interaction with $h > 0$ is to reduce the energy. Note that if there are any UV divergences in the energy they cannot appear at linear order in h, since the interaction involves just one field in each CFT.

At least at first order in h, the entropy of entanglement S_{EE} between the left and right boundaries should also be well-defined (and time dependent) even during the period of time when the interaction is turned on, if one thinks of the state as evolving by the deformed Hamiltonian in the original tensor product Hilbert space. By the first law of entanglement, at linear order in h, the change in S_{EE} is equal to $\beta\delta H_R$, thus it also decreases until the turn-off time t_f after which it remains constant (as it must under decoupled unitary evolution on the left and right).

The change in S_{EE} is $\mathcal{O}(1)$ in a $1/c \sim 1/N \sim G_N/L_{AdS}$ expansion.[7] At this order, in the bulk interpretation S_{EE} has two parts, namely the small gravitational correction to the area $A/4G_N$ of the extremal surface, and the entanglement entropy of bulk fields S_{bulk} on the spacelike slice from the extremal surface to the boundary slice at time t [25, 9].

In our situation, causality implies that the geometry near the bifurcation surface is unaffected by the perturbation. Thus, at order h, the area of the quantum extremal surface is unchanged from the original state. On the other hand, S_{bulk} has nonlocal aspects. Therefore, the decrease of S_{EE} at first order must be entirely due to a corresponding decrease in S_{bulk} evaluated at the bifurcation surface.

[6] We consider global AdS here so that the total energy is finite.

[7] These are the correct scaling relations for $2+1$ dimensional bulk. In other dimensions, the scaling with G_N is the same, but the scaling with the number of species N may vary.

However, after the time t_{trav} on the boundary, the bifurcation surface (E_1 of Fig. 2.4) is no longer spacelike to the AdS boundary, and one cannot define a bulk entanglement wedge using the surface E_1. This would render S_{bulk} ill-defined. The resolution is to use the *quantum extremal* surface.

More generally, it was proposed in [23] (and proven in [22]) that, at general orders in $1/N$, one should consider the entropy outside the quantum extremal surface, obtained by extremizing the total generalized entropy $S_{\text{gen}} = A/4G_N + S_{\text{bulk}}$. When calculating the $\mathcal{O}(1)$ piece of the entropy, these two prescriptions agree on the value of the entropy but [23, 21] argued that the location of the quantum extremal surface is also physically important, because it provides a natural boundary for how much of the bulk can be reconstructed from the CFT state on a single boundary. One useful constraint on the location quantum extremal surface is the GSL, which states that S_{gen} is nondecreasing on any future horizon.

On a Cauchy slice prior to the time when the interaction is turned on, the geometry and bulk quantum state are that of the Hartle-Hawking state. Thus the quantum (and classical) extremal surface is located at the bifurcation surface of the original black hole (E_1 of Fig. 2.4). On the other hand, after the interaction is over, the bulk quantum state of the fields changes and thus the quantum extremal surface must move. By left-right symmetry of the spacetime (together with the fact that the joint state of the entire system is pure so that S_{EE} is the same on both sides) it can it can only move along the vertical axis of symmetry of the spacetime. Also, the GSL implies that the new location must be on or behind the causal horizon [23], because otherwise it lies on a future horizon whose S_{gen} is generically increasing.

In fact, at first order in h, the GSL implies that the quantum extremal surface must lie exactly at the point E_2 in Fig. 2.4, where the two future horizons intersect. For since the GSL is true in every state [83], and saturated for the Hartle-Hawking state, it must also be saturated for any first order perturbation to the Hartle-Hawking state [81]. But if S_{gen} is stationary along two linearly independent normal directions of E_2, then it must be a quantum extremal surface.

As noted above, the area and bulk entanglement entropies are identical for E_1 and E_2 at linear order in h (as long as they are well-defined). Any effects arising from differences between E_1 and E_2 are suppressed by additional powers of h.

At second order in h, the GSL should no longer be saturated on the future horizon. Hence S_{bulk} is increasing with time at E_2, and the quantum extremal surface will instead be located slightly above the point E_2.

We have not followed the evolution of the quantum extremal surface at intermediate times, but it seems that it must gradually move upwards from E_1 to its final location above E_2. After the interaction is over the boundary evolution is unitary, and hence neither S_{EE} nor the quantum extremal surface changes.

[23] argued that the quantum extremal surface should always be spacelike to its corresponding CFT region. In a sense this continues to be true, since E_1 is spacelike to all the boundary points prior to turning on the interaction, while E_2 is spacelike to all the points after the interaction is turned off. But neither one is spacelike to the entire boundary for all time. For example, a unitary operator applied to the right boundary at sufficiently early times might affect the value of $S_{\text{gen}}(E_2)$, and hence the right CFT entropy after the interaction. But that does not contradict any of the properties of the right CFT, since it does not have unitary time evolution (independent of the left CFT) during the period of the interaction.

Note that, if we assume that our holographic entropy prescription is correct when the CFT's are not coupled, it must necessarily also be correct when the CFT's are coupled. Before the interaction is turned on, we can simply consider the Hartle-Hawking spacetime as if there were no interaction. Similarly, after the interaction is over, we can consider a new spacetime which is dual to extrapolating the final state backwards in time, without any interaction. Neither of these spacetimes corresponds to a traversable wormhole, but they can be used for purposes of calculating S_{EE} before or after the interaction is turned on. It is only when these two spacetimes are patched together, that they are seen to be a traversable wormhole geometry.

2.5 Discussion

We have demonstrated that the Einstein-Rosen bridge of a BTZ black hole becomes slightly traversable after the addition of a two-boundary coupling. (We expect that a similar effect also occurs in $D > 3$ bulk spacetime dimensions, although it is harder to calculate the exact form of the stress-tensor.)

From (2.38), we see that the integral $\int dU T_{UU}$, giving the deviation of null rays from the horizon, is proportional to h, which implies that the wormhole opens up by an amount (in units where $\hbar = 1$)

$$\Delta V \sim \frac{h G_N}{R^{D-2}} \tag{2.41}$$

where ΔV is the difference of V coordinate between the future horizon and the first lightray

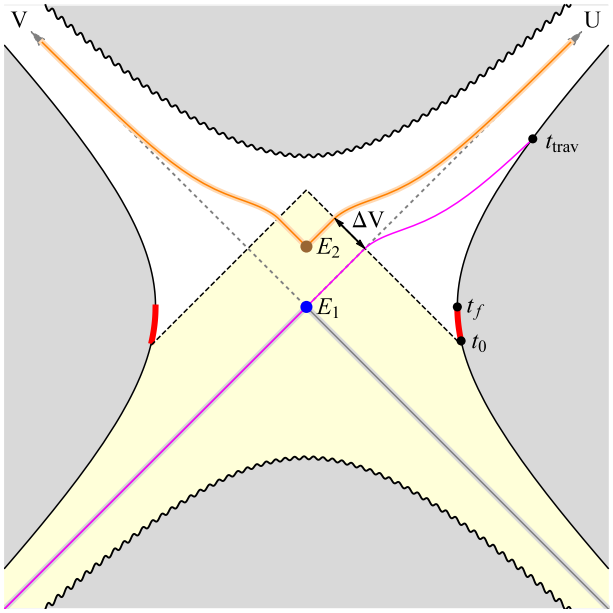

Figure 2.4: The throat size is $\Delta V \sim h$. The red thick interval on the boundary is the duration of the deformation beginning at t_0 and ending at t_f. The metric in the light yellow region is unchanged and only that of the white region will have a nonzero backreaction correction. The orange thick curve is the future event horizon and the grey thick curve is the past event horizon. E_1 is the original bifurcation surface. E_2 is the location where the right and left future horizons cross. The magenta curve is a null ray that passes through wormhole, deviating to right boundary.

which can get through the wormhole (see Fig. 2.4), and we assume that the black hole radius r_h, the AdS length L_{AdS}, and the amount of time Δt the interaction is turned on for are all of the same characteristic length scale R.

The wormhole is only open for a small proper time in the interior region. This is quite different from the usual static wormhole solutions which do not have event horizons (e.g. [57]). Nevertheless, radial lightrays originating on the boundary at arbitrarily early times will cross through the portal to the other side; in this sense the wormhole is open at arbitrarily early boundary times on either side.

A (test) astronaut from one boundary can only go through the wormhole before it closes, and she reaches the other boundary long after the boundary-boundary interaction is turned on. One should note that since the coupling we add breaks the Killing symmetry $H_L - H_R$, there is no way to boost her back to a time before she entered the worm hole. Thus the way we glue the two boundaries fixes the relative time coordinate between them,

excluding the possibility of having closed time-like curves [58]. Note that the traversable throat size depends on the strength of the coupling and a signal transmitted through the wormhole is only received at the other end after a very long time delay if the gravitational effects of the coupling are small. Furthermore, the thermofield double state that we require is an extremely fine tuned state, so it would be very difficult to prepare such a configuration in which the astronaut could enter at early times from the left.

We have not yet considered the backreaction on the geometry coming from an actual (non-test) astronaut traversing the wormhole throat. An object travelling at light speed from left to right contributes to T_{VV} but not to T_{UU}, so at the level of linearized gravity it will prevent objects from traversing in the *other direction* (i.e. from right to left) but it will have no tendency to close the wormhole in the same direction that it is travelling. This suggests that the objects can still traverse the wormhole even after taking into account their own gravitational back-reaction.[8]

Another question concerns the interaction of the astronaut with the negative energy pulse of radiation travelling in the other direction. In the frame of reference defined by Kruskal coordinates, a quantum traversing the wormhole must be blueshifted up to a frequency $1/\Delta V$, while the pulse coming in the other direction has a frequency of order $1/R$. Here we are assuming that the interaction is turned on for about one light-crossing time R, and that there is no other time scale of relevance in the problem. Although an incoming pulse with negative total energy is not allowed in classical scattering problems, we will nevertheless attempt to build intuition by comparing the situation to a normal field theory scattering problem. The center-of-mass energy scale of the collision is given by

$$\sqrt{s} \sim \sqrt{\frac{R^{D-4}}{hG_N}}. \tag{2.42}$$

Since $G_N \sim L_{\text{planck}}^{D-2}$, the center-of-mass energy is below the Planck scale in $D = 3$ (i.e. a BTZ black hole with any extra dimensions compactified at the Planck scale) but not when $D > 3$. However, even in higher dimensions we do not expect that full quantum gravity effects will be important. We nevertheless expect that it is legitimate to use the eikonal approximation, in which one solves for the propagation of each particle on the background

[8] Presumably there is *some* limit on how much information can get through, since the black hole on the other side cannot radiate more energy than its initial mass, but determining the precise limit would require going beyond the linearized regime. There might also be an interesting limit on the total amount of *information* which can get through the wormhole, coming from the Bousso bound [13] (see [29] for a proof in classical case) or its quantum generalization [14, 71].

field generated by the other particle. This corresponds to resumming ladder Feynman diagrams, whose amplitude scales with various powers of

$$\frac{G_N s}{b^{D-4}} \sim h^{-1}, \tag{2.43}$$

where b is the impact parameter, and we have used the fact that $b \sim R$ (except for small tails of the wavefunction). Non-eikonal Feynman diagrams should be suppressed by additional powers of G_N relative to eikonal diagrams with the same s dependence [2]. Therefore we can consistently consider scenarios in which only the eikonal scattering is relevant, in which our calculation of the geometry shows that the wormhole is traversable if the particle is sent in before a time $\Delta t \approx R \ln(R/hL_{\text{planck}})$ prior to the interaction being turned on. However if the particle is sent in more than $\frac{3}{2}\Delta t$ prior to the interaction time, then the eikonal approximation breaks down and there may be large back-reaction, invalidating our analysis. When $h \sim 1$, these times are of order the scrambling time.

It is interesting to consider what would happen if the two black holes were in the same component of space, rather than in different asymptotic regions. If the black holes were in a suitably entangled state, they should be connected by an Einstein-Rosen bridge [53], with the QFT state near the horizon close to the Hartle-Hawking state. The direct boundary interaction could then be produced by propagation through the ambient spacetime—this would be the same as the interaction we studied, except with a time delay. A similar calculation would then lead to a traversable wormhole. The negative ANE could be understood as coming from the Casimir effect associated to the cycle in space going from one black hole to the other in the ambient space and then threading the wormhole. Of course, the effect would be enhanced if the signals sent between the black holes were directed and amplified (otherwise the Casimir energy would be extremely tiny if the black holes were far apart). No causal paradoxes would arise because the traversability depends on backreaction due to the existence of a casual path between the black holes in the ambient spacetime.

Since any infinite null geodesic which makes it through a wormhole must be chronal (as discussed in the Introduction), such wormholes do not enable one to travel faster than light over long distances through space. Hence traversable wormholes are like getting a bank loan: you can only get one if you are rich enough not to need it.

The traversable wormhole we found has an interesting interpretation in the context of ER=EPR [53]. Maldacena and Susskind conjectured that any pair of entangled quantum systems are connected by an Einstein-Rosen bridge (the non-traversable wormhole). The crucial difference in our work is that we allow interaction between the entangled systems,

which is assumed to be negligible in ER=EPR. What we have shown is that in this case the Einstein-Rosen bridge can open to become a traversable wormhole.

Our example thus provides a way to operationally verify a salient feature of ER=EPR that observers from opposite sides of an entangled pair of systems may meet in the connected interior. Since in [53] any such meeting is trapped behind the horizon, it is not obvious how its occurrence could be confirmed by exterior or CFT measurements. What we found is that if, after the observers jump into their respective black holes, a boundary-boundary coupling is activated, then the Einstein-Rosen can be rendered traversable, and the meeting inside may be seen from the boundary. This seems to suggest that the ER=EPR wormhole connection was physically "real". But since all measurements in the CFT description are governed by the rules of linear quantum mechanics, it seems like any explicit operational verification of the existence of the wormhole would also correspond to a linear quantum measurement. It might be interesting to check the compatibility of these ideas with the linearity of measurements made behind the horizon, discussed in [56].

What is the quantum information theory interpretation of such a traversable wormhole? A curious feature of the transmission of a qubit, Q, through the wormhole is that it appears to be sent "via the entanglement", rather than directly by the inter-boundary coupling. (Note that the traversable portion of the wormhole is close to the bifurcation point, which describes the subspaces of the left and right Hilbert spaces that are the most entangled in the thermofield double state.) There are several ways to see that the quantum information of Q is not simply being sent directly through the boundaries. First, the commutator of Q (for example when it is first injected into the interior from the left boundary) with the interaction Hamiltonian is extremely small near the thermofield double state. Furthermore, at the time the interaction is activated, Q is in fact spacelike separated from the boundary in the bulk picture, so in the bulk approximation Q and $\mathcal{O}$ are independent quantum variables. From the CFT perspective, this is because Q has thermalized into the left system before the $\mathcal{O}_L\mathcal{O}_R$ interaction is turned on, so no quantum information about Q appears to be accessible to the operator $\mathcal{O}$. Of course, the boundary coupling is nevertheless crucial for the existence of the traversable wormhole.

This situation is somewhat analogous to what occurs in quantum teleportation. Entanglement alone cannot be used to transmit information, and no qubit, Q, from the left can traverse the bridge to the right if the left and right systems are dynamically decoupled. However, if additional classical information is sent from the left to the right, a qubit can be transmitted - this is referred to as quantum teleportation. Suppose Alice and Bob share a maximally entangled pair of qubits, A and B. Alice can then transmit the qubit Q to Bob by sending only the classical output of a measurement on the Q-A system. Depending on

which of the 4 possible results are obtained, Bob will perform a given unitary operation on the qubit B, which is guaranteed to turn it into the state Q.

Unlike the usual description of quantum teleportation, in our example it is essential that the channel between the left CFT, A, and the right CFT, B, is a quantum one. For example, if one projected onto eigenstates of the operator $\mathcal{O}_L$, then the configuration would simply look like a particular quantum state (the projection of $|\text{tfd}\rangle$) evolving under the decoupled Hamiltonians together with an action by a purely right unitary, which can never lead to a traversable wormhole. This makes sense, because in the standard description of quantum teleportation, the measurement performed by Alice is a projection onto an eigenstate, which instantly results in the pattern of Q being contained in the system B. This would not be described by a physical motion through the wormhole in the bulk. Teleportation in this sense has been discussed in the dual gravity language by [73, 60, 56].

However, in the exact, fully quantum description of the quantum teleportation protocol, there is a particular dynamical process given by the unitary evolution $V = \sum_i P_i^{QA} U_i^B$ that governs the transmission of the "classical" information and the subsequent appropriate transformation of a qubit in the B quantum system. Here P_i^{QA} are a complete mutually exclusive set of projectors on the Q-A system that describe Alice's measurement, and U_i^B is the unitary transformation performed by Bob given the data i. The classical information transmitted from Alice to Bob was encoded by the index i.

Treating V as a time dependent interaction Hamiltonian can result in negative ANE along the horizon if the original entanglement between A and B was well described by a large Einstein-Rosen bridge, which will render the wormhole traversable. This is a description in which the time scales and processes of decoherence and measurement by Alice are resolved, and treated as physical dynamical evolution. In such a "microscopic" description of quantum teleportation, the qubit Q must physically evolve from the left to the right. Of course in the limit that Alice's measurement is essentially instantaneous and classical, the traversable window will be very small (and not well described by a semiclassical spacetime) - just enough to let the single qubit Q pass through. Therefore, we propose that the gravitational dual description of quantum teleportation understood as a dynamical process is that the qubit passes through the ER=EPR wormhole of the entangled pair, A and B, which has been rendered traversable by the required interaction.

Another possible interpretation of our result is to relate it to the recovery of information described in [36]. Assuming that black hole evaporation is unitary, it is in principle possible to eventually recover a qubit which falls into a black hole, from a quantum computation acting on the Hawking radiation. Assuming that you have access to an auxiliary system

maximally entangled with the black hole, and that the black hole is an efficient scrambler of information, it turns out that you only need a small (order unity) additional quantity of Hawking radiation to reconstruct the qubit. In our system, the qubit may be identified with the system that falls into the black hole from the left and gets scrambled, the auxiliary entangled system is the CFT on the right, and the boundary interaction somehow triggers the appropriate quantum computation to make the qubit reappear again, after a time of order the scrambling time $R\ln(R/L_{\text{planck}})$.[9]

Acknowledgements

We thank Ofer Aharony, Daniel Harlow, Juan Maldacena, Sudipta Sarkar, Douglas Stanford and Andy Strominger for helpful and stimulating discussions. DLJ and PG were supported in part by NSFCAREER grant PHY-1352084 and by a Sloan Fellowship. AW was supported by the Institute for Advanced Study, by the Martin A. and Helen Chooljian Membership Fund, and NSF grant PHY-1314311. AW is grateful for typing support from Geoff Penington.

2.A $\int dUT_{UU}$

Using (2.28), the integrated null energy is

$$\int_{U_0}^{\infty} dUT_{UU} = -4h\Delta C_0 \int_{U_0}^{\infty} dU \lim_{U'\to U} \partial_U G(U,U';U_0), \tag{2.44}$$

where

$$G(U,U';U_0) \equiv \int_{U_0}^{U} dU_1 \int_1^{\frac{U}{U_1}} \frac{dy}{\sqrt{y^2-1}} \frac{U_1^{\Delta}}{(U-U_1 y)^{\Delta}(U'U_1+y)^{\Delta+1}}. \tag{2.45}$$

Note that

$$\lim_{U'\to U} \partial_U G(U,U';U_0) = \partial_U G(U,U;U_0) - \partial_U^{(2)} G(U,U;U_0), \tag{2.46}$$

where $\partial_U^{(2)}$ indicates a derivative with respect to the second variable. (2.44) becomes

$$\int_{U_0}^{\infty} dUT_{UU} = -4h\Delta C_0 \left(G(\infty,\infty;U_0) - G(U_0,U_0;U_0) - \int_{U_0}^{\infty} dU \partial_U^{(2)} G(U,U;U_0) \right) \tag{2.47}$$

[9] We thank Juan Maldacena for suggesting this interpretation.

By (2.29), and changing to the z variable,

$$\begin{aligned}G(U,U;U_0) &\propto \int_{U_0}^{U} dU_1 \frac{U_1^{\Delta-1/2}}{(U-U_1)^{\Delta-1/2}(1+UU_1)^{\Delta+1}} F_1(\frac{1}{2};\frac{1}{2},\Delta+1;\frac{3}{2}-\Delta;\frac{U_1-U}{2U_1},\frac{U_1-U}{U_1(1+UU_1)}) \\ &= \int_0^1 dz \frac{((U-U_0)z+U_0)^{\Delta-1/2}}{(U-U_0)^{\Delta-3/2}(1-z)^{\Delta-1/2}(1+U((U-U_0)z+U_0))^{\Delta+1}} \\ &\times F_1(\frac{1}{2};\frac{1}{2},\Delta+1;\frac{3}{2}-\Delta;\frac{(U-U_0)(z-1)}{2((U-U_0)z+U_0)},\frac{(U-U_0)(z-1)}{((U-U_0)z+U_0)(1+U((U-U_0)z+U_0))})\end{aligned} \tag{2.48}$$

which immediately implies $G(U_0,U_0;U_0)=0$ given that $\Delta<3/2$. For the large U limit, $G(\infty,\infty;U_0)$, the prefactor of F_1 above decays at least as fast as $U^{-\Delta}$ and the F_1 part becomes

$$F_1(\frac{1}{2};\frac{1}{2},\Delta{+}1;\frac{3}{2}{-}\Delta;-\frac{1-z}{2z},0) = {}_2F_1(\frac{1}{2},\frac{1}{2};\frac{3}{2}{-}\Delta;\frac{z-1}{2z}) = \left(\frac{2z}{z+1}\right)^{1/2} {}_2F_1(\frac{1}{2},\frac{1}{2};\frac{3}{2}{-}\Delta;\frac{1-z}{1+z}) \tag{2.49}$$

which leads to

$$G(\infty,\infty;U_0) \sim U^{-\Delta}\int_0^1 dz \left(\frac{2z}{z+1}\right)^{1/2}(1-z)^{-\Delta+1/2}{}_2F_1(\frac{1}{2},\frac{1}{2};\frac{3}{2}-\Delta;\frac{1-z}{1+z}) \to 0 \tag{2.50}$$

where in the last step we used the fact that the z integral is finite due to the property of hypergeometric function:

$${}_2F_1(\frac{1}{2},\frac{1}{2};\frac{3}{2}-\Delta;0)=1, \qquad \lim_{z\to 0} z^{1/2}{}_2F_1(\frac{1}{2},\frac{1}{2};\frac{3}{2}-\Delta;\frac{1-z}{1+z}) \sim z^{1/2}\log\frac{2z}{z+1}\to 0 \tag{2.51}$$

The integral of T_{UU} is simplified to be

$$\begin{aligned}&-\frac{1}{4h\Delta C_0}\int_{U_0}^{\infty} dU T_{UU} \\ &= -\int_{U_0}^{\infty} dU \int_{U_0}^{U} dU_1 \int_1^{\frac{U}{U_1}} \lim_{U'\to U}\partial_{U'}\frac{dy}{\sqrt{y^2-1}}\frac{U_1^{\Delta}}{(U-U_1y)^{\Delta}(U'U_1+y)^{\Delta+1}} \\ &= \int_{U_0}^{\infty} dU_1 \int_{U_1}^{\infty} dU \int_1^{\frac{U}{U_1}} \frac{dy}{\sqrt{y^2-1}}\frac{(\Delta+1)U_1^{\Delta+1}}{(U-U_1y)^{\Delta}(UU_1+y)^{\Delta+2}} \\ &= \int_{U_0}^{\infty} dU_1 \int_{U_1}^{\infty} dU \frac{(\Delta+1)\Gamma(\frac{1}{2})\Gamma(1-\Delta)U_1^{2\Delta+3}(U+U_1)^{-1/2}}{\Gamma(\frac{3}{2}-\Delta)(U-U_1)^{\Delta-1/2}U^{\Delta+2}(1+U_1^2)^{\Delta+2}} \\ &\times F_1(1-\Delta;\frac{1}{2},\Delta+2;\frac{3}{2}-\Delta;\frac{U-U_1}{U+U_1},\frac{U-U_1}{U(1+U_1^2)})\end{aligned} \tag{2.52}$$

For further simplification, we use (2.37) and define $w = \frac{U-U_1}{U+U_1}$ to rewrite (2.52) as

$$\begin{aligned}
&-\frac{1}{4h\Delta C_0}\int_{U_0}^{\infty} dU T_{UU} \\
=&\sum_m \frac{(\Delta+1)\Gamma(\frac{1}{2})\Gamma(1-\Delta)(1-\Delta)_m(\Delta+2)_m 2^{m+1-\Delta}}{m!\Gamma(\frac{3}{2}-\Delta)(\frac{3}{2}-\Delta)_m}\int_{U_0}^{\infty} dU_1 \frac{U_1^2}{(1+U_1^2)^{\Delta+m+2}} \\
&\times \int_0^1 dw \frac{w^{m-\Delta+1/2}(1-w)^{2\Delta}}{(1+w)^{\Delta+m+2}} {}_2F_1(1-\Delta+m;\frac{1}{2};\frac{3}{2}-\Delta+m;w) \\
=&\sum_m \frac{(\Delta+1)\Gamma(\frac{1}{2})\Gamma(1-\Delta)(1-\Delta)_m(\Delta+2)_m 2^{m+1-\Delta}}{m!\Gamma(\frac{3}{2}-\Delta)(\frac{3}{2}-\Delta)_m}\int_{U_0}^{\infty} dU_1 \frac{U_1^2}{(1+U_1^2)^{\Delta+m+2}} \\
&\times \frac{\Gamma(\frac{3}{2}-\Delta+m)\Gamma(2\Delta+1)^2}{2^{\Delta+m+2}\Gamma(\frac{3}{2}+2\Delta)\Gamma(2+\Delta+m)} {}_2F_1(2\Delta+1,2\Delta+1;\frac{3}{2}+2\Delta;\frac{1}{2}) \\
=&\sum_m \frac{\Gamma(\frac{1}{2})\Gamma(1-\Delta)\Gamma(2\Delta+1)^2(1-\Delta)_m}{m!\Gamma(\frac{3}{2}+2\Delta)\Gamma(\Delta+1)2^{2\Delta+1}} {}_2F_1(2\Delta+1,2\Delta+1;\frac{3}{2}+2\Delta;\frac{1}{2}) \\
&\times \frac{(U_0^{-2})^{\Delta+m+1/2}}{2(\Delta+m+1/2)} {}_2F_1(\frac{1}{2}+\Delta+m,2+\Delta+m;\frac{3}{2}+\Delta+m;-U_0^{-2}) \\
=&\frac{\Gamma(\frac{1}{2})\Gamma(1-\Delta)\Gamma(2\Delta+1)^2}{2^{2\Delta+2}(\Delta+\frac{1}{2})\Gamma(\frac{3}{2}+2\Delta)\Gamma(\Delta+1)} \frac{1}{(1+U_0^2)^{\Delta+1/2}} {}_2F_1(2\Delta+1,2\Delta+1;\frac{3}{2}+2\Delta;\frac{1}{2}) \\
&\times \sum_m \frac{(1-\Delta)_m(\frac{1}{2}+\Delta)_m}{m!(\frac{3}{2}+\Delta)_m}\left(\frac{1}{1+U_0^2}\right)^m {}_2F_1(\frac{1}{2}+\Delta+m,-\frac{1}{2};\frac{3}{2}+\Delta+m;\frac{1}{1+U_0^2}) \\
=&\frac{\pi\Gamma(1-\Delta)\Gamma(2\Delta+1)^2}{2^{2\Delta+2}(\Delta+\frac{1}{2})\Gamma(\Delta+1)^3} \frac{{}_2F_1(\frac{1}{2}+\Delta,\frac{1}{2}-\Delta;\frac{3}{2}+\Delta;\frac{1}{1+U_0^2})}{(1+U_0^2)^{\Delta+1/2}}
\end{aligned} \tag{2.53}$$

where in fifth line we used [63]

$$\begin{aligned}
&\int_0^y \frac{x^{c-1}(y-x)^{\beta-1}}{(1-zx)^\rho} {}_2F_1(a,b;c;\frac{x}{y})dx \\
=&\frac{y^{c+\beta-1}}{(1-yz)^\rho}\frac{\Gamma(c)\Gamma(\beta)\Gamma(c-a-b+\beta)}{\Gamma(c-a+\beta)\Gamma(c-b+\beta)} {}_3F_2(\beta,\rho,c-a-b+\beta;c-a+\beta,c-b+\beta;\frac{yz}{yz-1}) \\
&[y,\mathrm{Re}\,c,\mathrm{Re}\,\beta,\mathrm{Re}(c-a-b+\beta)>0;|\arg(1-yz)|<\pi]
\end{aligned} \tag{2.54}$$

in sixth line we used

$$\int_b^\infty dx \frac{x^2}{(1+x^2)^a} = \frac{b^{-2a+3}}{2a-3} {}_2F_1(a-\frac{3}{2},a;a-\frac{1}{2};-b^{-2}) \tag{2.55}$$

and in last step we used [63]

$$\sum_{k=0}^{\infty}\frac{(a)_k(b')_k}{k!(c)_k}x^k {}_2F_1(a+k,b;c+k;x) = {}_2F_1(a,b+b';c;x) \tag{2.56}$$

$$ {}_2F_1(2\Delta+1, 2\Delta+1; \frac{3}{2}+2\Delta; \frac{1}{2}) = \frac{\pi^{1/2}\Gamma(\frac{3}{2}+2\Delta)}{\Gamma(1+\Delta)^2} \tag{2.57} $$

In the end, restoring ℓ, we find the following relatively simple result

$$ \int_{U_0}^{\infty} dU T_{UU} = -\frac{h\Gamma(2\Delta+1)^2}{2^{4\Delta}(2\Delta+1)\Gamma(\Delta)^2\Gamma(\Delta+1)^2\ell} \frac{{}_2F_1(\frac{1}{2}+\Delta, \frac{1}{2}-\Delta; \frac{3}{2}+\Delta; \frac{1}{1+U_0^2})}{(1+U_0^2)^{\Delta+1/2}} \tag{2.58} $$

If we turn off the interaction at U_f, the integral is just the difference between $\int_{U_0}^{\infty} dU T_{UU}$ and $\int_{U_f}^{\infty} dU T_{UU}$.

Chapter 3

Regenesis and Quantum Traversable Wormholes

This thesis chapter originally appeared in the literature as
Gao, P. and Liu, H., *2018. Regenesis and quantum traversable wormholes. arXiv preprint arXiv:1810.01444.*

3.1 Introduction

When a circuit is disconnected from its battery, the electric current flowing through it quickly stops, due to dissipation.

Using modern language, treating the circuit and its environment as a single isolated quantum system, we say the current is scrambled among other degrees of freedom of the system. Once a signal is dissipated (or scrambled), it cannot be recovered in practice, as to do that one needs to have control over the full quantum state of the system, which in practice is never possible for a system of many degrees of freedom.

In this paper we discuss a new phenomenon, based on the recent discussion of a traversable wormhole [31, 52, 74, 72, 75], where the current signal can re-appear with the need of only performing some simple operations.

Let us first describe the setup using field theory language (see also Fig. 3.1). Consider two identical uncoupled quantum systems, to which we will refer as L, R systems. The Hamiltonians for them are respectively H^L and H^R which by definition have the same set

of eigenvalues $\{E_n\}$ with respective energy eigenstates $|n\rangle_{L,R}$. Suppose L, R systems are arranged in a special entangled state such that at $t = 0$ it is given by a thermal field double state [76]

$$|\Psi_\beta\rangle = \frac{1}{Z_\beta}\sum_n e^{-\frac{\beta E_n}{2}}|\bar{n}\rangle_L|n\rangle_R\,, \qquad Z_\beta = \sum_n e^{-\beta E_n} \tag{3.1}$$

where $|\bar{n}\rangle$ denotes time reversal of $|n\rangle$. $|\Psi_\beta\rangle$ has the property that if one operates solely in one of the systems one finds a thermal state at inverse temperature β. Consider at some time $t = -t_s < 0$ turning on an external source φ^R for some few-body Hermitian operator J^R for a short interval.[1] In the R system there is an induced expectation value $\langle J^R(t)\rangle \equiv \langle\Psi_\beta|J^R(t)|\Psi_\beta\rangle$, but there is no response in the L system as by definition $[J^L, J^R] = 0$. As usual $\langle J^R(t)\rangle$ will dissipate and decay quickly to zero after φ^R is turned off.

Now couple the two systems at $t = 0$, with the total Hamiltonian

$$H = H^L + H^R - gV\delta(t = 0) \tag{3.2}$$

where g is a coupling and V is an operator involving both L and R systems, e.g. a simplest choice is

$$V = \mathcal{O}^L(0)\mathcal{O}^R(0) \tag{3.3}$$

for some few-body operator $\mathcal{O}(x)$. The surprising result from the gravity analysis of [52] is that a signal will re-appear in the L-system if t_s is larger than the *scrambling time* t_* of the L, R system.[2] Note that here $\mathcal{O}$ and J are generic few-body operators which do not need to have any common degrees of freedom between them.

The purpose of this paper is to argue that this phenomenon, to which we will refer below as "regenesis," is universal for generic quantum chaotic systems, to elucidate its underlying physics, to study it in detail in a class of field theories, and to discuss its gravity implications.

A general result we obtain is that in a generic chaotic system for $t, t_s \gg t_*$: (i) $\langle J^L(t)\rangle_g$ is supported only for $t \approx t_s$ where $\langle\cdots\rangle_g$ denotes expectation value in (3.1) with a nonzero g; (ii) as a function of t_s, $\langle J^L(t = t_s, \vec{x})\rangle_g$ has the following behavior

$$\langle J^L(t_s, \vec{x})\rangle_g \approx C(g)\,\varphi^R(-t_s, \vec{x}), \qquad t_s \gg t_* \tag{3.4}$$

[1] The time interval is taken to be much smaller than t_s.

[2] Scrambling time is defined here as the time scale when $\langle[V(t), W(0)]^2\rangle$ between generic few-body operators V, W become $O(1)$.

where $C(g)$ is an $O(1)$ constant depending on g. We thus find the "input signal" φ^R from the R system at $t = -t_s$ regroups at $t = t_s$ in the L system long after it has dissipated![3] The result (3.4) is insensitive to the specific form of $L - R$ interaction V. The behavior for a system with $t_s \sim t_*$ is more complicated and will be mentioned later.

The essential elements behind the regenesis behavior (3.4) are: (i) scrambling in a chaotic system makes out-of-time-ordered correlation functions (OTOCs) vanish for $t \gg t_*$ [68, 51], and (ii) the entanglement structure of (3.1) which strongly correlates an operator inserted at $(-t, \vec{x})$ with an operator at $(t, \vec{x})$. Compared to other manifestations of quantum chaos such as the initial growth of OTOCs which deals with early times, and a random matrix-type energy spectrum which reflects very large time behavior, the regenesis phenomenon concerns with intermediate times, of order the scrambling time of a system. Instead of making the signal to appear at the same spatial location $\vec{x}$, by considering a slight variation of (3.1) one could also make the signal from $(-t, \vec{x})$ to regroup at $(t, \vec{x} + \vec{a})$ for some $\vec{a}$.

One may wonder what happens if we consider the same setup in a few-body or integrable system. In general, with $g \neq 0$, some response will be generated in the L-system: interactions among each subsystem will manage to communicate the effects of φ^R to J^L. But there are two crucial differences: (1) it will not be "regenesis," as in a few-body system (or in integrable systems) there is no dissipation, so the original signal in the R-system will remain there forever; (2) the signal generated in the L-system will depend sensitively on the specifics of an individual system and the operators used. In contrast, in chaotic systems, the behavior is universal, independent of all the details.

At first sight, the regenesis phenomenon appears to be miraculous: how can a dissipated signal regroup with a very simple operation like (3.3)? If one wants to be melodramatic, we could imagine that by turning on φ^R, we create a "cat" in the R system. The cat lives for a while, and dies. Eventually her body will be fully scrambled with the environment. Now it appears that we could bring her back to life in the L-system by simply turning on a gV! There are two important catches here. Firstly, the success of the operation in fact requires extreme fine tuning in how we prepare the initial state at $-t_s$ when we turn on the external source φ^R. The state should be prepared such that as the system evolves to $t = 0$, the system is in the thermal field double state (3.1). This is a highly nontrivial requirement as the scrambling time t_* could be macroscopic for a macroscopic system, and as we will see explicitly the regenesis phenomenon is somewhat fragile: various modifications could

[3]Note that in (3.4) signals which are input earlier in the R systems appear later in the L system, so in fact what one finds is the *time reversed* form of the input signal.

destroy the behavior (3.4). A second catch is that as we will discuss later (in Sec. 3.2.4), at least for the regime $t, t_s \gg t_*$, the signal (3.4) is quantum in nature, i.e. the variance is always comparable to the expectation value itself, and one cannot cut down fluctuations using macroscopic measurements.

We also study the regenesis phenomenon in two-dimensional conformal field theories (CFT) in the large central charge limit which is known to be chaotic [64]. That is, we take L and R systems to be (1+1)-dimensional and described by a CFT. We consider $c \gg \Delta_J \gg \Delta_{\mathcal{O}} \sim O(1)$ where c is the central charge of the system, and $\Delta_{\mathcal{O}}, \Delta_J$ are respectively the scaling dimensions of few-body operators $\mathcal{O}$ and J. In this regime we can obtain the behavior of $\left\langle J^L(t)\right\rangle_g$ in detail by applying the techniques of [26, 27, 28]. In addition to (3.3) we will also consider two other types of couplings (in (3.5) α denotes different operator species)

$$V = \frac{1}{k}\sum_{\alpha=1}^{k} \mathcal{O}_\alpha^L(0)\mathcal{O}_\alpha^R(0) \tag{3.5}$$

which were considered in [52] in the large k limit, and

$$V = \frac{1}{L}\int_{-\frac{L}{2}}^{\frac{L}{2}} dx\, \mathcal{O}^L(x)\mathcal{O}^R(x)\ . \tag{3.6}$$

For (3.5) our CFT results are fully consistent with the gravity results of [52] for a $(0+1)$-dimensional holographic system.

We will refer to (3.3) as a single-channel coupling, while (3.5)–(3.6) as multiple-channel, one from multiplicity of operators, one from spatial integrations. Their local spacetime structure is chosen to maximally take advantage of the entanglement structure of (3.1). Here is a brief summary of the main features found in explicit CFT calculations (some of these features are also present in the gravity results of [52] for (3.5)):

1. In all cases, as a function of t_s, one can separate the behavior of $\left\langle J^L(t_s)\right\rangle_g$ into three different regions: (1) $t_s \ll t_*$ (sub-scrambling region), where $\left\langle J^L(t_s)\right\rangle_g$ is exponentially small and can be considered to be zero for practical purposes; (2) $t_s \sim t_*$ (transition region), where $\left\langle J^L(t_s)\right\rangle_g$ becomes $O(1)$; (3) $t_s \gg t_*$ (stable region), where $\left\langle J^L(t_s)\right\rangle_g$ is given by (3.4). Here the scrambling time is given by $t_* = \frac{\beta}{2\pi}\log\frac{c}{6\pi}$.

2. For (3.3) and (3.5) the transition region is very narrow, of order $O(\beta)$, while for (3.6) the transition regions is lengthened to $O(L)$ for $L \gg \beta$. See Fig. 3.2.

3. An interesting effect for (3.5) in the transition region is that, with a choice of a sign for g, the magnitude of $\left\langle J^L(t_s)\right\rangle_g$ could be exponentially large in g, to which we refer as resonant enhancement. See Fig. 3.2(a) for a cartoon.

4. For (3.5)–(3.6), $C(g)$ in (3.4) is given by

$$C(g) = 2G_J \sin(gG) \tag{3.7}$$

is oscillatory in g. G_J and G are some constants. For (3.3) there appears no oscillation in g, and we find for large g

$$C(g) \propto g^{-1} \ . \tag{3.8}$$

Our field theory studies also have important implications for the understanding of the traversability of a wormhole on the gravity side. In [31, 52], the basic picture is that the two-sided coupling (3.3) (or (3.5)–(3.6)) generates negative-energy excitations which in turn deform the spacetime causal structure of the wormhole geometry, allowing signals to propagate between the two boundaries of a wormhole. Combining our results and those from gravity calculations of [52], we argue that there exist physically distinct scenarios for traversability from causal propagation through the wormhole. For example, in the regime as described by (3.4), the traversability appears quantum in nature, i.e. cannot be associated with a semi-classical spacetime causal structure. Instead it appears to involve breaking of a delicate destructive interference, see Fig. 3.3 for a cartoon picture (which is appropriate for $t_s \gg t_*$).

The plan of this chapter is as follows. In Sec. 3.2 we present a general argument for the regenesis phenomenon, explain the quantum nature of the signal, and discuss its robustness. We also present a simple qubit model as a contrast study of this phenomenon in a few-body system. In Sec. 3.3 we outline the main steps of the calculation of $\left\langle J^L(t)\right\rangle_g$ in a two-dimensional CFT in the large central charge limit, with details of the calculation given in Appendix 3.C and Appendix 3.D. Details on the CFT calculation of the robustness of the phenomenon is given in Appendix 3.E. In Sec. 3.4 we analyze the results obtained in Sec. 3.3 and various Appendices. In Sec. 3.5 we discuss gravity interpretation of our results, including a detailed comparison with the results of [52]. In Sec. 3.6 we conclude with various discussions, including future directions and experimental realizations.

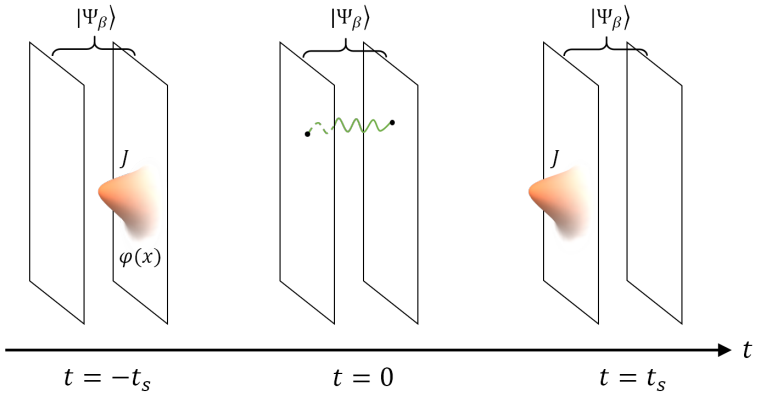

Figure 3.1: The setup for the regenesis phenomenon. At $t = -t_s$, uncoupled systems L, R are in an entangled state (3.1). The signal in J^R disappears shortly after we turn off the source φ^R. At $t = 0$, we turn on a local coupling between L and R for a short time, which we have approximated as a delta function in time in (3.2). At $t = t_s$, the signal reappears in the L system if t_s is sufficiently large. The reappeared signal is not identical to the original signal, but related by a transformation.

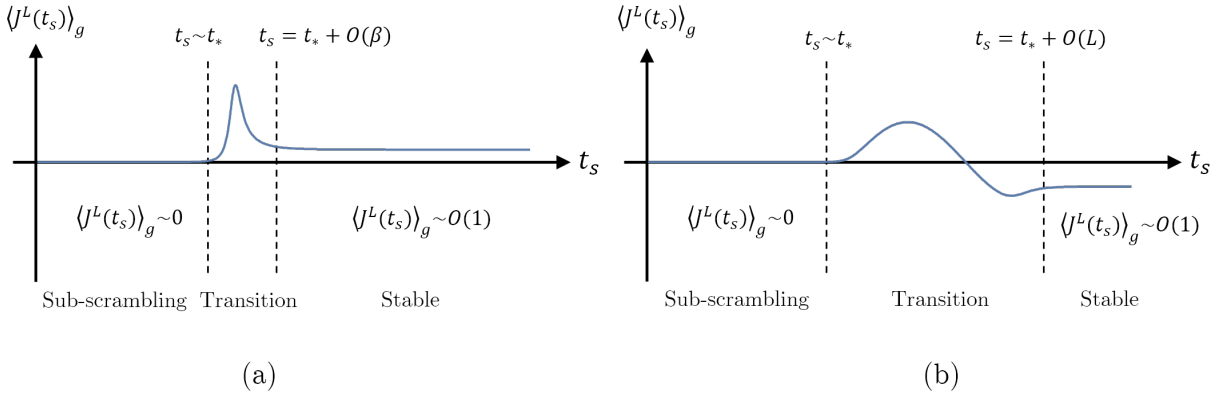

Figure 3.2: The behavior of $\langle J^L(t_s)\rangle_g$ for three regimes of t_s. (a) is a cartoon for (3.5) with transition regime of length $O(\beta)$, and the resonant enhancement could be pronounced. (b) is for (3.6) with the size of the transition region of order $O(L)$ for $L \gg \beta$.

3.2 A general argument for the regenesis phenomenon

In this section we present a simple argument for the regenesis behavior (3.4) for a general quantum chaotic system and discuss the robustness of the phenomenon, i.e. how it fares against imperfections of the preparation of $|\Psi_\beta\rangle$. The results of this section are consistent with the gravity results of [52] for holographic systems, and will be further confirmed through explicit calculations in two-dimensional CFTs in the large central charge limit in subsequent sections.

3.2.1 More on the general setup

As discussed in the Introduction we consider L and R systems in a thermal field double state (3.1). In this state, the expectation value of any set of operators which act only on one of the systems is given by the thermal average with inverse temperature β, e.g.

$$\langle \Psi_\beta | \mathcal{O}_1^L \cdots \mathcal{O}_n^L | \Psi_\beta \rangle = \frac{1}{Z_\beta} \mathrm{Tr}\left(e^{-\beta H} \mathcal{O}_1 \cdots \mathcal{O}_n\right) \equiv \langle \mathcal{O}_1 \cdots \mathcal{O}_n \rangle_\beta \tag{3.9}$$

where on the right hand side the trace is performed in the left system and $\langle \cdots \rangle_\beta$ denotes thermal average at inverse temperature β. For notational simplicity we have dropped L labels. We will do this for the rest of the paper: below any quantities with no explicit labels should be understood as in the L system.

By definition any operators from L system commute with those of R system, i.e.

$$[\mathcal{O}^L(x), J^R(x')] = 0, \qquad \forall\ \mathcal{O}, J, x, x' \tag{3.10}$$

where x denotes spacetime coordinates, i.e. $x = x^\mu = (t, \vec{x})$ and $\vec{x}$ are spatial coordinates. Consider turning on a source φ^R for some generic (hermitian) few-body operator J^R, i.e. perturbing the action S^R of the right system by

$$S^R \to S^R + \int d^d x\, \varphi^R(x) J^R(x)\ . \tag{3.11}$$

We will choose J such that its thermal expectation value is zero. Then at linear order in φ^R we have

$$\big\langle J^R(x) \big\rangle = \int d^d x'\, G^{RR}(x, x') \varphi^R(x'), \qquad G^{RR}(x, x') = i\theta(t - t') \big\langle [J^R(x), J^R(x')] \big\rangle_\beta\ . \tag{3.12}$$

For $g = 0$, there is no response in the left system

$$\big\langle J^L(x) \big\rangle = 0 \tag{3.13}$$

due to (3.10). On general ground one expects that the thermal response function G^{RR} for a non-conserved quantity to behave for large $t-t'$ or large $|\vec{x}-\vec{x}'|$ as

$$G^{RR}(t,\vec{x},t',\vec{x}') \sim e^{-\frac{|t-t'|}{\tau_r}}, \qquad G^{RR}(t,\vec{x},t',\vec{x}') \sim e^{-\frac{|\vec{x}-\vec{x}'|}{\ell_r}} \tag{3.14}$$

where τ_r, ℓ_r are respectively relaxation time and length, both of which will be treated as microscopic, i.e. much smaller than typical scales involved in φ^R. For a scale invariant system, they are both of $O(\beta)$, see e.g. (3.64). Thus $\langle J^R \rangle$ will quickly decay to zero in a time scale of order τ_r after the source is turned off.

Now with g nonzero in (3.2) we would like to see whether there is a response on the L side. We take the source φ^R to be turned on for a short period around $t=-t_s<0$ such that $\langle J^R(t)\rangle$ will have long decayed to zero before V is turned on at $t=0$. From Appendix 3.A, we find at full nonlinear level in φ^R

$$\langle J^L(t)\rangle_g = \langle \Phi|J^L(t)|\Phi\rangle = \langle\Psi_\beta| e^{-i\int ds\,\varphi^R(s)J^R(s)} e^{-igV} J^L(t) e^{igV} e^{i\int ds\,\varphi^R(s)J^R(s)} |\Psi_\beta\rangle \tag{3.15}$$

with $|\Phi\rangle$ defined as

$$|\Phi\rangle \equiv e^{igV} e^{i\int ds\,\varphi^R(s)J^R(s)} |\Psi_\beta\rangle \ . \tag{3.16}$$

Expanding (3.15) to linear order in φ^R we then find

$$\langle J^L(x)\rangle_g = \int d^dx'\, G^{LR}(x,x')\varphi^R(x'), \tag{3.17}$$

with (note we take both J and $\mathcal{O}$ to be Hermitian operators)

$$G^{LR}(x,x') = i\theta(t-t')\langle\Psi_\beta|[J^L(x),J^R(x')]|\Psi_\beta\rangle_g = i\theta(t-t')(W(x,x')-W^*(x,x')), \tag{3.18}$$

$$W(x,x') = \langle\Psi_\beta|e^{-igV}J^L(x)\,e^{igV}J^R(x')\,|\Psi_\beta\rangle \ . \tag{3.19}$$

3.2.2 Entanglement structure

The thermal field double state (3.1) has a rather specific entanglement structure between L and R systems. It can be checked that the state generated from a Hermitian operator J^R acting on $|\Psi_\beta\rangle$ can be reproduced from the action of J^L in the L system with a shift in imaginary time, i.e.

$$J^R|\Psi_\beta\rangle = \eta^* J^L(i\beta/2)|\Psi_\beta\rangle \tag{3.20}$$

where η is the phase factor associated with time reversal on J and will be dropped subsequently as it will not play any role. Furthermore,

$$(H^L-H^R)|\Psi_\beta\rangle = 0, \quad \to \quad e^{-iH^Lt}|\Psi_\beta\rangle = e^{-iH^Rt}|\Psi_\beta\rangle \ . \tag{3.21}$$

The combination of (3.20)–(3.21) implies that

$$\begin{aligned} J^R(t)\,|\Psi_\beta\rangle &= e^{iH^Rt}J^Re^{-iH^Rt}\,|\Psi_\beta\rangle = e^{-iH^Lt}e^{iH^Rt}J^R\,|\Psi_\beta\rangle \\ &= e^{-iH^Lt}J^L(i\beta/2)e^{iH^Lt}\,|\Psi_\beta\rangle = J^L(-t+i\beta/2)\,|\Psi_\beta\rangle \end{aligned} \tag{3.22}$$

where we have used L and R operators commute and (3.21) repeatedly. Note that (3.22) applies to a complex t with $\mathrm{Im}\,t \in (0,\beta/2)$. By using the above equation repeatedly we further find that

$$J_1^R(t_1)J_2^R(t_2)\cdots J_n^R(t_n)\,|\Psi_\beta\rangle = J_n^L(-t_n+i\beta/2)\cdots J_2^L(-t_2+i\beta/2)J_1^L(-t_1+i\beta/2)\,|\Psi_\beta\rangle \tag{3.23}$$

where subscripts label different operators. Due to the entanglement structure of $|\Psi_\beta\rangle$, we see from (3.22)–(3.23) that operators inserted at $(t,\vec{x})$ in the R system are strongly correlated with those inserted at $(-t,\vec{x})$ in the L system. In other words, there appears a "time reversal symmetry" between L and R systems. We will refer to such a pair of points as an entangled pair. This simple fact will play a key role in understanding the results of the paper. Moreover, the interactions (3.3) and (3.5)–(3.6) are chosen to involve couplings between operators inserted at entangled points, which as we will see makes the teleportation most efficient.

From (3.22) we have

$$\langle\Psi_\beta|J^L(t,\vec{x})J^R(-t',\vec{x}')|\Psi_\beta\rangle = \langle J^L(t,\vec{x})J^L(t'+i\beta/2,\vec{x}')\rangle_\beta \sim \begin{cases} e^{-\frac{|t-t'|}{\tau_r}} & |t-t'|\gg\tau_r \\ e^{-\frac{|\vec{x}-\vec{x}'|}{\ell_r}} & |\vec{x}-\vec{x}'|\gg\ell_r \end{cases} \tag{3.24}$$

where in the second equality we have again displayed the usual behavior for a thermal two-point function. An explicit example of (3.24) is given by (3.65) for a two-dimensional CFT, for which $\tau_r = \ell_r = \frac{\beta}{2\pi}$. Treating τ_r, ℓ_r as microscopic, we see that the two-side correlation function (3.24) is essentially nonzero only for $t \approx t'$ and $\vec{x} \approx \vec{x}'$, and we will denote

$$G_J \equiv \langle\Psi_\beta|J^L(t,\vec{x})J^R(-t,\vec{x})|\Psi_\beta\rangle \tag{3.25}$$

which is a constant from spacetime translational symmetries.

3.2.3 Regenesis behavior for quantum chaotic systems

Now let us examine the behavior of (3.15) (or its linear version (3.19)) for a general chaotic system. We will take $x = (t,\vec{x})$ and $x' = (-t_s,\vec{x}')$ with $t_s > 0$. First consider $g = 0$. Since J^R commutes with J^L, equation (3.15) then reduces to $\langle\Psi_\beta|J^L|\Psi_\beta\rangle = 0$. For $g \neq 0$, at

small t, since $\mathcal{O}$ and J are generic few-body operators, whose degrees of freedom in general do not overlap, $[J(t), V] \approx 0$, which again leads to $\langle J^L(t)\rangle_g \approx 0$. As time increases, $J(t)$ grows and scrambles in the space of degrees of freedom. At sufficiently large t, $[J(t), V]$ becomes non-negligible; the time scale that this happens defines the scrambling scale t_*. Thus $\langle J^L(t)\rangle_g$ (thus also G^{LR}) can be non-negligible only when t is of the scrambling scale t_*.

Also due to the entanglement structure of (3.1), as manifested in (3.24), we expect W defined in (3.19) to be non-vanishing only when t_s and t are close. So t_s also has to be of order or larger than t_* for G^{LR} to be nonzero. Similarly for the full nonlinear expression (3.15).

When t, t_s are of order the scrambling scale, even at linear order in φ^R, the expression for $\langle J^L\rangle_g$ is complicated. We will study the behavior of W and G^{LR} in detail for various choices of V in subsequent sections in two-dimensional CFTs. Here we show that when $t, t_s \gg t_*$ the behavior of full nonlinear expression (3.15) is very simple .

For clarity we will illustrate the main argument using the linear expression (3.19). Consider expanding the exponential e^{igV} between J^L and J^R in power series of g, then at n-th order one gets correlation functions of the form

$$M_n = \langle \Psi_\beta | e^{-igV} J^L(t) (\mathcal{O}^L(0)\mathcal{O}^R(0))^n J^R(-t_s) | \Psi_\beta \rangle \tag{3.26}$$

where we have suppressed all the spatial dependence. Note that the precise form of V is not important and we have only schematically indicated that it has the form of some product of $\mathcal{O}^L\mathcal{O}^R$ inserted at $t = 0$. Now using repeatedly (3.23), we can write (3.26) as

$$M_n = \langle \Psi_\beta | e^{-igV} J^L(t) (\mathcal{O}^L(0))^n J^L(t_s + i\beta/2) (\mathcal{O}^L(i\beta/2))^n | \Psi_\beta \rangle \tag{3.27}$$

with J and $(\mathcal{O}^L)^n$ out-of-time-ordered.

Now for a general quantum chaotic system, due to scrambling, we expect

$$M_n \to 0, \qquad t, t_s \gg t_* \quad \text{for} \quad n \geq 1 \tag{3.28}$$

with t_* the scrambling time of the system. Thus for $t, t_s \gg t_*$, equation (3.19) should reduce to

$$W = \langle \Psi_\beta | e^{-igV} J^L(t, \vec{x}) J^R(-t_s, \vec{x}') | \Psi_\beta \rangle \ . \tag{3.29}$$

Notice that expanding the exponential e^{igV} in (3.29) in power series of V will now give rise to only time-ordered correlation functions (TOCs). On general grounds, one expects that

such TOCs to factorize at large time separations between J and $\mathcal{O}$ insertions, we then find[4]

$$W \approx \langle e^{-igV} \rangle \langle J^L(t,\vec{x}) J^R(-t_s,\vec{x}') \rangle \ . \tag{3.30}$$

From (3.18), (3.25) and the discussion below (3.24), we thus find that $G^{LR}(t,\vec{x};-t_s,\vec{x}')$ is nonzero only for $t \approx t_s$ and $\vec{x} \approx \vec{x}'$ with

$$G^{LR}(t_s,\vec{x};-t_s,\vec{x}) = C(g) = \text{const} \tag{3.31}$$

and

$$C(g) = -2G_J \, \text{Im} \langle e^{-igV} \rangle \ . \tag{3.32}$$

For φ^R slowly varying at the scales of τ_r, ℓ_r, we thus see (3.17) reduces to

$$\langle J^L(t_s,\vec{x}) \rangle_g \approx C(g) \, \varphi^R(-t_s,\vec{x}), \qquad t_s \gg t_* \ . \tag{3.33}$$

Note that generically we expect $\langle e^{-igV} \rangle$ to be complex and $O(1)$ as already mentioned the operator V is designed to couple $\mathcal{O}^{L,R}$ at entangled points.

It is interesting that the sole effect of turning on the interaction V between two subsystems is to generate a phase so that W is no longer real, resulting a nonzero G^{LR}. Through the entanglement structure of Ψ_β, information of the source φ^R is already present in the L system, just as in the usual EPR story. Heuristically, the effect of turning on V is to turn this information into "real" physical signals.

The above discussion can be immediately generalized to the full nonlinear expression (3.15). In fact for any few-body operator $X^L(t)$, setting all OTOCs to zero, we find in the limit $t \sim t_s \gg t_*$,

$$\langle X^L \rangle_g \equiv \langle \Phi | X^L(t) | \Phi \rangle = (1 - 2 \, \text{Re} \, a) \langle \Psi_\beta | X^L(t) | \Psi_\beta \rangle + \left(a \langle \Psi_\beta \left| X^L(t) U^R \right| \Psi_\beta \rangle + h.c. \right) \tag{3.34}$$

where $|\Phi\rangle$ is given by (3.16) and we have introduced

$$U^R = e^{i \int ds \, \varphi^R(s) J^R(s)}, \qquad a = \langle e^{-igV} \rangle_\beta - 1 \ . \tag{3.35}$$

See Appendix 3.B for a derivation of (3.34). For $X^L = J^L$, we then find

$$\langle J^L(t) \rangle_g \approx a \langle \Psi_\beta \left| J^L(t) U^R \right| \Psi_\beta \rangle + h.c. \ . \tag{3.36}$$

[4]The conclusion was obtained before in the large k limit of (3.5) for holographic systems using gravity calculation in [52].

Equation (3.36) again has the form of a complex factor times correlation functions in the thermal field double state (plus its hermitian conjugate).

To summarize, equation (3.33) and its full nonlinear version (3.36) can be understood as due to the following three key elements: (i) vanishing of OTOCs at large times due to scrambling; (ii) factorization of TOCs at large times; (iii) entanglement structure of Ψ_β. Note that the factorization assumption can in principle be weakened or dropped. One only needs that (3.29) is complex and not small at large times.

The discussion of this subsection does not apply to $t, t_s \sim t_*$ for which we will examine in two-dimensional CFTs in Sec. 3.4.

3.2.4 Quantum nature of the regenesis signal

In this section we show that the regenesis signal (3.33) is quantum in nature.[5] We do this by comparing (3.36) and the corresponding variance with those in a standard response setup.

For this purpose, let us first recall the standard response story,[6]

$$\tilde{J} \equiv \left\langle \Psi_\beta | U_L^\dagger J^L U_L | \Psi_\beta \right\rangle, \quad \delta\tilde{J} \equiv \left(\left\langle \Psi_\beta | U_L^\dagger (J^L - \tilde{J})^2 U_L | \Psi_\beta \right\rangle \right)^{\frac{1}{2}}, \tag{3.37}$$

where U_L is the unitary operation for turning on some source φ^L in the L-system. $\tilde{J}$ is the corresponding signal and $\delta\tilde{J}$ is the variance. Note that since both U_L and J^L belong to the L-system, (3.37) just reduce to thermal averages. In this context we will thus suppressed index L. We also denote the variance and fourth moment of J in the thermal state (recall $\langle J \rangle_\beta = 0$) as

$$J_2 = \sqrt{\langle J^2 \rangle_\beta}, \qquad J_4 = \left(\langle J^4 \rangle_\beta \right)^{\frac{1}{4}} . \tag{3.38}$$

To make the discussion explicit, let us imagine a lattice system of interacting spins. Suppose J is given by some operator at a single site, say σ_z, then clearly both $\tilde{J}$ and $\delta\tilde{J}$ are

[5] The content of this section is developed from discussions with Juan Maldacena, Douglas Stanford and Zhenbin Yang. The main conclusions have also been anticipated by them.

[6] In a field theory we assume J is suitably smeared such that both J and J^n are bounded operators with a finite norm

order $O(1)$, and one needs multiple measurements to detect the effects of U. One can make life easier by measuring the average polarization, say,

$$J = \frac{1}{N}\sum_i Z_i \tag{3.39}$$

and considering a source which acts on all spins

$$U = Pe^{i\sum_j \int ds\, \varphi^L(s) Z_j(s)} \tag{3.40}$$

where Z_i is σ_z at i-th site and N is the total number of sites. Putting (3.39)–(3.40) into (3.37), and assuming there is no long-range spin correlation, one then finds, in the thermodynamic limit $N \to \infty$, the following scalings

$$\tilde{J} \sim O(1), \qquad \delta\tilde{J} \sim N^{-\frac{1}{2}} \ . \tag{3.41}$$

The signal $\tilde{J}$ is then much larger than fluctuations $\delta\tilde{J}$, and thus it is enough to make one single measurement. In other words, the signal is macroscopic or "classical." Also note pure thermal fluctuations have the scaling

$$J_2 \sim N^{-\frac{1}{2}}, \qquad J_4 \sim N^{-\frac{1}{2}} \ . \tag{3.42}$$

Similar scaling behavior can also be obtained in a large N matrix-type theory (including two-dimensional CFTs in the large central charge limit). In this case take J to be a single-trace operator and $U \sim e^{iNJ\varphi}$. We then find scalings

$$\tilde{J} \sim O(N), \qquad \delta\tilde{J} \sim O(1), \qquad J_2, J_4 \sim O(1) \tag{3.43}$$

and thus the signal $\tilde{J}$ is again "classical."

Now coming back to (3.36), using the Cauchy-Schwarz inequality we find that

$$\bar{J}_g(t) \equiv \left\langle J^L(t)\right\rangle_g \leq 2|a|\ \left(\left\langle \Psi_\beta | J^L J^L | \Psi_\beta\right\rangle\right)^{\frac{1}{2}} = 2|a| J_2 \ . \tag{3.44}$$

In other words, up to an $O(1)$ constant $\left\langle J^L(t)\right\rangle_g$ is bounded from above by the variance of J in the thermal ensemble. Now consider the variance of J^L with $g \neq 0$. Using (3.34) with various choices of $X(t)$, we find

$$\begin{aligned}(\delta J_g)^2 &\equiv \left\langle (J^L(t) - \bar{J}_g(t))^2\right\rangle_g \\ &= (1 - 2\,\mathrm{Re}\, a) J_2^2 - \bar{J}_g^2 + b\end{aligned} \tag{3.45}$$

with

$$b \equiv a\langle \Psi_\beta \left| (J^L(t))^2 U^R \right| \Psi_\beta \rangle + h.c. \leq 2|a| J_4^2 \tag{3.46}$$

where we have again used Cauchy-Schwarz in the last step. Given that $\bar{J}_g \sim J_2$, and in general $J_4 \sim J_2$, all terms in (3.45) are of order J_2^2. We thus find that modulo miraculous cancellations $\delta J_g \sim \bar{J}_g$, i.e. the variance is always of the same of order as the signal regardless of the choice of J and U^R.

More explicitly, let us consider the three situations mentioned above for the standard response story. For J to be a spin operator at a single site, again all quantities are of order $O(1)$. For J^L of the form (3.39) with U^R of the form (3.40), then from (3.44) and (3.42) we find that

$$\bar{J}_g \sim J_2 \sim \delta J_g \sim N^{-\frac{1}{2}} \ . \tag{3.47}$$

In fact in this case considering the average polarization not only does not help to reduce the fluctuations, but also reduces the signal itself. One might as well just measure a single spin. Note that if one considers linear order in φ^R as in (3.18)–(3.19) one may conclude that $\bar{J}_g \sim O(1)$ instead of (3.47). This suggests that the linear response analysis for $\bar{J}_g$ could be potentially misleading in this regime.

Finally for J given by a single-trace operator in a large N matrix-type theory, the counterparts of (3.43) are

$$\bar{J}_g \sim \delta J_g \sim O(1) \tag{3.48}$$

with again reduced signal.

To summarize, the regenesis signal $\bar{J}_g$ in the L-system due to U^R and coupling V is intrinsically quantum in all situations!

3.2.5 Robustness of the regenesis phenomenon

Let us now consider the robustness of the regenesis phenomenon, i.e. how it fares against imperfections in the preparation of the initial state at the time $-t_s$ when we turn on the external field φ^R. For simplicity, we will restrict to our discussion to linear order in φ^R, i.e. (3.18)–(3.19). The arguments presented below generalize straightforwardly to full nonlinear level.

Here we consider two types of "small" perturbations. One type is that at $t = 0$ instead of $|\Psi_\beta\rangle$ we get

$$|\Psi(t=0)\rangle = |\Psi_\beta\rangle + \epsilon\, |\Phi\rangle \tag{3.49}$$

where ϵ is a small parameter. Physically this means that in preparation of the system at $t = -t_s$ to aim for $|\Psi_\beta\rangle$ at $t = 0$, the aiming is not perfect, but misses a bit. Such perturbations may result if at $-t_s$ in addition to φ^R there are some other "small" sources present (whose strengths are characterized by ϵ). With (3.49) in (3.19) instead of $|\Psi_\beta\rangle$, the corrections are clearly controlled by ϵ, and thus the qualitative conclusion above should not be modified.

Another possibility is that at $t = 0$ instead of $|\Psi_\beta\rangle$ we have

$$|\Psi(t=0)\rangle = \gamma^L(t_0, \vec{x}_0)\,|\Psi_\beta\rangle \tag{3.50}$$

with some t_0 for some few-body operator $\gamma(x)$ (suitably smeared so that (3.50) is normalizable). Heuristically, this describes a state obtained adding a "γ^L-particle" to the thermal field double at time t_0. One could consider similar states obtained by acting with some operator in the R-system, but from (3.22) that is equivalent to an operation in the L system with inverted time, so (3.50) covers all cases. Strictly speaking, (3.50) is not a small perturbation of $|\Psi_\beta\rangle$ as it is orthogonal to $|\Psi_\beta\rangle$ since a generic few-body operator γ will have negligible expectation value in $|\Psi_\beta\rangle$. There is, however, a physical sense that such perturbations are "small": at $t = t_0$, it is hard to tell the difference between (3.50) and $|\Psi_\beta\rangle$ by making measurements using generic few-body operators, such as J, as they generically commute with γ.

With (3.50), we should replace (3.19) by

$$W_\gamma \equiv \frac{\langle\Psi|\,\gamma^L(t_0)e^{-igV}J^L(t)e^{igV}J^R(-t_s)\gamma^L(t_0)\,|\Psi\rangle}{\langle\Psi|\,\gamma^L(t_0)\gamma^L(t_0)\,|\Psi\rangle} \tag{3.51}$$

where the spatial coordinates are suppressed. Consider first $g = 0$, then

$$\begin{aligned} W_\gamma(g=0) &= \frac{\langle\Psi|\,\gamma^L(t_0)J^L(t)J^R(-t_s)\gamma^L(t_0)\,|\Psi\rangle}{\langle\Psi|\,\gamma^L(t_0)\gamma^L(t_0)\,|\Psi\rangle} \\ &= \frac{\langle\Psi|\,\gamma^L(t_0)J^L(t)\gamma^L(t_0)J^L(t_s+i\beta/2)\,|\Psi\rangle}{\langle\Psi|\,\gamma^L(t_0)\gamma^L(t_0)\,|\Psi\rangle} \end{aligned} \tag{3.52}$$

which is an OTOC. Equation (3.52) is small whenever

$$|t - t_0| \gg t_* \quad \text{(destroy correlation of } J^L \text{ and } J^R\text{)} \tag{3.53}$$

in which case insertion of γ^L will destroy the correlation between points $(t, \vec{x})$ and $(-t_s, \vec{x})$ in $|\Psi_\beta\rangle$, and destroy regenesis even without worrying about possible effects of γ on the interaction between two subsystems. For example, for $t \sim t_s \sim t_*$, equation (3.53) means

any $t_0 \ll 0$ or $t_0 \gg 2t_*$. The latter can be more intuitively understood as insertion of γ^R of order t_* before we send the signal at time $-t_*$.

Now look at (3.51) with $g \neq 0$. Notice that the ordering between $\gamma^L(t_0)$ and any V insertions are also out-of-time-ordered. From the same argument we then expect the effects of V will be destroyed when

$$|t_0| \gg t_* \quad \text{(destroy the coupling between two systems)} \ . \tag{3.54}$$

Hence we expect regenesis is no longer present in (3.50) for $t_0 \gg t_*$ and $t_0 \ll 0$. See Fig. 3.4 for regions of insertion of γ which will destroy the regenesis phenomenon.

We will confirm the above qualitative expectations in Sec. 3.4.5 by explicit calculations in two-dimensional CFTs. Our conclusion is also qualitatively consistent with gravity expectations discussed in [52], which we will elaborate more in Sec. 3.5.

3.2.6 A contrast study: "regenesis" in a qubit model

Here we study the regenesis phenomenon a simple qubit model to help sharpen some essence aspects of the phenomenon in a quantum chaotic many-body system.

Consider a system consists of four qubits: $L_{1,2}$ and $R_{1,2}$, with the Hilbert space $\mathcal{H} = \mathcal{H}_L \otimes \mathcal{H}_R = \mathcal{H}_{L_1} \otimes \mathcal{H}_{L_2} \otimes \mathcal{H}_{R_1} \otimes \mathcal{H}_{R_2}$. We will write 2 by 2 identity matrix and Pauli matrices as $\sigma^\mu = \{I, X, Y, Z\}$. We take the Hamiltonian to be like an Ising model

$$H_0 = H^L + H^R, \quad H^L = \frac{\nu}{2}(Z_{L_1}Z_{L_2}) + \frac{\mu}{2}(Z_{L_1} + Z_{L_2}), \quad H^R = \frac{\nu}{2}(Z_{R_1}Z_{R_2}) + \frac{\mu}{2}(Z_{R_1} + Z_{R_2}) \ . \tag{3.55}$$

For simplicity we will consider the thermal field double (3.1) with $\beta = 0$, which is then giving by the following state of 2 EPR pairs

$$|\Psi\rangle = |EPR_1\rangle \otimes |EPR_2\rangle \, , \quad |EPR_i\rangle = \frac{1}{\sqrt{2}}(|0_{L_i}0_{R_i}\rangle + |1_{L_i}1_{R_i}\rangle) \tag{3.56}$$

as one can readily check that each component $|i_{L_1}j_{L_2}; i_{R_1}j_{R_2}\rangle$ $(i, j = 0, 1)$ in $|\Psi\rangle$ is an energy eigenstate.

A general hermitian J^L operator on L_1 site is $a_\mu\sigma^\mu$, where a_μ is a real vector. The corresponding operator J^R acting on R_1 is then (note $\beta = 0$)

$$J^R|\Psi\rangle = J^L|\Psi\rangle \quad \text{with} \quad J^R = a_0 I + a_1 X - a_2 Y + a_3 Z \tag{3.57}$$

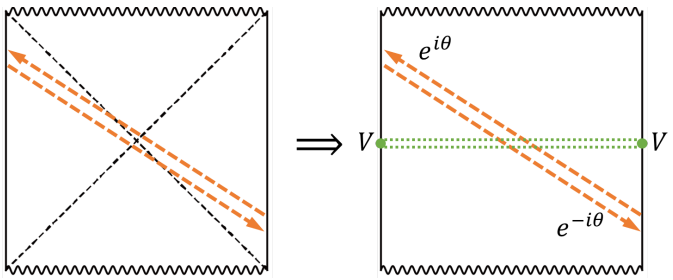

Figure 3.3: Left: in a wormhole described by (3.1), due to entanglement between the two boundaries, there are virtual particles which can propagate between them. The non-traversability can be understood as coming from perfect destructive interference between the process of a virtual particle traveling from R to L, and the mirror process of traveling from L to R. Right: turning on interaction V subtly changes the entanglement structure and gives a phase for each propagation. Now the destructive interference is no longer perfect, resulting propagations of "real" particles between the boundaries. Note that the interference is not a process between "future" and "past" as the related two boundaries are actually spacelike separated. It is possible to boost the frame such that it occurs on one spatial slice.

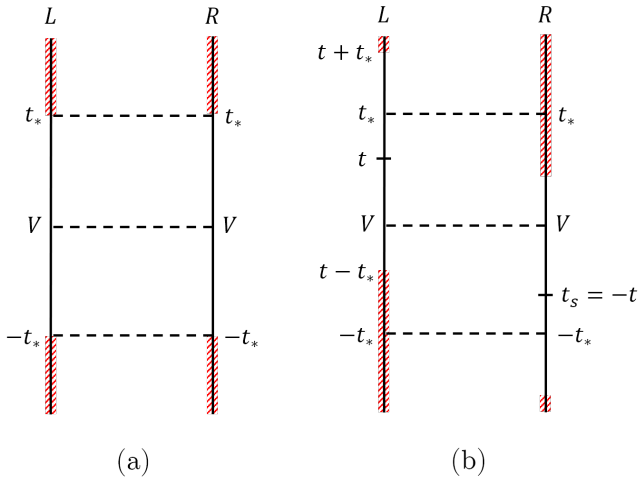

Figure 3.4: The regenesis phenomenon is destroyed by insertion of γ from either side when t_0 is in the red shaded regions. (a) shows the destruction by diminishing effective coupling when $|t_0| \gg t_*$, and (b) shows the destruction by diminishing $J^L J^R$ correlation when $|t - t_0| \gg t_*$.

We choose V to act on site L_2 and R_2, i.e. it commutes with J^L and J^R as they act on different sites, so as to model the situation described in the many-body context that V and J are generic few-body operators whose degrees of freedom do not overlap. We will take $\mathcal{O} = X$, and therefore

$$V = X_{L_2} X_{R_2} \ . \tag{3.58}$$

With $g = 0$, we have

$$\begin{aligned} \langle \Psi | \, J^R(-t) J^R(-t_s) \, | \Psi \rangle &= \langle \Psi | \, J^R(t) J^L(-t_s) \, | \Psi \rangle \\ &= a_0^2 + a_3^2 + (a_1^2 + a_2^2) \cos \nu (t - t_s) \cos \mu (t - t_s) \end{aligned} \tag{3.59}$$

which as expected is a function of only $t - t_s$. Since the above expression is real we have both $G^{RR} = G^{LR} = 0$. That even $G^{RR} = 0$ is an artifact of that we are considering a $\beta = 0$ state. G^{RR} is nonzero for other values of β. Now turn on V at $t = 0$, we the have

$$\begin{aligned} W &\equiv \langle \Psi | \, e^{-igV} J^L(t) e^{igV} J^R(-t_s) \, | \Psi \rangle \\ &= a_0^2 + a_3^2 + (a_1^2 + a_2^2) e^{-ig} \cos \mu (t - t_s) (\cos g \cos \nu (t - t_s) + i \sin g \cos \nu (t + t_s)) \end{aligned} \tag{3.60}$$

with

$$G^{LR}(t, -t_s) = i(W - W^*) = 2(a_1^2 + a_2^2) \sin(2g) \sin \nu t \sin \nu t_s \cos \mu (t - t_s) \ . \tag{3.61}$$

$G^{RR}(t, -t_s)$ is given by the same expression as above with $t - t_s$ replaced by $t + t_s$.

This simple example provides an interesting contrast which highlights some key elements of the regenesis phenomenon for a chaotic many-body system: (1) for a few-body system, there is no dissipation, and thus G^{RR} does not dissipate, i.e. even with φ^R turned off, the signal will remain in the R-system forever (turning on g only modifies the signal somewhat). (2) With $g \neq 0$, the signal also appears in the L-system. The effect of V is not regenesis, more like "double genesis." The reason is of course trivial: interactions among degrees of freedom within each subsystem will manage to communicate φ^R to the L-system through V. (3) The response in the L-system depends sensitively on time, choice of the specific operator J, the Hamiltonian $H^{L,R}$ of the subsystems, and choice of interaction V.

In other words, in a few-body system or an integrable many-body systems, some kind of signal in the L-system will be generated by turning on V. But it is not "regenesis," and the signal will depend on all the specifics of an individual system and the operators used. In contrast, in chaotic systems, the behavior is universal, independent of all the details.

3.2.7 A generalization: regenesis between spatially separated points

With the understanding of the entanglement structure, the set can be trivially generalized to be between any spatial points. Instead of Ψ_β we could use a one-side spatially shifted thermal field double state $e^{i\vec{P}\cdot\vec{a}}|\Psi_\beta\rangle$ where $\vec{P}$ is the spatial translation operator in either left or right system. Two choices are equivalent as $\vec{P}_L+\vec{P}_R$ is a symmetry of $|\Psi_\beta\rangle$, and for definiteness we take $\vec{P}=\vec{P}_R$. The entangled pair of points for the shifted state are $(t,\vec{x})$ and $(-t,\vec{x}-\vec{a})$, and the regenesis is now between them. We will also modify the interaction V between L and R accordingly, e.g. replacing (3.3) by

$$V_a=\mathcal{O}_L(0,\vec{0})\mathcal{O}_R(0,-\vec{a})\ . \tag{3.62}$$

The story is then exactly same as before, with equation (3.19) becoming

$$\begin{aligned}W_a(t,\vec{x};t',\vec{x}')&=\left\langle\Psi_\beta|e^{-i\vec{P}_R\cdot\vec{a}}e^{-igV_a}J^L(t,\vec{x})e^{igV_a}J^R(t',\vec{x}')e^{i\vec{P}_R\cdot\vec{a}}|\Psi_\beta\right\rangle\\&=\left\langle\Psi_\beta|e^{-igV}J^L(t,\vec{x})e^{igV}J^R(t',\vec{x}'+\vec{a})|\Psi_\beta\right\rangle=W(t,\vec{x};t',\vec{x}'+\vec{a})\end{aligned} \tag{3.63}$$

where we have used $e^{-i\vec{P}_R\cdot\vec{a}}V_a e^{i\vec{P}_R\cdot\vec{a}}=V$.

3.3 Explicit computations in large c CFTs

To calculate (3.15) explicitly for a general quantum many-body system is a difficult task. In [52] it was calculated at leading order in φ^R (i.e. (3.18)) for a $(0+1)$-dimensional holographic system by summing over scattering diagrams on gravity side. In this paper we will compute it in $(1+1)$-dimensional CFTs in the large central charge limit, again restricting to (3.18). This will enable us to obtain the behavior for J^L for $t,t_s\sim t_*$ which one could not access using general arguments of Sec. 3.2.

We will take $\mathcal{O}$ to be a scalar primary operator with conformal dimension $\Delta_\mathcal{O}=2h_\mathcal{O}$, and J to be a scalar operator with dimension $\Delta_J=2h_J$. Furthermore, for convenience of calculation we will consider the regime $O(1)\sim h_\mathcal{O}\ll h_J\ll c$. This regime is natural physically. We do not want the coupling V to change the UV behavior of the system, i.e. would like to take it to be a relevant operator, and thus $\Delta_\mathcal{O}\sim O(1)$. h_J should be much smaller than c as c is a measure of total number of degrees of freedom of a CFT. In our calculation we will neglect terms suppressed by $\frac{1}{c}$ and $\frac{h_\mathcal{O}}{c}$ while keeping all dependence

on h_J.[7] Here we will outline the main steps and results, leaving technical details to Appendix 3.C. Readers who are only interested in the final expressions can skip this section.

A remark on notation: below all x's refer to spatial coordinate in $(1+1)$-dimension, although earlier we have used it as a shorthand for spacetime coordinates.

3.3.1 Some useful expressions

Here we first mention some standard results on two-point functions in the state Ψ_β for a two-dimensional CFT, which we will use later. The Wightman function for two J's in the same subsystem is given by

$$\left\langle J^R(t_1,x_1)J^R(t_2,x_2)\right\rangle_\beta = \frac{C_J\left(\frac{2\pi}{\beta}\right)^{2\Delta_J}}{\left(2\cosh\left(\frac{2\pi x_{12}}{\beta}\right)-2\cosh\left(\frac{2\pi(t_{12}+i\epsilon_{12})}{\beta}\right)\right)^{\Delta_J}} \tag{3.64}$$

where $\epsilon_{12}<0$ assigns the ordering of two J^R operators and avoids singularity. The response function (3.12) is obtained from the imaginary part of (3.64). The two-point function of J's from different subsystems is given by

$$\begin{aligned}\left\langle\Psi_\beta|J^L(t_1,x_1)J^R(-t_2,x_2)|\Psi_\beta\right\rangle &= \left\langle J^L(t_1,x_1)J^L(t_2+i\beta/2,x_2)\right\rangle_\beta \\ &= \frac{C_J\left(\frac{2\pi}{\beta}\right)^{2\Delta_J}}{\left(2\cosh\left(\frac{2\pi x_{12}}{\beta}\right)+2\cosh\left(\frac{2\pi t_{12}}{\beta}\right)\right)^{\Delta_J}}\end{aligned} \tag{3.65}$$

where C_J is a constant and $x_{12}=x_1-x_2$. Note that in (3.64)–(3.65), the correlators decay exponentially for (t_2,x_2) lying outside the region $(t_1\pm\frac{\beta}{2\pi},x_1\pm\frac{\beta}{2\pi})$, as indicated earlier in (3.14) and (3.24). The form of (3.65) is a manifestation of the entanglement structure of (3.1) discussed in Sec. 3.2.2: the two systems are entangled in such a way that an operator inserted at point $(-t,x)$ in R system is highly correlated with the same operator inserted in a region of size $\frac{\beta}{2\pi}$ around (t,x) in L system.

Similarly we have

$$\left\langle\mathcal{O}(0,x_i)\,\mathcal{O}(0,x_j)\right\rangle_\beta = \frac{C_{\mathcal{O}}(2\pi/\beta)^{2\Delta_O}}{\left(2\cosh\frac{2\pi}{\beta}x_{ij}-2\right)^{\Delta_O}}, \tag{3.66}$$

[7] This is slightly more general than the regime discussed in [27], where the limit $h_J,c\to\infty$ with h_J/c fixed was considered. See Appendix 3.C.

$$\left\langle \Psi_\beta | \mathcal{O}^L(0,x_i)\,\mathcal{O}^R(0,x_j)\,|\Psi_\beta\right\rangle = \frac{C_{\mathcal{O}}(2\pi/\beta)^{2\Delta_O}}{\left(2\cosh\frac{2\pi}{\beta}x_{ij}+2\right)^{\Delta_O}}\ . \tag{3.67}$$

In our discussion below we will also use the following notations

$$\left\langle \Psi_\beta | \mathcal{O}^L(0)\,\mathcal{O}^R(0) | \Psi_\beta\right\rangle = C_{\mathcal{O}}\left(\frac{\pi}{\beta}\right)^{2\Delta_{\mathcal{O}}} \equiv G\ . \tag{3.68}$$

3.3.2 More elaborations on W

Equation (3.19) is the central object that we would like to calculate and analyze. Here we elaborate a bit further on its structure. We can expand it in an infinite series (for definiteness using (3.6) as an example)

$$W(t,x;-t_s,x_s) = \sum_{n=0}^{\infty}\frac{(-ig)^n}{L^n n!}\int_{-\frac{L}{2}}^{\frac{L}{2}}\left(\prod_{k=1}^{n}dx_k\right)W_n \tag{3.69}$$

with

$$W_n = \left\langle \Psi_\beta | [v_n,[v_{n-1},\cdots[v_1,J(t,x)]\cdots]J^R(-t_s,x_s)|\Psi_\beta\right\rangle, \tag{3.70}$$

$$v_i \equiv \mathcal{O}(0,x_i)\mathcal{O}^R(0,x_i) \equiv \mathcal{O}_i\mathcal{O}_i^R, \quad \mathcal{O}_i \equiv \mathcal{O}(0,x_i) \tag{3.71}$$

where we have suppressed superscripts L for operators in L system. More explicitly,

$$W_0 = \left\langle \Psi_\beta | J J^R | \Psi_\beta\right\rangle = \left\langle J\tilde{J}\right\rangle_\beta, \qquad W_1 = \left\langle \Psi_\beta | [\mathcal{O}_1,J]\mathcal{O}_1^R J^R|\Psi_\beta\right\rangle = \left\langle [\mathcal{O}_1,J]\tilde{J}\tilde{\mathcal{O}}_1\right\rangle_\beta, \tag{3.72}$$

$$W_2 = \left\langle \Psi_\beta | [\mathcal{O}_2,[\mathcal{O}_1,J]]\mathcal{O}_1^R\mathcal{O}_2^R J^R|\Psi_\beta\right\rangle = \left\langle [\mathcal{O}_2,[\mathcal{O}_1,J]]\tilde{J}\tilde{\mathcal{O}}_2\tilde{\mathcal{O}}_1\right\rangle_\beta \tag{3.73}$$

$$W_n = \left\langle [\mathcal{O}_n,[\mathcal{O}_{n-1},\cdots[\mathcal{O}_1,J]\cdots]\ \tilde{J}\tilde{\mathcal{O}}_n\cdots\tilde{\mathcal{O}}_1\right\rangle_\beta \tag{3.74}$$

where we have used (3.23) repeatedly and introduced short-hand notations

$$J \equiv J(t,x), \qquad \mathcal{O}_i \equiv \mathcal{O}(0,x_i), \qquad \tilde{\mathcal{O}}_i \equiv \mathcal{O}(i\beta/2,x_i), \qquad \tilde{J} \equiv J(t_s+i\beta/2,x_s)\ . \tag{3.75}$$

Note that all $\tilde{\mathcal{O}}$'s commute with one another.

3.3.3 Evaluating W: part I

We will proceed by first evaluating (3.74) and then performing the sum (3.69). The thermal correlation functions (3.74) are in turn obtained by analytic continuation from those in the

Euclidean signature. Let us first describe how to compute a multiple-point function of the form

$$w_n = \langle J(t_a, x_a) J(t_b, x_b) \mathcal{O}(t_1, x_1) \cdots \mathcal{O}(t_{2n}, x_{2n}) \rangle_\beta \tag{3.76}$$

in the Euclidean signature, i.e. with all the $t = -i\tau$ understood as being pure imaginary. Following the standard procedure, we first perform a conformal transformation

$$z = e^{\frac{2\pi}{\beta}(x+t)}, \qquad \bar{z} = e^{\frac{2\pi}{\beta}(x-t)} \tag{3.77}$$

to map the cylinder (τ, x) (τ is periodic in β) to the full complex z plane. Note that for pure imaginary t, $z, \bar{z}$ are complex conjugates of each other, but are independent variables for general complex t. The calculation of (3.76) on the z-plane is still nontrivial. Fortunately, in the regime $h_\mathcal{O} \ll h_J \ll c$, one could do it by applying techniques developed recently in [27].

For example, at the level of 4-point function we find that

$$\frac{\langle J_a J_b \mathcal{O}_1 \mathcal{O}_2 \rangle}{\langle J_a J_b \rangle \langle \mathcal{O}_1 \mathcal{O}_2 \rangle} = \mathcal{V}(u)\mathcal{V}(\bar{u}) + O(1/c, h_\mathcal{O}/c) \tag{3.78}$$

where for notational simplicity we have used the subscripts to denote the positions of operators, and ($\bar{u}$ is defined as u with z's replaced by $\bar{z}$'s)

$$\mathcal{V}(u) = \left(\frac{\alpha^2 u^2 (1-u)^{\alpha-1}}{(1-(1-u)^\alpha)^2} \right)^{h_\mathcal{O}}, \quad u = \frac{z_{12} z_{ab}}{z_{1a} z_{2b}}, \quad z_{12} = z_1 - z_2, \tag{3.79}$$

$$\alpha = \sqrt{1 - \frac{24 h_J}{c}} \, . \tag{3.80}$$

More generally, for (3.76) we have

$$\frac{\langle J_a J_b \mathcal{O}_1 \cdots \mathcal{O}_{2n} \rangle}{\langle J_a J_b \rangle} = \sum_{\text{all pairings}} \prod_{i=1}^{n} \left[\mathcal{V}(u_i) \mathcal{V}(\bar{u}_i) \langle \mathcal{O}_{i1} \mathcal{O}_{i2} \rangle \right] + O(1/c, h_\mathcal{O}/c), \quad u_i \equiv \frac{z_{i1,i2} z_{ab}}{z_{i1,a} z_{i2,b}} \tag{3.81}$$

where the sum is over all possible pairings of $\mathcal{O}$'s with $(\mathcal{O}_{i1}, \mathcal{O}_{i2})$ denoting the i-th pair. See Appendix 3.C for details.

We now analytically continue the above expressions to Lorentzian signature to obtain (3.74). Correlation function of Lorentzian operators with a specific ordering can be obtained from continuation of the corresponding Euclidean correlation function by assigning appropriate $i\epsilon$'s [70]. For example,

$$\langle \mathcal{O}(t_1) \cdots \mathcal{O}(t_n) \rangle = \lim_{\{\epsilon_j\} \to 0} \langle \mathcal{O}(t_1 + i\epsilon_1) \cdots \mathcal{O}(t_n + i\epsilon_n) \rangle, \quad \epsilon_1 < \cdots < \epsilon_n \tag{3.82}$$

where the left hand side denotes Lorentzian correlation function of a specified order, while the right hand side denotes Euclidean correlation function with the time argument $t = -i\tau_i$ for each operator replaced by $t = t_i + i\epsilon_i$, and ϵ_i ordered as indicated. This $i\epsilon$-prescription instructs how one continues through possible branch cuts encountered when analytically continuing from imaginary to real times.

Therefore for each term in (3.72)–(3.74) we just need to continue (3.81) by assigning different orderings of ϵ_i's. For example, from (3.78), we find that (recall (3.75))

$$W_1 = \left\langle \mathcal{O}_1 J \tilde{J} \tilde{\mathcal{O}}_1 \right\rangle - \left\langle J \mathcal{O}_1 \tilde{J} \tilde{\mathcal{O}}_1 \right\rangle = G\Big\langle J\tilde{J}\Big\rangle A(u_1, \bar{u}_1) \tag{3.83}$$

where we have used (3.68) and

$$A(u_1, \bar{u}_1) = \mathcal{V}^+(u_1)\mathcal{V}^+(\bar{u}_1) - \mathcal{V}^-(u_1)\mathcal{V}^-(\bar{u}_1), \tag{3.84}$$

with

$$\begin{aligned} u_1 &= \frac{e^{\frac{2\pi}{\beta}x_1}(e^{i\epsilon_1} + e^{i\tilde{\epsilon}_1})(e^{\frac{2\pi}{\beta}(x+t)+i\epsilon_J} + e^{\frac{2\pi}{\beta}(x_s+t_s)+i\tilde{\epsilon}_J})}{(e^{\frac{2\pi}{\beta}x_1+i\epsilon_1} - e^{\frac{2\pi}{\beta}(x+t)+i\epsilon_J})(e^{\frac{2\pi}{\beta}(x_s+t_s)+i\tilde{\epsilon}_J} - e^{\frac{2\pi}{\beta}x_1+i\tilde{\epsilon}_1})}, \\ \bar{u}_1 &= \frac{e^{\frac{2\pi}{\beta}x_1}(e^{-i\epsilon_1} + e^{-i\tilde{\epsilon}_1})(e^{\frac{2\pi}{\beta}(x-t)-i\epsilon_J} + e^{\frac{2\pi}{\beta}(x_s-t_s)-i\tilde{\epsilon}_J})}{(e^{\frac{2\pi}{\beta}x_1-i\epsilon_1} - e^{\frac{2\pi}{\beta}(x-t)-i\epsilon_J})(e^{\frac{2\pi}{\beta}(x_s-t_s)-i\tilde{\epsilon}_J} - e^{\frac{2\pi}{\beta}x_1-i\tilde{\epsilon}_1})} . \end{aligned} \tag{3.85}$$

In (3.84) $\mathcal{V}^+$ denotes (3.79) with ordering $\epsilon_1 < \epsilon_J < \tilde{\epsilon}_J < \tilde{\epsilon}_1$, while $\mathcal{V}^-$ denotes (3.79) with ordering $\epsilon_J < \epsilon_1 < \tilde{\epsilon}_J < \tilde{\epsilon}_1$.

For simplicity we will take $t_s = t$ and $x_s = x$, which as discussed earlier is the most relevant case. By tracking the motions of $u_1, \bar{u}_1$ as one varies t, we can write $A(u_1, \bar{u}_1)$ more explicitly as

$$A(u_1, \bar{u}_1) = (\mathcal{V}_1(u_1) - \mathcal{V}_2(u_1))\mathcal{V}_1(\bar{u}_1) \tag{3.86}$$

where $\mathcal{V}_1(u)$ and $\mathcal{V}_2(u)$ denote respectively the values of (3.79) along the negative real axis on its first and second sheet ($\mathcal{V}(u)$ has a branch cut along $(1, +\infty)$)

$$\mathcal{V}_1(u) = \left(\frac{\alpha(-u)}{\sqrt{1-u}} \frac{1}{-(1-u)^{-\alpha/2} + (1-u)^{\alpha/2}}\right)^{2h_\mathcal{O}}, \tag{3.87}$$

$$\mathcal{V}_2(u) = \left(\frac{\alpha(-u)}{\sqrt{1-u}} \frac{1}{(1-u)^{-\alpha/2}e^{i\pi\alpha} - (1-u)^{\alpha/2}e^{-i\pi\alpha}}\right)^{2h_\mathcal{O}} \tag{3.88}$$

and for convenience we have slightly redefined $u_1, \bar{u}_1$ as

$$u_1 \equiv -\frac{4e^{\frac{2\pi}{\beta}(t-|x-x_1|)}}{(1-e^{\frac{2\pi}{\beta}(t-|x-x_1|)})^2}, \qquad \bar{u}_1 \equiv -\frac{4e^{\frac{2\pi}{\beta}(t+|x-x_1|)}}{(1-e^{\frac{2\pi}{\beta}(t+|x-x_1|)})^2} . \tag{3.89}$$

The explicit evaluation of (3.86) is given in Appendix 3.C.3.

3.3.4 Evaluating W: part II

For general W_n, let us first look at the case of V given by (3.5), for which

$$W_n = \frac{1}{k^n}\left(\prod_{i=1}^{n}\sum_{\alpha_i=1}^{k}\right)\left\langle [\mathcal{O}_{\alpha_n},[\mathcal{O}_{\alpha_{n-1}},\cdots[\mathcal{O}_{\alpha_1},J]\cdots]\ \tilde{J}\tilde{\mathcal{O}}_{\alpha_1}\cdots\tilde{\mathcal{O}}_{\alpha_n}\right\rangle \tag{3.90}$$

where subscripts denote different types of operators all inserted at $t,x=0$. Applying (3.81) to a term obtained by expanding commutators in (3.90), we see that there are two types of contractions among $\mathcal{O}$'s: two-sided contractions between a $\mathcal{O}_{\alpha_i}$ and a $\tilde{\mathcal{O}}_{\alpha_j}$ which are given by $\left\langle \mathcal{O}_{\alpha_i}\tilde{\mathcal{O}}_{\alpha_j}\right\rangle_\beta = G\delta_{\alpha_i\alpha_j}$ (recall (3.68)), and same-sided contractions between $\mathcal{O}$'s (or between $\tilde{\mathcal{O}}$'s) which are in fact divergent. We will assume that $\mathcal{O}$ and $\tilde{\mathcal{O}}$ are smeared such that same-sided contractions are finite. The two-sided contractions can be further separated into contractions among operators in the same sums or different sums. Note there is an enhancement factor k if in a sum each $\mathcal{O}_{\alpha_i}$ is contracted with the corresponding $\tilde{\mathcal{O}}_{\alpha_i}$ from the same sum [52]. Thus in the large k limit, this type of contractions will dominate over all others, including same-sided contractions. Also note that for various terms obtained by expanding commutators of (3.90) only orderings between $\mathcal{O}$ and J matter (all the $\mathcal{O}$ and $\tilde{\mathcal{O}}$ commute with one another). We then conclude that to leading order in large k

$$W_n = G^n A_0^n\left\langle J\tilde{J}\right\rangle + O(1/k) \quad \rightarrow \quad W = \left\langle J\tilde{J}\right\rangle e^{-igGA_0} + O(1/k) \tag{3.91}$$

where $A_0 \equiv A(u_0,\bar{u}_0)$ with $u_0,\bar{u}_0$ obtained by setting $x_1=0$ in $u_1,\bar{u}_1$.

At finite k, which includes (3.3) as a special case with $k=1$, one has to keep track of all other contractions, which is very complicated. The detailed derivations are given in Appendix 3.D. The final result can be written in a form

$$W = \left\langle J\tilde{J}\right\rangle\left(1+\frac{igG(A_0+\eta B_0)}{k}\right)^{-k/2}\left(1+\frac{igG(A_0-\eta B_0)}{k}\right)^{-k/2} \tag{3.92}$$

where $\eta = H/G$ and H is defined as $\langle \mathcal{O}_{\alpha_i}\mathcal{O}_{\alpha_j}\rangle = \left\langle \tilde{\mathcal{O}}_{\alpha_i}\tilde{\mathcal{O}}_{\alpha_j}\right\rangle = H\delta_{\alpha_i\alpha_j}$.[8] In (3.92) B_0 is given by

$$B_0^2 = [(\mathcal{V}_1(\mu_0)-\mathcal{V}_{-1}(\mu_0))\mathcal{V}_1(\bar{\mu}_0)+(\mathcal{V}_1(-\mu_0)-\mathcal{V}_2(-\mu_0))\mathcal{V}_1(-\bar{\mu}_0)]\,\mathcal{V}_1(\mu_0)\mathcal{V}_1(\bar{\mu}_0) \tag{3.93}$$

[8] We are assuming that the smearing is such that same-sided contractions of $\mathcal{O}$ and $\tilde{\mathcal{O}}$ are the same. There is no qualitative change if one takes them to be different.

where $\mathcal{V}_1, \mathcal{V}_2$ were given before in (3.87)–(3.88), $\mathcal{V}_{-1}$ is the corresponding value on -1 sheet, given by

$$\mathcal{V}_{-1}(u) = \left(\frac{\alpha(-u)}{\sqrt{1-u}} \frac{1}{(1-u)^{-\alpha/2} e^{-i\pi\alpha} - (1-u)^{\alpha/2} e^{i\pi\alpha}} \right)^{2h_{\mathcal{O}}} . \tag{3.94}$$

In (3.93), the arguments of $\mathcal{V}$-functions are defined as

$$\mu_0 = \frac{2i \sin\frac{\pi\epsilon}{\beta}}{\sinh\frac{2\pi}{\beta}(t-|x|) + 2i\sin\frac{\pi\epsilon}{\beta}}, \quad \bar{\mu}_0 = \frac{2i \sin\frac{\pi\epsilon}{\beta}}{\sinh\frac{2\pi}{\beta}(t+|x|) + 2i\sin\frac{\pi\epsilon}{\beta}}, \tag{3.95}$$

where $0 < \epsilon < \beta$ is a regulator which makes same-sided contractions finite. A couple of further comments on (3.92). In the limit $\eta \to \infty$, W becomes real and thus G^{LR} is zero in that limit. In large k limit, B_0 terms cancel out in the exponential and recovers (3.91).

Now finally consider (3.6), which we will take L to be much larger than β.[9] The discussion here is similar to the large k story described above, with the sums over indices α replaced by integrations over x. The counterpart of k is $\frac{L}{\beta}$. In the large $\frac{L}{\beta}$ limit we will need to include contractions between $\mathcal{O}_i$ and $\tilde{\mathcal{O}}_i$ which belong to the same integral. Parallel discussion as (3.91) then leads to leading order in $\frac{\beta}{L}$

$$W = \left\langle J\tilde{J} \right\rangle \exp\left(-\frac{igG}{L} \int_{-L/2}^{L/2} dx_1 \, A(u_1, \bar{u}_1) \right) . \tag{3.96}$$

3.4 Analysis of the results

In this section we analyze the expression for W obtained in last section. The main expressions are (3.91) for (3.5) in the large k limit, (3.92) for (3.5) at any finite k, which includes (3.3) as a special case ($k = 1$), and (3.96) for (3.6) in the limit $L \gg \beta$. $A(u_1, \bar{u}_1)$ in those expressions are given by (3.86)–(3.89) with α given by (3.80), and A_0 is obtained from $A(u_1, \bar{u}_1)$ by setting $x_1 = 0$. B_0 is given by (3.93).

3.4.1 General remarks

We first note that in all cases (i.e. (3.91), (3.92) and (3.96)) W is proportional to

$$\left\langle J\tilde{J} \right\rangle_\beta = \langle \Psi_\beta | J^L(t,x) J^R(-t_s, x_s) | \Psi_\beta \rangle \tag{3.97}$$

[9] For L comparable or smaller than β, it is not that different from (3.3).

which from (3.65) is supported for $|t-t_s| \lesssim \frac{\beta}{2\pi}$ and $|x-x_s| \lesssim \frac{\beta}{2\pi}$. As commented earlier that the form of (3.65) is in turn determined by the entanglement structure of thermal field double state $|\Psi_\beta\rangle$. Thus possible spacetime points (t,x) to which one could send signal from $(-t_s,x_s)$ is determined by the entanglement structure with $\frac{\beta}{2\pi}$ characterizing the size of the window for possible nonzero signal. Now consider (3.17) which we copy here for convenience,

$$\left\langle J^L(t,x)\right\rangle_\varphi = \int dt_s dx_s\, G^{LR}(t,x;-t_s,x_s)\varphi^R(-t_s,x_s)\ . \tag{3.98}$$

Since $G^{LR}(t,x;t_s,x_s) \propto \mathrm{Im}W$ falls off rapidly outside the window $|t-t_s| \lesssim \frac{\beta}{2\pi}$ and $|x-x_s| \lesssim \frac{\beta}{2\pi}$, for sources $\varphi^R(t,x)$ which are slowly varying in spacetime at the scale of $\frac{\beta}{2\pi}$ we can approximate (3.98) as

$$\left\langle J^L(t,x)\right\rangle_\varphi \approx \bar{G}^{LR}(t,x;-t,x)\varphi^R(-t,x) \tag{3.99}$$

where $\bar{G}^{LR}(t,x;-t,x)$ is obtained by averaging $G^{LR}(t,x;-t_s,x_s)$ in (t_s,x_s) over the region defined by $|t-t_s| \lesssim \frac{\beta}{2\pi}$ and $|x-x_s| \lesssim \frac{\beta}{2\pi}$. Below without loss of qualitative features, instead of considering the averaged $\bar{G}^{LR}(t,x;-t,x)$, we will simply examine the behavior of $G^{LR}(t,x;-t_s,x_s)$ for $t_s=t$ and $x_s=x$. In this case we then have

$$\left\langle J\tilde{J}\right\rangle_\beta = C_J\left(\frac{\pi}{\beta}\right)^{2\Delta_J} \equiv G_J\ . \tag{3.100}$$

One interesting feature of (3.99) is that signals which are sent earlier in the R systems appear later in the L system, which is of course a direct consequence of the entanglement structure discussed in Sec. 3.2.2.

Also notice that in (3.91), (3.92) and (3.96), the coupling g always comes with G, which is the (maximal) correlation between $\mathcal{O}^L$ and $\mathcal{O}^R$ as following from (3.67). This is due to interactions (3.3), (3.5)–(3.6) are between $\mathcal{O}^L$ and $\mathcal{O}^R$ inserted at entangled spacetime points. Were we to couple $\mathcal{O}^L$ and $\mathcal{O}^R$ at general spatial locations or times, then one effectively diminishes the value of G, and weakens the effects of V. Below we will use

$$g_{\text{eff}} \equiv gG \tag{3.101}$$

which may be interpreted as the effective coupling between two systems.

For notational simplicity we will write $G^{LR}(t,x;-t,x)$ as $G^{LR}(t,x)$, and then from (3.18) we find for (3.91)

$$G^{LR}(t,x) = 2G_J e^{g_{\text{eff}}\,\mathrm{ImA}_0}\sin\left(g_{\text{eff}}\,\mathrm{ReA}_0\right) \tag{3.102}$$

and for (3.96)

$$G^{LR}(t,x) = 2G_J e^{g_{\text{eff}}\,\text{Im}\mathcal{A}} \sin\left(g_{\text{eff}}\,\text{Re}\mathcal{A}\right) \tag{3.103}$$

with

$$\mathcal{A} \equiv \frac{1}{L}\int_{-\frac{L}{2}}^{\frac{L}{2}} dx_1\, A(u_1,\bar{u}_1)\ . \tag{3.104}$$

The expression of G^{LR} for (3.3) can be straightforward obtained by taking the imaginary part of (3.92) with $k=1$, but the formal expression is not very illuminating, so we will not write it explicitly.

Now recall that A is the normalized four-point function

$$A(u_1,\bar{u}_1) = \frac{\langle[\mathcal{O}(0,x_1),J(t,x)]J(t+i\beta/2,x)\mathcal{O}(i\beta/2,x_1)\rangle_\beta}{\langle\mathcal{O}(0,x_1)\mathcal{O}(i\beta/2,x_1)\rangle_\beta\langle J(t,x)J(t+i\beta/2,x)\rangle_\beta} \tag{3.105}$$

with A_0 are given by setting x_1 to zero. The commutator upstairs is the difference between $\left\langle \mathcal{O}J\tilde{J}\tilde{O}\right\rangle_\beta$ and $\left\langle J\mathcal{O}\tilde{J}\tilde{O}\right\rangle_\beta$, with the latter one being an OTOC. It has been known from previous discussion in [64] that as $t\to\infty$ the OTOC $\left\langle J\mathcal{O}\tilde{J}\tilde{O}\right\rangle_\beta$ goes to zero, while $\left\langle \mathcal{O}J\tilde{J}\tilde{O}\right\rangle_\beta$ factorizes into $\left\langle \mathcal{O}\tilde{\mathcal{O}}\right\rangle_\beta\left\langle J\tilde{J}\right\rangle_\beta$ and thus

$$A\to 1,\quad t\to\infty \tag{3.106}$$

which can also be checked explicitly from (3.86).[10] We then find that G^{LR} goes a constant, e.g. for (3.102)–(3.103)

$$G^{LR}(t\to\infty,x) = 2G_J\sin g_{\text{eff}}\ . \tag{3.107}$$

Similarly for (3.92) we find as $t\to\infty$, $B_0\to\sqrt{2}$, and thus

$$W(t\to\infty,x) = G_J\left(1+\frac{ig_{\text{eff}}(1+\sqrt{2}\eta)}{k}\right)^{-\frac{k}{2}}\left(1+\frac{ig_{\text{eff}}(1-\sqrt{2}\eta)}{k}\right)^{-\frac{k}{2}}\ . \tag{3.108}$$

Note that while (3.107) is oscillatory in g_{eff} with period 2π, for $k=1$ it is not, and goes to zero as g_{eff}^{-1} for large g_{eff}.

From (3.99) we then find that in all cases

$$\left\langle J^L(t,x)\right\rangle_\varphi \approx C(g)\,\varphi^R(-t,x),\qquad t\to\infty\ , \tag{3.109}$$

[10] Note as $t\to\infty$, $u_1,\bar{u}_1\to 0$ and we find $\mathcal{V}_1(u)\to 1, \mathcal{V}_2(u)\to 0$.

with $C(g)$ a constant, which is consistent with (3.31)–(3.32) deduced on general ground.

We will now proceed to understand the behavior of G^{LR} at general times in more detail.

3.4.2 A scaling limit

Based on general discussion of Sec. 3.2 we expect the nontrivial behavior of G^{LR} to arise when t becomes of order of the scrambling time t_* which for a CFT at large c is proportional to $\log c$ [64]. Since in general we do not expect $x - x_1$ to scale with c, thus for values of t of interest we should have $t \gg |x - x_1|$ for which

$$u_1 \approx -4e^{\frac{2\pi}{\beta}(-t+|x-x_1|)} \ll 1, \qquad \bar{u}_1 \approx -4e^{-\frac{2\pi}{\beta}(t+|x-x_1|)} \ll 1 \ . \tag{3.110}$$

Denoting $\mathcal{V}_{1,2}(u) = U_{1,2}(u)^{2h_\mathcal{O}}$ and expanding in small u we find from (3.87)

$$U_1(u) = 1 + O(u^2) \ . \tag{3.111}$$

We are interested in $h_J \ll c$, i.e. $\alpha \approx 1$. It can be readily checked all the coefficients of higher powers of u in U_1 going to zero as $\alpha \to 1$ ($U_1 = 1$ for $\alpha = 1$). Expanding for small $u_1 < 0$ in U_2 we find from (3.88) that

$$U_2(u_1) = \frac{\alpha|u_1|}{2i\sin\pi\alpha} - \frac{\alpha|u_1|^2(-i + \alpha\cot\pi\alpha)}{4\sin\pi\alpha} + \cdots \ . \tag{3.112}$$

Now we notice that as $\alpha \to 1$, each coefficient becomes singular. There is a scaling regime

$$u_1 \to 0, \qquad \alpha \to 1, \qquad Q \equiv \frac{2\pi(1-\alpha)}{|u_1|} = \text{finite} \tag{3.113}$$

in which one can resum the whole series (3.112)

$$U_2(u_1) = \frac{1}{1+iQ} + O(1/c) \tag{3.114}$$

Q can be written more explicitly as

$$Q = \frac{6\pi h_J}{c}\exp\left(\frac{2\pi}{\beta}(t - |x-x_1|)\right) \equiv \exp\left(\frac{2\pi}{\beta}(\mathfrak{t} - |x-x_1|)\right) \tag{3.115}$$

where we have introduced

$$\mathfrak{t} \equiv t + t_J - t_* \qquad t_* \equiv \frac{\beta}{2\pi}\log\frac{c}{6\pi}, \qquad t_J \equiv \frac{\beta}{2\pi}\log h_J \ . \tag{3.116}$$

We then find

$$A(u_1, \bar{u}_1) = 1 - \left(\frac{1}{1+iQ}\right)^{2h_{\mathcal{O}}} + O(1/c) \ . \tag{3.117}$$

Similarly, in the scaling limit, from (3.93) we find B_0 can be written as

$$B_0^2 = 2\left[1 - \left(1 + \frac{1}{\sin\frac{\pi\epsilon}{\beta}} Q_0\right)^{-2h_{\mathcal{O}}}\right](1 + O(1/c)) \,, \quad Q_0 \equiv Q(x_1 = 0) \ . \tag{3.118}$$

Note that in contrast to $A(u_1, \bar{u}_1)$ and A_0, B_0 is always real.

In the large c limit, $t_* \gg t_J, |x - x_1|$, the scaling limit helps us to focus on the time scale $t \sim t_*$ during which Q is $O(1)$ (in terms of large c scaling) and the commutator (3.105) between generic few-body operators $\mathcal{O}$ and J becomes sizable. This defines t_* as the scrambling time.

Note that it is curious that at leading order in (3.117)–(3.118) the only dependence on h_J is through a time shift t_J.

3.4.3 Three regimes of G^{LR}

Let us now look at the behavior of G^{LR} more closely, using (3.102) for (3.5) as the main example, and will comment on the differences at finite k. Equation (3.103) for (3.6) will be discussed in next subsection.

At leading order in $1/c$, A has simple dependence on Q which in turn is given by a simple exponential. So the behavior of (3.102) is straightforward to obtain. One immediate thing to notice is that G^{LR} is a function of $t - |x|$ only. From (3.99), points with the same $t - |x|$ then get multiplied by the same factor in going from source to signal. The behavior of A and G^{LR} can be separated into three distinct regimes:

1. Sub-scrambling regime: for $t - |x| \ll t_* - t_J$ (i.e. $\mathfrak{t} - |x|$ large and negative) we have $Q \ll 1$ and[11]

$$A_0 = h_{\mathcal{O}}\left(2i + \frac{24\pi h_J}{c}\left(1 + \frac{i}{\pi}\right)\right) e^{\frac{2\pi}{\beta}(\mathfrak{t}-|x|)} + h_{\mathcal{O}}(1 + 2h_{\mathcal{O}}) e^{\frac{4\pi}{\beta}(\mathfrak{t}-|x|)} + \cdots \tag{3.119}$$

[11]Note that the first term is not pure imaginary when including h_J/c corrections.

and

$$G^{LR} = 2G_J g_{\text{eff}} h_{\mathcal{O}} \left(\frac{24\pi h_J}{c} e^{\frac{2\pi}{\beta}(\mathfrak{t}-|x|)} + (1+2h_{\mathcal{O}}) e^{\frac{4\pi}{\beta}(\mathfrak{t}-|x|)} \right) + \cdots \ . \tag{3.120}$$

Note that (3.119) is exponentially increasing with time with Lyapunov exponent $\frac{2\pi}{\beta}$ and butterfly velocity $v_B = 1$ [64], but the leading behavior is pure imaginary and does not contribute to G^{LR}. In this regime, the signal one sent in at time $-t$ just started getting scrambled before we set up the communication channel V at time 0. The signal is very weak in this regime and can be considered as being approximately zero for practical purpose. G^{LR} for a finite k has very similar behavior.

2. Transition regime: for a narrow window of size $\frac{\beta}{2\pi}$ around $t - |x| = t_* - t_J$, both real and imaginary parts of A_0 are $O(1)$, and G^{LR} also becomes $O(1)$. In this window, the exponential factor $e^{g_{\text{eff}} \text{Im} A_0}$ in (3.102) can enhance the magnitude of G^{LR} significantly when g_{eff} has the right sign and not too small. Note as can be explicitly checked from the expression of A_0 (see Fig. 3.5(a) for an example), for $\Delta_{\mathcal{O}} \sim O(1)$, $\text{Im} A_0$ is always positive and smaller than 1.[12] Thus enhancement requires g_{eff} to be positive. See Fig. 3.5(b) for some examples.

   In contrast, at a finite k including the case for (3.3), from the imaginary part of (3.92) we find there is no enhancement in the transition region for generic values of regulation parameter $\epsilon \sim O(\beta)$. See Fig. 3.5(c) for some examples.

   One may understand the exponential enhancement in the large k limit as coming from constructive interference of different channels.

3. Stable regime: as we further increase t beyond the transition regime, i.e. for $t - |x| \gg t_* - t_J$ ($\mathfrak{t} - |x|$ large and positive), Q quickly grows to be $Q \gg 1$, for which A_0 approaches to 1 exponentially (quasi-normal behavior)

$$A_0 = 1 - e^{-ih_{\mathcal{O}}\pi} e^{-\frac{4\pi h_{\mathcal{O}}}{\beta}(\mathfrak{t}-|x|)} + \cdots \tag{3.121}$$

   and for G^{LR} we have

$$G^{LR}(t,x) = G^{LR}(t=\infty) + O(e^{-\frac{4\pi h_{\mathcal{O}}}{\beta}(\mathfrak{t}-|x|)}) \ . \tag{3.122}$$

To conclude this subsection we should emphasize that the regimes described above are not evolutions; they correspond to different types of behavior when we vary the time separation between the time of turning on the source and the time we turn on interaction V between L and R systems.

[12] From (3.117), $\text{Im}\, A_0$ is proportional to $\sin(2h_{\mathcal{O}} \arctan Q)$. Since the value of Q ranges between 0 and ∞, $\text{Im}\, A_0$ is always positive for $h_{\mathcal{O}} < 1$. For any relevant V, $h_{\mathcal{O}}$ is within this range.

3.4.4 Multiple channel from integration

Let us now examine the behavior of (3.103)–(3.104). We will consider $t_* \gg L \gg \beta$ as for $L \lesssim \beta$ the story is essentially the same as that of single-channel. There are some new elements in (3.103) compared with (3.102). Firstly due to the integration over x_1, G^{LR} is no longer a function of $t - |x|$ only. Secondly, as we will see the transition regime can be significantly lengthened.

For illustration let us consider $x = 0$ for which we have to leading order in $1/c$

$$\mathcal{A} = \frac{2}{L}\int_0^{\frac{L}{2}} dx_1 \left[1 - \left(\frac{1}{1+iQ(x_1)}\right)^{2h_\mathcal{O}}\right], \quad Q(x_1) = e^{\frac{2\pi}{\beta}(\mathfrak{t}-x_1)} . \tag{3.123}$$

The sub-scrambling regime is for $\mathfrak{t} \ll 0$ such that $Q(x_1)$ is exponentially small for the whole integration range. The stable regime is for $\mathfrak{t} \gg \frac{L}{2}$, for which $Q(x_1)$ is exponentially large for the whole integration range. The behavior of $\mathcal{A}$ for these regimes is completely parallel to the corresponding regimes of A_0 discussed in last subsection (with only differences in some constant prefactors), and thus the behavior of G^{LR} is also parallel to those of (3.102). Things are more interesting for $\mathfrak{t}$ in the window $\mathfrak{t} \in (0, \frac{L}{2})$ (i.e. $t \in (t_* - t_J, t_* - t_J + \frac{L}{2})$) for which as x_1 changes from 0 to L, $Q(x_1)$ varies from exponentially large to exponentially small.[13] To find $\mathcal{A}$ for such values of $\mathfrak{t}$ we note that (3.123) can in fact be exactly integrated, yielding

$$\mathcal{A}(\mathfrak{t}) = 1 - \frac{\beta e^{-2\pi i h_\mathcal{O}}}{\pi L}\left[B\left(\frac{i}{Q(\frac{L}{2})}, 2h_\mathcal{O}, 1-2h_\mathcal{O}\right) - B\left(\frac{i}{Q(0)}, 2h_\mathcal{O}, 1-2h_\mathcal{O}\right)\right] \tag{3.124}$$

where $B(x,a,b)$ is the incomplete beta function. Using that $Q(0)$ is exponentially large and $Q(\frac{L}{2})$ exponentially small we find that

$$\mathcal{A} \to \frac{2}{L}\left(\mathfrak{t} + c_0\frac{\beta}{2\pi}\right) + i\frac{\beta}{2L} + \cdots \tag{3.125}$$

where c_0 is a numerical constant. This behavior is extremely simple with linear dependence on $\mathfrak{t}$ and a constant imaginary part, leading to

$$G^{LR}(t, x=0) = 2G_J e^{\frac{g_{\text{eff}}\beta}{2L}} \sin\left(\frac{2g_{\text{eff}}}{L}\left(\mathfrak{t} + c_0\frac{\beta}{2\pi}\right)\right), \quad \mathfrak{t} \in (0, L/2) . \tag{3.126}$$

Thus we see that for (3.103), the size of transition regime is extended to a region of size $\frac{L}{2}$ (in contrast to $\frac{\beta}{2\pi}$ for (3.102)), but the imaginary part of $\mathcal{A}$ is down by an order $\frac{\beta}{L}$ compared

[13] We will be concerned about $\mathfrak{t}$'s in the middle of the window $(0, \frac{L}{2})$, i.e. not close to either edges.

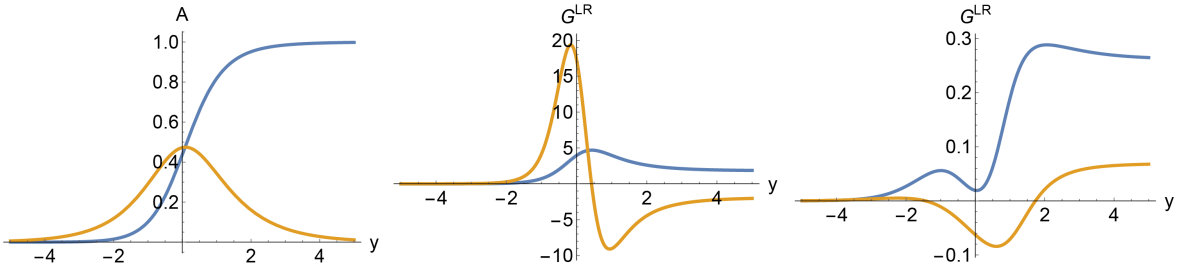

(a) (b) (c)

Figure 3.5: (a) Plots of real (blue) and imaginary (yellow) part of A_0 for $\Delta_{\mathcal{O}} = 8/9$. The horizontal axis is $y = \frac{2\pi}{\beta}(\mathfrak{t} - |x|)$. (b) Plots G^{LR} for (3.102) for two values of g_{eff}: blue for $g_{\text{eff}} = 2$ and yellow for $g_{\text{eff}} = 5$. (c) Plots of G^{LR} for $k = 1$ in (3.92) with $\epsilon = \beta/2$ in (3.118). Blue is for $g_{\text{eff}} = 2$ and yellow is for $g_{\text{eff}} = 5$.

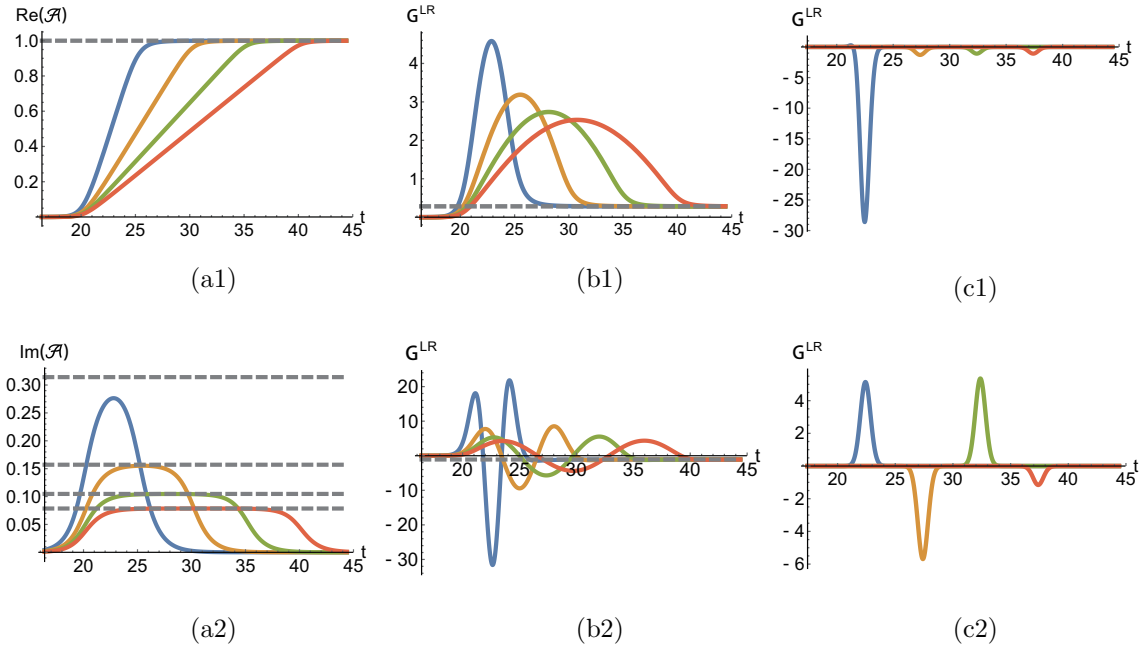

(a1) (b1) (c1)

(a2) (b2) (c2)

Figure 3.6: Plots of $\mathcal{A}$ and G^{LR} in various cases. We take $h_{\mathcal{O}} = 4/9$, $\beta = 2\pi$, $\Delta_J = 2h_J = 10$, $x = x_s = 0$, $h_J/c = 10^{-10}$. Plots (a1) and (a2) are respectively real and imaginary parts of $\mathcal{A}(t)$ with $g_{\text{eff}} = 3$. Blue, yellow, green, red curves are for $L/2 = 5,\ 10,\ 15,\ 20$ respectively, and the gray dashed lines are $\beta/(2L) = \pi/L$. Plots (b1) and (b2) are respectively $G^{LR}(t, t_s = t)$ with $g_{\text{eff}} = 3$ and $g_{\text{eff}} = 10$. Blue, yellow, green, red curves are for $L/2 = 5,\ 10,\ 15,\ 20$ and gray lines are asymptotic values $2\sin(g_{\text{eff}})$ for large t. In (c1) and (c2) we plot $G^{LR}(t, t_s)$ as a function of t for different t_s, with $g_{\text{eff}} = 10$. For (c1) $L/2 = 5$ and for (c2) $L/2 = 15$. Blue, yellow, green and red curves are for $t_s = t_* + 3,\ t_* + 8,\ t_* + 13,\ t_* + 18$ respectively.

with A_0. Thus while the resonant enhancement is extended to a much larger range of time period, the enhancement effect is more moderated. See Fig. 3.6 for various numerical plots of $\mathcal{A}$ and the corresponding G^{LR}.

The behavior for general x is qualitatively similar. The only difference is that the transition regime is now from $t_* + \theta(|x| - L/2)(|x| - L/2)$ to $t_* + L/2 + |x|$, which has maximal length of L when $|x| \geq L/2$. Here $\theta(x)$ is step function. See Fig. 3.7. Finally let us note that when $L \to \infty$, the behavior (3.125)–(3.126) will last forever and one never reaches the stable regime.

3.4.5 Robustness of regenesis from CFT calculations

We now turn to the explicit calculation of (3.51) for CFTs in the large c limit. For simplicity we will take $t_s = t$ and consider the regime $c \gg \Delta_\gamma \gg \Delta_J \gg \Delta_\mathcal{O} \sim O(1)$, for which we will be able to confirm explicitly the conclusion of Sec. 3.2.5. We will present only the results here leaving details to Appendix 3.E.

For simplicity we will consider only (3.5) in the large k limit and (3.6) when $L \gg \beta$. For these cases we find

$$\frac{W_\gamma(t;t_0)}{\left\langle J\tilde{J}\right\rangle} = \mathcal{J}(t,t_0) \times \begin{cases} \exp\left(-ig_{\text{eff}}\mathcal{G}_0(t,t_0)\tilde{A}_0(t,t_0)\right) & \text{large } k \\ \exp\left(-\frac{ig_{\text{eff}}}{L}\int_{-L/2}^{L/2} dx_1\, \mathcal{G}(t,t_0;x_1)\tilde{A}(t,t_0;x_1)\right) & \text{large } L \end{cases} \tag{3.127}$$

where for notational simplicity we have suppressed x, x_0 in the arguments of various functions. Function $\tilde{A}_0(t,t_0)$ is obtained from $\tilde{A}(t,t_0;x_1)$ by setting $x_1 = 0$ and $\mathcal{G}_0$ is obtained from $\mathcal{G}$ in the same way.

By comparing (3.127) with (3.91) and (3.96), we see that the following three differences between the corresponding expressions for (3.50) and Ψ_β which reflect three distinct aspects how an insertion of γ in Ψ_β affects the regenesis phenomenon :

1. The prefact factor $\left\langle J\tilde{J}\right\rangle$ is multiplied by another function $\mathcal{J}$, which modifies correlation between $J^L(t,x)$ and $J^R(-t,x)$.

2. the effective coupling g_{eff} is multiplied by a function $\mathcal{G}$, which modifies correlation between $\mathcal{O}^L(0)$ and $\mathcal{O}^R(0)$ and thus the effective coupling between L and R systems.

3. the function A is replaced by another function $\tilde{A}$ which reflects how "interactions" between $\mathcal{O}$ and J operators are modified due to presence of γ.

Note that item (1) and (2) can be interpreted as coming from modification of the entanglement structure of Ψ_β.

Now let us look at the explicit expressions of $\mathcal{J}, \mathcal{G}$ and $\tilde{A}$. Note that if the spatial location x_0 is sufficiently far away, e.g. if $|x_0 - x| \gg t - t_0$, clearly from causality γ cannot have any effect on J. Similar statement applies to $\mathcal{O}$. Now from Appendix 3.E we find that (assuming $x - x_0$ is much smaller than t_*)

$$\mathcal{J}(t, x; t_0, x_0) = \left(1 + \frac{2h_\gamma}{\epsilon_\gamma} Q_J\right)^{-2h_J}, \qquad Q_J = e^{\frac{2\pi}{\beta}(|t-t_0|-t_*-|x_0-x|)} \tag{3.128}$$

where ϵ_γ is a UV regulator need to make (3.50) normalizable. Note that $\mathcal{J} \leq 1$, and $\mathcal{J} \to 0$ when $|t - t_0| \gg t_*$ as anticipated in (3.53). From Appendix 3.E, $\mathcal{G}$ has the form

$$\mathcal{G} = \left(1 + \frac{2h_\gamma}{\epsilon_\gamma} Q_1\right)^{-2h_\mathcal{O}}, \qquad Q_1 = e^{\frac{2\pi}{\beta}(|t_0|-t_*-|x_0-x_1|)} . \tag{3.129}$$

Again $\mathcal{G} \leq 1$ and we see that $\mathcal{G} \to 0$, and thus the effective coupling is destroyed, when $|t_0| \gg t_*$, which confirms the expectation (3.54).

The behavior of $\tilde{A}$ is much more difficult to work out explicitly. This is also easy to understand physically: to see how the presence of γ modifies "interactions" between $\mathcal{O}$ and J is warranted to be complicated in a strongly interacting system. Fortunately the conclusion does not depend on the detailed form $\tilde{A}$. We expect $\tilde{A} \approx A$ if $|t_0| \ll t_*$ and $|t - t_0| \ll t_*$, i.e. the effect of γ on $J - \mathcal{O}$ correlation functions will be small if γ excitation does not have enough time to grow. Outside this region, the form of $\tilde{A}$ is expected to be complicated, but we do not really care as from (3.53)–(3.54) and (3.128)–(3.129), outside this region, the correlations between two systems already become too weak to have the regenesis phenomenon.

3.5 Gravity interpretation

In this section we compare with the gravity discussion of [31, 52] and discuss implications of our results for wormhole physics in the context of holography. Other recent papers on traversable wormholes from gravity perspective include [50, 4, 49, 17, 30]. Note that our two-dimensional CFT calculation in the large c limit may be considered as describing a BTZ black hole.

In the gravity description, thermal field double (3.1) is described by an eternal black hole which has two asymptotic boundaries connected by a non-traversable wormhole (see

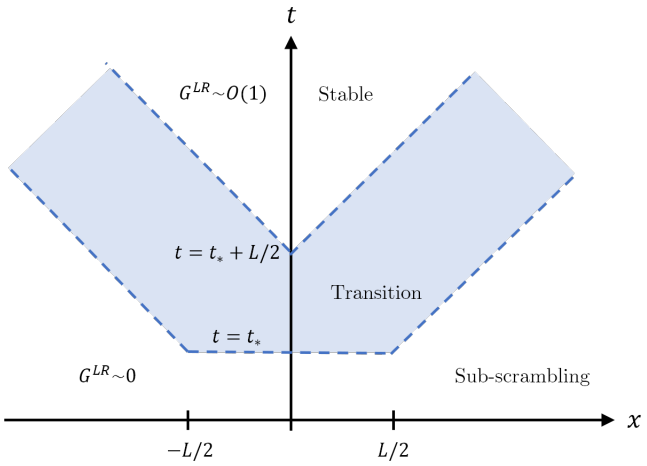

Figure 3.7: The sub-scrambling, transition, and stable regions for different values of x for (3.96).

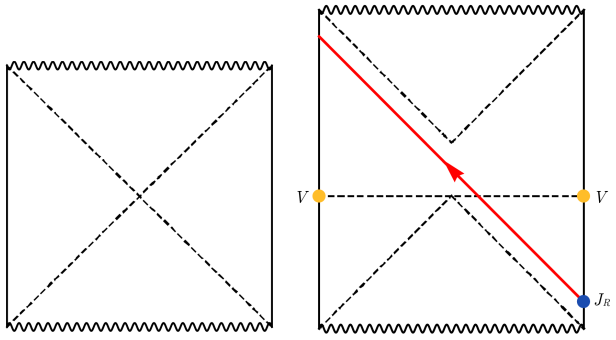

(a) (b)

Figure 3.8: (a): Penrose diagram of an eternal black hole. The two boundaries are causally disconnected. (b): in the picture of [31, 52], presence of V deforms the bulk geometry, especially the causal structure, allowing signals to pass from right to left, now following a timelike geodesic.

Fig. 3.8(a)). The regenesis phenomenon corresponds to the statement that with a coupling like (3.3), one could send signals between two boundaries, i.e. the wormhole becomes traversable.

Turning on the source φ^R for a short time on the right boundary generates bulk excitations dual to J. These excitations fall toward and are absorbed by the black hole membrane, which corresponds to the dissipation of $\langle J^R \rangle$. The process happens very fast, with time of order $O(\beta)$, as also seen in our earlier CFT calculation. When we briefly couple the two boundaries at $t = 0$, the physical picture of [31, 52] is that, the interaction V deforms the bulk geometry, especially the causal structure, making the wormhole traversable, as indicated in Fig. 3.8(b). It is important in the discussion of [31] that only one sign of the coupling g, i.e. $g > 0$ which generates negative bulk energy, allows for the traversability.

Below we will first compare our CFT results with that of [52] obtained from gravity scatterings. We then discuss implications of the regenesis phenomenon on gravity side. In particular, we will argue that there are other scenarios for wormhole traversability in addition to that suggested by Fig. 3.8(b). For example, the regime for $t_s \gg t_*$ should correspond to a "quantum traversable wormhole."

3.5.1 Explicit comparison with gravity results

Here we compare our explicit expression for W calculated from two-dimensional CFTs with that of [52] calculated for a $(0+1)$-dimensional boundary theory from gravity. By using graviton scattering amplitudes between $J\tilde{J}$ and $\mathcal{O}\tilde{\mathcal{O}}$ near horizon, for V given by (3.5) they

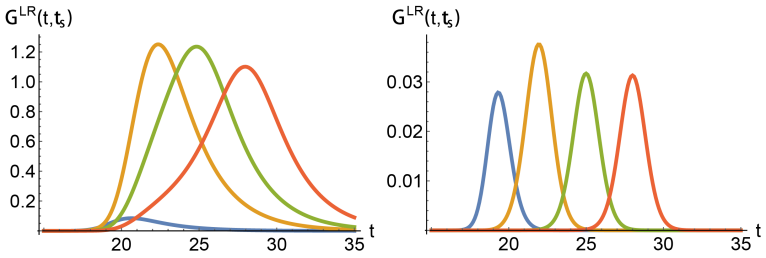

(a) (b)

Figure 3.9: Plot of $G^{LR}(t, t_s)$ as a function of t for fixed t_s. In (a) we choose $\Delta_J = \Delta_{\mathcal{O}} = 4/9$, in (b) we enlarge Δ_J as $\Delta_J = 3$. Blue, yellow, green and red curves are for $t_s = t_* + 0.5,\ t_* + 3.5,\ t_* + 6.5,\ t_* + 9.5$.

derived the following expression for W (below β has been set to 2π, and we have rescaled p and used notations introduced in Sec. 3.4.1)

$$W(t,-t_s)=e^{-ig_{\text{eff}}}\left\langle J\tilde{J}\right\rangle_\beta\frac{(-i)^{2\Delta_J}}{\Gamma(2\Delta_J)}\int_0^\infty dp\,p^{2\Delta_J-1}e^{ip}\exp\left[\frac{ig_{\text{eff}}}{\left(1+\frac{p\hat{Q}}{2\Delta_J}\right)^{2\Delta_\mathcal{O}}}\right], \tag{3.130}$$

where p is a bulk momentum of the J-quantum, and

$$\left\langle J\tilde{J}\right\rangle_\beta=\left(\frac{1}{2\cosh\frac{t-t_s}{2}}\right)^{2\Delta_J},\qquad \hat{Q}=\frac{\Delta_J G_N}{8}\frac{e^{\frac{t+t_s}{2}}}{\cosh\frac{t-t_s}{2}}\ . \tag{3.131}$$

To compare (3.130) with our results, it is convenient to deform the integral contour to be along the imaginary p axis from 0 to $i\infty$ (note the integral along the arc from $+i\infty$ to $+\infty$ vanishes). We then find (after a scaling $p\to ip$) for $t_s=t$

$$W(t)=G_J\frac{e^{-ig_{\text{eff}}}}{\Gamma(2\Delta_J)}\int_0^\infty dp\,p^{2\Delta_J-1}e^{-p}\exp\left[\frac{ig_{\text{eff}}}{\left(1+\frac{ipQ}{2\Delta_J}\right)^{2\Delta_\mathcal{O}}}\right] \tag{3.132}$$

where

$$G_J=2^{-2\Delta_J},\qquad Q=\hat{Q}|_{t=t_s}=\frac{\Delta_J G_N}{8}e^t=e^{t+t_J-t_*},\quad t_J\equiv\log\Delta_J,\quad t_*\equiv\log\frac{G_N}{8}\ . \tag{3.133}$$

Let us now consider Δ_J large. Assuming the exponential factor involving g_{eff} in (3.132) is slowly varying in p we can approximate the factor $p^{2\Delta_J-1}e^{-p}$ in the integrand of (3.132), which is a Poisson distribution by Gaussian distribution with center value

$$p_J=2\Delta_J-1\approx 2\Delta_J \tag{3.134}$$

and variance $\sqrt{2\Delta_J}$. Evaluated at (3.134), equation (3.132) becomes

$$W(t)=G_J\exp\left[-ig_{\text{eff}}\left(1-\left(\frac{1}{1+iQ}\right)^{2\Delta_\mathcal{O}}\right)\right], \tag{3.135}$$

which has exactly the same form as (3.91) with A_0 given by (3.117) (with $x=x_1=0$).[14] To make sure our Gaussian approximation is valid, we need the exponential term involving g_{eff} in (3.130) to be slowly varying within the variance of the Gaussian distribution, i.e.

$$\frac{g_{\text{eff}}\Delta_\mathcal{O}}{\sqrt{\Delta_J}}Q\,|1+iQ|^{-2\Delta_\mathcal{O}-1}\ll 1\ . \tag{3.136}$$

[14] $h_\mathcal{O}$ and h_J in our (1+1)-dimensional expressions are replaced respectively here in (0+1)-dimension by $\Delta_\mathcal{O}$ and Δ_J.

The above equation is satisfied for all values of Q if

$$g_{\text{eff}}\Delta_{\mathcal{O}} \ll \sqrt{\Delta_J}\ . \tag{3.137}$$

Our CFT calculation was performed for $\Delta_J \gg \Delta_{\mathcal{O}} \sim O(1)$ with g independent of Δ_J, so is consistent.

For $\Delta_J \sim \Delta_{\mathcal{O}} \sim O(1)$, while we do not have explicit counterpart from CFT calculation, equation (3.130) is consistent with various general features we discussed earlier. For example, in the limit $t, t_s \to \infty$, it reduces to (3.30). Another important aspect of our discussion is the reversed time ordering between the input signal φ^R and output signal $\langle J^L \rangle$ as indicated for example in (3.99). It can be checked that (3.130) also has this property, as can be seen explicitly from the plots of the resulting G^{LR} in Fig. 3.9.

3.5.2 A semi-classical regime

We now elaborate on a "semi-classical" regime of (3.130) which was identified in [52].[15] Consider smearing J-operator so that its high energy component is suppressed. One can represent such a smearing by inserting a Gaussian factor $e^{-\frac{p^2}{2\sigma^2}}$ in the momentum integral of (3.130). Then one finds that, in the large g_{eff} limit (with σ and $\Delta_J, \Delta_{\mathcal{O}} \sim O(1)$ fixed), there exists a regime corresponding to the picture of Fig. 3.8(b).

More explicitly, consider expanding in $\hat{Q}$ in the exponent of (3.130)

$$\left(1 + \frac{p\hat{Q}}{2\Delta_J}\right)^{-2\Delta_{\mathcal{O}}} = 1 - \frac{\Delta_{\mathcal{O}}}{\Delta_J} p\hat{Q} + \frac{\Delta_{\mathcal{O}}(2\Delta_{\mathcal{O}}+1)}{4\Delta_J^2} p^2\hat{Q}^2 + \cdots \tag{3.138}$$

and keeping only the linear term in $\hat{Q}$. Equation (3.130) can then be approximated by

$$W_\sigma(t, -t_s) \approx \left\langle J\tilde{J} \right\rangle \frac{(-i)^{2\Delta_J}}{\Gamma(2\Delta_J)} \int_0^\infty dp\, p^{2\Delta_J - 1} e^{ipX - \frac{p^2}{2\sigma^2}}, \quad X \equiv 1 - \frac{g_{\text{eff}}\Delta_{\mathcal{O}}}{\Delta_J}\hat{Q}\ . \tag{3.139}$$

Note that the prefactor $e^{-ig_{\text{eff}}}$ has now been canceled. Without the Gaussian factor in (3.139), the integral in (3.139) would yield

$$\left\langle J\tilde{J} \right\rangle \frac{1}{(X + i\epsilon)^{2\Delta_J}} = G_J \frac{1}{(\cosh\frac{t-t_s}{2} - g_{\text{eff}}\Delta_{\mathcal{O}} e^{\frac{t+t_s}{2} - t_*})^{2\Delta_J}} \tag{3.140}$$

[15] See Appendix B.1 there. We than Douglas Stanford and Zhenbin Yang for clarifications.

which has a "light-cone" singularity at

$$\cosh\frac{t-t_s}{2} = g_{\text{eff}}\Delta_{\mathcal{O}} e^{\frac{t+t_s}{2}-t_*} \quad \to \quad t = t_l \equiv t_* - \log\left(2\Delta_{\mathcal{O}} g_{\text{eff}} - e^{t_*-t_s}\right) . \tag{3.141}$$

Thus we can view (3.139) as the propagator of a smeared field in a spacetime where points on two boundaries satisfying (3.141) are connected by light rays, as indicated in Fig 3.8 (b).

Let us make some further remarks:

1. For the approximation in (3.139) to be valid, we need for the range of p allowed by the Gaussian factor, the terms of $O(Q^2)$ and higher in (3.138) are suppressed, i.e.

$$\frac{\hat{Q}\sigma}{\Delta_J} \ll 1, \quad \frac{g_{\text{eff}}\Delta_{\mathcal{O}}}{\Delta_J}\hat{Q}\sigma \gg 1, \quad \frac{g_{\text{eff}}\Delta_{\mathcal{O}}^2}{\Delta_J^2}(\hat{Q}\sigma)^2 \ll 1 \quad \to \quad \frac{1}{g_{\text{eff}}\sigma} \ll \frac{\Delta_{\mathcal{O}}}{\Delta_J}\hat{Q} \ll \frac{1}{\sqrt{g_{\text{eff}}}\sigma} \tag{3.142}$$

   Equation (3.141) (which corresponds to $\frac{g_{\text{eff}}\Delta_{\mathcal{O}}}{\Delta_J}\hat{Q} = 1$) lies within the range (3.142) provided that (recall we have $\beta = 2\pi$ which sets the unit)

$$\sqrt{g_{\text{eff}}} \gg \sigma \gg 1 . \tag{3.143}$$

2. Note that equation (3.141) has a solution only for $g_{\text{eff}} > 0$ and

$$t_s \geq t_* - \log(2\Delta_{\mathcal{O}} g_{\text{eff}}) \equiv t_c \tag{3.144}$$

   and for t_s satisfying (3.144), a corresponding $t_l(t_s)$ always exists. Note $\frac{dt_l}{d(-t_s)} > 0$ when (3.144) is satisfied, which means the light-cone structure is such that the earlier a signal (smaller $-t_s$) is sent, the earlier (smaller t_l) the arrival of the signal at the other boundary. In particular, as $-t_s \to -\infty$, $t_l(t_s) \to t_c$ which is the earliest possible arrival time, and as $-t_s \to -t_c$, $t_l(t_s) \to +\infty$.

   This is consistent with the heuristic picture of Fig. 3.8(b), but is sharply different from the behavior exhibited in (3.135) or for general $\Delta_{\mathcal{O}}, \Delta_J, g_{\text{eff}}$, for which the signal sent from $-t_s$ arrives at $t \approx t_s$. We contrast these two different types of behavior in Fig. 3.10.

3. For $\sigma \sim \sqrt{g_{\text{eff}}}$ or larger, terms with quadratic and higher powers in $\hat{Q}$ in the expansion of $(1 + \frac{p\hat{Q}}{2\Delta_J})^{-2\Delta_{\mathcal{O}}}$ become important. Note since $\hat{Q} \propto G_N$, these terms may be understood as due to backreaction of J-quanta on the geometry. Without the momentum suppression factor $e^{-\frac{p^2}{2\sigma^2}}$ (i.e. $\sigma \to \infty$), such backreactions are always important.

3.5.3 Old cats never die

Connecting the boundary and bulk pictures for the regenesis phenomenon in the semi-classical regime discussed in the last subsection raises leads to a rather amusing scenario.

To make the contrast of the two pictures a bit sharper, let us imagine by turning on φ^R, we create a "cat," which contains only "low energy" constituents compared with the coupling g_{eff} which we will eventually turn on (i.e. with their bulk momenta satisfying (3.143)). From the boundary picture, the cat lives for a while, but eventually her body gets more and more scrambled with the environment. We wait until her body is fully scrambled, turn on the interaction gV. From normal standards, it should be safe to say by this time the cat has long died (in other words, her body should have long been decomposed). From the genesis phenomenon, after another scrambling time, the cat is reborn in the other universe. As emphasized in the Introduction this process requires extreme fine tuning of the initial state at the time we created the cat.

Now let us refer to the bulk dual of the cat as the bulk cat, which we suppose is also a living object. Then in the bulk picture, the bulk cat travels in the deformed geometry created by the interaction gV. She never "dies"[16], just sailing through the bulk geometry. The journey should be smooth as no regions of large curvature will be encountered. In this picture, the reborn cat simply corresponds to the arrival of the bulk cat through a wormhole. In fact if she travels close to the light cone, the proper time that the cat experiences might not be too long.

From the holographic duality, these two pictures must be equivalent. In particular, since all boundary events should have a bulk version, the bulk cat should be able to "see" her own funeral on the boundary. This is the bulk way to say that the regenesis cat in fact contains the "memory" of her previous life.

3.5.4 Quantum traversable wormholes

In Sec. 3.5.2 we discussed in detail that the semi-classical scenario of Fig 3.8(b) corresponds to the parameter region of (3.143) and $k \to \infty$, as well as the ranges of t, t_s satisfying (3.142). Outside these parameter regions, how do we interpret the traversability of a wormhole? Here we offer some qualitative discussions by combining the general discussion of Sec. 3.2,

[16]By dying here we refer to something a bit more general, i.e. the body remains as a whole.

the explicit CFT results of Sec. 3.4, as well as discussion of (3.130). One can identify the following different physical scenarios/regimes:

1. A most straightforward scenario is that the picture of Fig. 3.8(b) still qualitatively applies, but with the deformed geometry interpreted as including both effects of gV and the backreaction of J itself. Since the deformed geometry now depends on the quanta propagating through it, strictly speaking, one can no longer talk about a background causal structure as in the case of a linear wave moving in a fixed geometry. Nevertheless, the essential physics picture remains qualitatively similar. So we will still refer to this scenario as the semi-classical scenario. For example, consider (3.130) (which is $k \to \infty$ limit) with a large g_{eff} and a momentum suppression factor $e^{-\frac{p^2}{2\sigma^2}}$, and slowly increase σ beyond the range of (3.143). As we increase σ, the backreactions of J become more and more important. One should be able to include them perturbatively, say first including the $\hat{Q}^2$ term in (3.138) but neglecting higher order terms, and then the $\hat{Q}^3$ term, and so on.[17]

2. When $t \sim t_s \gg t_*$, the traversability should arise from a distinct physical picture from that of Fig. 3.8(b). In this regime, independent of the details of any theory (and for general g, k and V), we discussed in Sec. 3.2 that the sole effect of gV is to generate a complex factor in W proportional to $\langle e^{-igV} \rangle$ with no dependence on the quantum numbers of J at all. There is no scattering between J and $\mathcal{O}$ quanta. For a CFT, the conclusion also does not depend on the large c limit (as far as the theory is chaotic).

   Let us also highlight some features which are sharply different from those of the semi-classical regime discussed above:

   (a) Even in the $k \to \infty$ limit, the regenesis phenomenon, and thus traversability of the wormhole, does not depend on the sign of g, while the semi-classical scenario of item 1 requires $g > 0$ [31].

   (b) Regardless of the bulk geometry, the form of V, and details of how the signal is sent (i.e. its energy and direction etc.), a bulk signal departing from $(-t_s, \vec{x})$ from the R boundary can only arrive on the L boundary at $(t_s, \vec{x})$.[18] See Fig. 3.10. As

[17] In the limit $\sigma \to \infty$ (or $\sigma \gg g_{\text{eff}}$), one finds that for certain range of t around t_* the integral is dominated by the contribution of a (real) saddle-point with $p_{\text{saddle}} \propto g_{\text{eff}}$ (see Appendix B of [52]). Such a saddle point may have an interpretation in terms of bulk Einstein equations.

[18] Again we are treating relaxation time scales as microscopic.

emphasized in Sec. 3.2.2, the pairing of $(t_s, \vec{x})$ and $(-t_s, \vec{x})$ is solely determined by the entanglement structure of the thermal field double state (3.1).

Thus the traversability for this regime does not appear to be associated with any spacetime causal structure at all, and is in a sense driven by entanglement. In other words, one has a "quantum traversable wormhole."

We do not yet have a precise way to characterize the "quantum geometry" associate with such a traversable wormhole. Here we offer some preliminary thoughts. Heuristically, the transmission of a signal from the R to L boundary feels like a tunneling process across the horizon mediated by gV interaction. Directly translating the discussion of Sec. 3.2.3 to the bulk gives the following picture. Consider first $g = 0$, for which the wormhole in non-traversable. Nevertheless, the bulk Wightman and Feynman functions between L and R for the bulk field dual to J is nonzero. We may interpret the vanishing of $\langle [J^L, J^R] \rangle = \langle J^L J^R \rangle - \langle J^R J^L \rangle$ as perfect destructive interference between the process of a *virtual* particle traveling from R to L, and the mirror process of traveling from L to R, as indicated in the left plot of Fig. 3.3. Turning on a nonzero g gives a phase shift to each propagator, and in general the destructive inference is no longer perfect, resulting propagation of *real* particles. See right plot of Fig. 3.3. In (3.107) we saw that G^{LR} is periodic in g_{eff}, thus as one dials the value of g, perfect destructive interference can be again reached at various special values.

3. Now for general k, g and σ, and $t, t_s \sim t_*$, the picture is no longer so sharp. There is a continuous spectrum in going from the semi-classical regime of item 1 to the quantum regime of item 2.

   For example, for large, but finite k, while the bulk stress tensor induced from turning on V will have a finite spread, for g_{eff}, σ satisfying (3.143), we expect the physics should still be close to the semi-classical picture.

   On the other hand, for (3.91) and (3.102) (or its $(0+1)$-dimensional counterpart (3.135)), both feature (a) and (b) listed in item 2 also apply. So it appears reasonable to expect the traversability is governed by the mechanism of item 2 except that in general there are also scatterings between J and $\mathcal{O}$ involved. Note that from (3.130), equation (3.135) is obtained from a pure imaginary "saddle" $p_{\text{saddle}} \approx i2\Delta_J$, which also suggests that the underlying physics cannot be understood straightforwardly in terms of classical scatterings of $\mathcal{O}$ and J quanta.[19]

[19] Also note that once one adds the Gaussian suppression factor $e^{-\frac{p^2}{2\sigma^2}}$ to (3.130), one can no longer deform

3.6 Discussions and future directions

In this paper we presented a general argument for the regenesis phenomenon in a many-body chaotic system and studied it in detail in two-dimensional CFTs in the large central charge limit. We also discussed the implications of these field theory results for wormhole physics.

Here we end with some further discussion, including future directions:

1. *Teleportation?*

   As discussed in [31, 52] (see also [75]), the coupling V between L and R system is reminiscent of the operations in a teleportation process. During the time evolution of the system, the effect of having the $gV\delta(t=0)$ term in the Hamiltonian can be considered as being equivalent to the process of performing some measurements in the R system, communicating the results to the L system, and then performing operations on the L system. But we would like to stress that the regenesis phenomenon is in fact very different from quantum teleportation in the usual sense. In teleportation one would like to send an unknown state to another party. Here while the signal from the R system re-appears in the L system, in general there is no state teleportation. It can be readily checked in the qubit model of Sec. 3.2.6 that general $H^{L,R}$ and coupling V, do not implement teleportation of a state. Thus the regenesis phenomenon can at most be considered as a "signal teleportation". This conclusion is also supported by the discussion of [75] that the operation for a state teleportation involve a much larger complexity than that of the regenesis setup. As emphasized in [52] the regenesis setup also shares some similarities with that of Hayden-Preskill [37], but as we emphasized in the Introduction regenesis requires extra fine tuning in the preparation of the initial state. Thus for Hayden-Preskill, the decoding requires much higher level of complexity [86].

   It is an interesting question for further study, say if one wants to send some known signals (one knows the input signal φ^R one is applying) from R to L, whether the current protocol is an efficient one (see [7] for a discussion of treating the wormhole setup as a quantum channel).

2. *Nature of quantum traversable wormholes*

---

the contour to imaginary p, which also indirectly suggests that (3.139) and (3.135) are controlled by very different physics.

It is important to have a more precise bulk picture for "quantum traversable wormholes" which we argued in Sec. 3.5.4. In particular, it would be ideal to have a real-time evolution picture for it.

Equation (3.36) can be reproduced from (3.15) by replacing Φ of (3.16) by[20] $|\Phi\rangle \approx a^* |\Psi_\beta\rangle + U^R |\Psi_\beta\rangle$. Note that this cannot be a true identity as the right hand side does not have the right normalization (and it does not reproduce (3.34)). Nevertheless, this expression is suggestive as it indicates that Φ is a superposition of two macroscopic states, one from acting U^R on TFD, while the other corresponding to multiplying a TFD by a complex number. Equation (3.36), and thus traversability, arises from interference between them. How should we think the bulk geometry corresponding to Φ? Is there a firewall at the horizon?

3. *Other systems*

   It is clearly of interest to study this phenomenon in other systems like spin chains or using random unitary circuits (see e.g. [59]) which have generated lots of insights into chaotic systems. Note that since regenesis concerns with time scales of order the scrambling time, thus it should be insensitive to the early time behavior such as whether the system has a nonzero Lyapunov exponent.

4. *Using effective field theories (EFTs)*

   The computation of the behavior G^{LR} in the transition regime (i.e. for $t_s \sim t_*$) in two-dimensional CFTs is rather complicated and technical even in the large c limit. While there are reasons to believe that the qualitative behavior we obtained should apply to generic chaotic systems, it would be good to understand it in a system-independent way. Recently a class of EFTs which aims to capture scrambling of general operators in chaotic systems (at least for those close to being maximally chaotic) has been proposed in [12]. In particular, the EFT for two-dimensional CFT in the large c limit has been obtained in [20, 35]. The EFT approach could provide a simpler and system-independent way to study many aspects of the regenesis phenomenon and wormhole physics. We will leave this for future investigation.

5. *Experimental realizations*

   It would be interesting to observe the regenesis phenomenon experimentally. For example, one could imagine setting up the protocol in bilayer graphene or quantum hall systems. Experimentally realizing a thermal field double state in a many-body

[20] We thank J. Maldacena, D. Stanford and Z. Yang for this observation.

system appears difficult.[21] If one could realize (3.1), to fine tune the state at $t = -t_s$ is similar to realizing an OTOC, as one needs to run the system "backward" in time, turn on the source, and then move forward in time. Recently there has been significant progress in realizing OTOCs in the lab (see e.g. [33]), so perhaps such tuning is not that far-fetched. In the spirit of ER = EPR [54], realizing regenesis experimentally may be interpreted as creating a quantum traversable wormhole in the lab!

Acknowledgements

We would like to thank David Gross, Yingfei Gu, Gary Horowitz, Daniel Jafferis, Kristan Jensen, Patrick Ledwith, Patrick Lee, Leonid Levitov, Juan Maldacena, Don Marolf, Krishna Rajagopal, Moshe Rozali, Subir Sachdev, Douglas Stanford, Leonard Susskind, Zhenbin Yang, Yizhuang You, and Ying Zhao for conversations and discussions. This work is supported by the Office of High Energy Physics of U.S. Department of Energy under grant Contract Number DE-SC0012567. H. L. would also like to thank Galileo Galilei Institute for Theoretical Physics for the hospitality during the workshop "Entanglement in Quantum Systems" and the Simons Foundation for partial support during the completion of this work.

3.A Linear responses

Consider perturbing a system by

$$H = H_0 + H'_S(t) = H_0 + H_S^{(1)}(t) + H_S^{(2)}(t) \tag{3.145}$$

where subscripts S denote the Schrodinger picture operators. More explicitly

$$H_S^{(1)} = -g \int d^3\vec{x} f(t,\vec{x}) \mathcal{O}^L(\vec{x}) \mathcal{O}^R(\vec{x}), \quad H_S^{(2)} = -\int d^3\vec{x}\, \varphi^R(t,\vec{x}) J^R(\vec{x}) \ . \tag{3.146}$$

We will take the support of $f(t,\vec{x})$ to be around $t = 0$ and that for $\varphi^R(t,\vec{x})$ to be around some $-t_1 \ll 0$. The two functions can be considered to have no overlap.

We take the system at $t = -\infty$ to be given by some state ρ_0, and consider H'_S going to zero at $t \to \pm\infty$ (as well as at spatial infinity). Now let us consider the expectation value

[21] Perhaps discussions in [48, 50] could be relevant.

for some operator A

$$\langle A\rangle = \mathrm{Tr}(\rho(t,t_0)A_S) = \mathrm{Tr}(\rho_0 A_H(t,t_0)) \tag{3.147}$$

where

$$\rho(t,t_0) = U(t,t_0)\rho_0 U^\dagger(t,t_0), \qquad A_H(t,t_0) = U^\dagger(t,t_0)AU(t,t_0), \qquad t_0\to-\infty \tag{3.148}$$

and $U(t,t_0)$ is the evolution operator under the full Hamiltonian H,

$$U(t,t_0) = T\exp\left(-i\int_{t_0}^{t} ds\, H(s)\right)\ . \tag{3.149}$$

Below we will use

$$A(t,t_0) = e^{iH_0(t-t_0)}Ae^{-iH_0(t-t_0)} \tag{3.150}$$

to denote the Heisenberg operator associated with H_0 with reference time t_0, and $A(t)$ to denote the Heisenberg operator with t_0 set to zero.

Using the standard interaction picture technique we can write

$$U(t,t_0) = e^{-iH_0(t-t_0)}U_I(t,t_0), \qquad U_I(t,t_0) = T\exp\left(-i\int_{t_0}^{t} ds\, H'(s,t_0)\right) \tag{3.151}$$

where

$$H'(t,t_0) = e^{iH_0(t-t_0)}H'_S(t)e^{-iH_0(t-t_0)} = H^{(1)}(t,t_0) + H^{(2)}(t,t_0)\ , \tag{3.152}$$

where

$$H^{(1)}(t,t_0) = -g\int d^3\vec{x} f(t,\vec{x})\mathcal{O}^L(t,t_0)\mathcal{O}^R(t,t_0), \quad H^{(2)}(t,t_0) = -\int d^3\vec{x}\,\varphi^R(t,\vec{x})J^R(t,t_0)\ . \tag{3.153}$$

We consider to linear order in H_2 while to full nonlinear order in H_1, i.e.

$$U_I(t,t_0) = U_1(t,t_0)\left(1 - i\int_{t_0}^{t} ds\, H^{(2)}(s,t_0)\right), \quad U_1(t,t_0) = T\exp\left(-i\int_{t_0}^{t} ds\, H^{(1)}(s,t_0)\right) \tag{3.154}$$

where we have used that the support of $\varphi^R(x)$ is much earlier than that of $f(x)$. Now for simplicity we will take

$$f(x) = \delta(t)f(\vec{x}) \tag{3.155}$$

we will the have

$$U_1(t,t_0) = \begin{cases} 1 & t\le 0 \\ \exp(igV) & t>0 \end{cases}, \quad V = \int d^3\vec{x}\, f(\vec{x})\mathcal{O}^L(0,t_0)\mathcal{O}^R(0,t_0)\ . \tag{3.156}$$

We thus find that

$$A_H(t,t_0) = U_I^\dagger(t,t_0)A(t,t_0)U_I(t,t_0) = \begin{cases} A(t,t_0) - i\int ds[A(t,t_0), H^{(2)}(s,t_0)] & t<0 \\ A_V(t,t_0) - i\int ds[A_V(t,t_0), H^{(2)}(s,t_0)] & t>0 \end{cases} \tag{3.157}$$

where

$$A_V(t,t_0) = e^{-igV}A(t,t_0)e^{igV} \ . \tag{3.158}$$

3.B An identity

For an operator X in the L-system, consider

$$\langle X\rangle_g \equiv \langle\Phi|X(t)|\Phi\rangle \tag{3.159}$$

where

$$|\Phi\rangle \equiv e^{igV}U^R|\Psi_\beta\rangle\,, \qquad U^R = e^{i\int ds\,\varphi^R(s)J^R(s)}, \tag{3.160}$$

and the source $\varphi^R(t)$ is supported near $t=-t_s$, while V is supported at $t=0$. In the limit $t, t_s \gg t_*$, with OTOCs set to zero, $\langle X\rangle_g$ can be greatly simplified. More explicitly, we have (suppressing Ψ_β)

$$\begin{aligned}\langle X\rangle_g &= \left\langle U_R^\dagger e^{-igV}X(t)e^{igV}U_R\right\rangle = \left\langle (U_R^\dagger-1)e^{-igV}X(t)e^{igV}(U_R-1)\right\rangle \\ &\quad + \left\langle e^{-igV}X(t)e^{igV}\right\rangle + \left[\left\langle e^{-igV}X(t)e^{igV}(U_R-1)\right\rangle + h.c.\right] \\ &= \left\langle (U_R^\dagger-1)X(t)(U_R-1)\right\rangle + \left\langle e^{-igV}X(t)e^{igV}\right\rangle + \left[\left\langle e^{-igV}X(t)(U_R-1)\right\rangle + h.c.\right] \ .\end{aligned} \tag{3.161}$$

Note that X commutes with U_R. Now as in (3.30) we factorize parts of a correlator which are widely separated in time (with $\left\langle e^{-igV}X(t)e^{igV}\right\rangle = \langle X\rangle$), which then gives

$$\langle X\rangle_g = (1-2\,\mathrm{Re}\,a)\langle\Psi_\beta|X(t)|\Psi_\beta\rangle + \left(a\left\langle\Psi_\beta\left|X(t)U^R\right|\Psi_\beta\right\rangle + h.c.\right) \tag{3.162}$$

with

$$a = \left\langle e^{-igV}\right\rangle_\beta - 1 \ . \tag{3.163}$$

3.C Details of CFT calculation

3.C.1 Approximation of identity Virasoro block by conformal transformation

In this Appendix we first review a method developed in [27] to calculate correlation functions in a CFT in the large c limit, and then use it to calculate (3.76) in the regime of $c \gg h_J \gg h_{\mathcal{O}} \sim O(1)$. While their original method was considered in the limit of $c \to \infty$ with h_J/c fixed, we will justify the same method in the weaker limit stated above. We will keep general dependence for h_J but ignoring all $1/c$ and $h_{\mathcal{O}}/c$ corrections.

Consider first the four-point function $\langle J_a(z_a)J_b(z_b)\mathcal{O}_1(z_1)\mathcal{O}_2(z_2)\rangle$. Since $h_J \gg h_{\mathcal{O}}$, we can treat this four point function as if the two point function of $\mathcal{O}$ in the background of J. To be more precise, we are going to do the following conformal map from z plane to w plane:

$$1 - w = \left(1 - \frac{z_{ab} z}{z_b(z_a - z)}\right)^{\alpha}, \ \alpha = \sqrt{1 - 24\frac{h_J}{c}} \tag{3.164}$$

which maps $z_a \to w_a = \infty$, $z_b \to w_b = 1$ and $0 \to 0$. This map has a branch cut in z plane from z_b to z_a. The Jacobian is

$$\mathbb{J}(z) \equiv \frac{\partial z}{\partial w} = \frac{(z - z_a)(z - z_b)}{\alpha z_{ab}} \left[\frac{z_a(z - z_b)}{z_b(z - z_a)}\right]^{-\alpha} \tag{3.165}$$

The relation between 4-pt function in z and w planes is

$$\langle J_a J_b \mathcal{O}_1 \mathcal{O}_2 \rangle_w = \mathbb{J}_a^{h_J} \mathbb{J}_b^{h_J} \mathbb{J}_1^{h_{\mathcal{O}}} \mathbb{J}_2^{h_{\mathcal{O}}} \langle J_a J_b \mathcal{O}_1 \mathcal{O}_2 \rangle_z \tag{3.166}$$

where the subscript denotes the coordinate. Note that $\mathbb{J}_a$ and $\mathbb{J}_b$ are vanishing, so the above formula should be regarded as taken in a proper limit since the LHS is also vanishing as $w_a \to \infty$.

The advantage of this conformal transformation is that in w plane, 4-pt function $\langle J(w_a)J(w_b)T(w)\rangle$ does not depend on h_J explicitly. In large c limit, this amounts to the leading order approximation in $1/c$ expansion. To be more precise, by Ward identity, the 4-pt function in z plane is

$$\langle J(z_a)J(z_b)T(z)\rangle = \frac{1}{z_{ab}^{2h_J}} \frac{h_J z_{ab}^2}{(z - z_a)^2(z - z_b)^2} \tag{3.167}$$

Since stress tensor is not primary field, it has an extra Schwarzian term under conformal transformations. Given the transformation (3.164), the stress tensor transformations as

$$T(w) = \mathbb{J}(z)^2 \left(T(z) - \frac{h_J z_{ab}^2}{(z-z_a)^2(z-z_b)^2} \right) \tag{3.168}$$

Hence we find that in w plane

$$\langle J(w_a) J(w_b) T(w) \rangle = \mathbb{J}_a^{h_J} \mathbb{J}_b^{h_J} \mathbb{J}_z^2 \cdot 0 \tag{3.169}$$

where the Schwarzian cancels the term that is proportional to h_J. In w plane, the whole Virasoro block is summing over all Virasoro descendents just like z plane. We can Taylor expand $T(w)$ around $w = 0$:

$$T(w) = \sum_n w^{-n-2} \mathcal{L}_n \tag{3.170}$$

One can show that the commutation between $\mathcal{L}_n$ and general primary operator $X(w)$ obeys the same rule as in z plane:

$$[\mathcal{L}_n, X(w)] = h_X (1+n) w^n X(w) + w^{1+n} \partial_w X(w) \tag{3.171}$$

and Virasoro algebra still holds for all $\mathcal{L}_n$:

$$[\mathcal{L}_n, \mathcal{L}_m] = (n-m)\mathcal{L}_{n+m} + \frac{c}{12} n(n^2-1)\delta_{n,-m} \tag{3.172}$$

Indeed, above relations always hold when the Jacobian $\mathbb{J}(z)$ is nonsingular around w.

The relation between L_n, the Virasoro mode of $T(z)$, and $\mathcal{L}_n$ can be solved explicitly by the conformal transformation (3.168)

$$\begin{aligned} \sum_n w^{-n-2} \mathcal{L}_n &= J(z)^2 \left(\sum_n z(w)^{-n-2} L_n - \frac{h_J z_{ab}^2}{(z-z_a)^2(z-z_b)^2} \right) \\ &= \frac{(1-w)^{2/\alpha-2} z_a^2 z_b^2 z_{ab}^2}{\alpha^2 (z_a - (1-w)^{1/\alpha} z_b)^4} \sum_n \left[\frac{z_a z_b (1-(1-w)^{1/\alpha})}{z_a - (1-w)^{1/\alpha} z_b} \right]^{-n-2} L_n - \frac{h_J}{\alpha^2 (1-w)^2} \end{aligned} \tag{3.173}$$

which implies that all $\mathcal{L}_n$ are linear combinations of L_m with $m \geq n$. This immediately gives an important result

$$\mathcal{L}_n |h\rangle = 0, \ n \geq 0 \tag{3.174}$$

for any primary $|h\rangle$. However, since the expansion (3.170) is not convergent around infinity due to the existence of branch cut from 1 to ∞, we should not expect $\mathcal{L}_n^\dagger = \mathcal{L}_{-n}$. In other

words, the radius of convergence of series (3.170) is bounded by the location of branch cut. Formally we can define a "w-primary state" $\langle h_w|$ as

$$\langle h_w| = \lim_{w\to\infty} \langle 0_w|\, w^{2h_X} X(w) \tag{3.175}$$

with $\langle h_w|\, \mathcal{L}_{-n} = 0$ for $n \geq 0$ and normalization $\langle h_w|\, h\rangle = 1$. The whole Virasoro block in w plane can be calculated as insertion of projection P_{T^k} between $J_a J_b$ and $\mathcal{O}_1\mathcal{O}_2$, where

$$P_{T^k} \equiv \frac{\mathcal{L}_{-n_1}\cdots\mathcal{L}_{-n_k}\,|h\rangle\,\langle h_w|\,\mathcal{L}_{n_k}\cdots\mathcal{L}_{n_1}}{\langle h_w|\mathcal{L}_{n_k}\cdots\mathcal{L}_{n_1}\mathcal{L}_{-n_1}\cdots\mathcal{L}_{-n_k}|h\rangle} \tag{3.176}$$

Note that these P_{T^k}'s are not orthogonal, and in general we need to take all overlaps between different projectors into account. Let us take $h = 0$ for identity Virasoro block for now.

There are a few features of this construction. First, $\langle 0_w|\mathcal{L}_{n_1}\cdots\mathcal{L}_{n_k}|0\rangle_w = \langle 0|L_{n_1}\cdots L_{n_k}|0\rangle_z$ because $\mathcal{L}_n$ and L_n obey the same algebra. Therefore, we can simply estimate the denominator of (3.176) in large c limit. For $n_i \geq 2$,

$$\langle 0_w|\mathcal{L}_{n_k}\cdots\mathcal{L}_{n_1}\mathcal{L}_{-n_1}\cdots\mathcal{L}_{-n_k}|0\rangle = O(c^k) \tag{3.177}$$

Second, $\langle 0_w|\,\mathcal{L}_{n_k}\cdots\mathcal{L}_{n_1}\mathcal{O}(w_1)\cdots\mathcal{O}(w_n)|0\rangle$ is the same as that in z plane because of the same algebra (3.171) and (3.175). In particular, the two point function is

$$\langle 0_w|\,\mathcal{O}(w_1)\mathcal{O}(w_2)|0\rangle = \frac{1}{w_{12}^{2h_\mathcal{O}}} \tag{3.178}$$

Note that this is different from conformal transformed version of $\langle 0|\mathcal{O}(z_1)\mathcal{O}(z_2)|0\rangle_z$ to w plane. Physically, this means that ignoring the neighborhood of branch cut, we regard all other regions in w plane the same as ordinary CFT on complex plane. Third, $\langle 0|\,J_aJ_b\mathcal{L}_{-n_1}\cdots\mathcal{L}_{-n_k}\,|0\rangle$ is not the same as z-plane CFT due to the branch cut, but restricted to the conformal transformation rules from z-plane to w-plane. In particular, the two point function obeys

$$\langle 0|J(w_a)J(w_b)|0\rangle = \mathbb{J}_a^{h_J}\mathbb{J}_b^{h_J}\,\langle 0|J(z_a)J(z_b)|0\rangle \tag{3.179}$$

The advantage of this special conformal transformation is that in w plane,

$$\langle 0|J(w_a)J(w_b)\mathcal{L}_{-n}|0\rangle = 0 \tag{3.180}$$

for all $n \geq 0$ due to (3.169). This method can be generalized to multiple T insertion in (3.169) and one can show that the leading order of h_J vanishes in w-plane. Indeed, notice

that T is different from primary field only by a central term. Therefore, for multiple T insertion in a correlation function of primaries $\langle X\rangle$, there is a induction relation:

$$\begin{aligned}\langle T(z_1)\cdots T(z_k)X\rangle =&\sum_i\left(\frac{h_i}{(z_1-z_i)^2}+\frac{1}{z_1-z_i}\partial_i\right)\langle T(z_2)\cdots T(z_k)X\rangle\\&+\sum_{i=2}^{k}\frac{c/2}{(z_1-z_i)^4}\left\langle T(z_2)\cdots\hat{T}(z_i)\cdots T(z_k)X\right\rangle\end{aligned}\tag{3.181}$$

where hat means omiting $T(z_i)$. From above formula, the k insertion should have the following expansion

$$\langle T(z_1)\cdots T(z_k)J_aJ_b\rangle=\sum_{i=0}^{[k/2]}\sum_{j=0}^{k-2i}c^ih_J^jF_{ij}(z_n),\qquad F_{00}(z_n)=0\tag{3.182}$$

where z_n denote coordinates collectively. In $c\gg h_J$ limit, the expansion has the orders from high to low as

$$c^{[k/2]}h_J^{k-2[k/2]},c^{[k/2]-1}h_J^{k-2[k/2]+2},\cdots,h_J^k,\cdots\tag{3.183}$$

Note that if we are considering L_{-n} rather than $\mathcal{L}_{-n}$, the powers of c does not contribute to $\langle 0|\,J_aJ_bL_{-n_1}\cdots L_{-n_k}\,|0\rangle$. But transforming to w plane, these powers are leading contributions to $\langle 0|\,J_aJ_b\mathcal{L}_{-n_1}\cdots\mathcal{L}_{-n_k}\,|0\rangle$. On the other hand, terms involving $\mathcal{O}_1$ and $\mathcal{O}_2$ after inserting P_{T^k} has scaling

$$\langle 0_w|\mathcal{L}_{n_k}\cdots\mathcal{L}_{n_1}\mathcal{O}_1\mathcal{O}_2\rangle\sim\sum_{n=1}^{k}O(h_{\mathcal{O}}^n)\sim O(1)\tag{3.184}$$

Therefore, the highest order terms in first a few orders of P_{T^k} insertion are

$$O(1)+O(h_J/c)+O(1/c)+O(h_J/c^2)+O(1/c^2)+O(h_J/c^2)+\cdots\tag{3.185}$$

where above explicit terms are from $k=0$ to $k=5$.

The purpose of the transformation (3.164) is to cancel all $O(h_J/c^{[k/2]})$ order terms in odd k and leave highest orders of the expansion (3.185) as

$$O(1)+O(1/c)+O(1/c^2)+\cdots\tag{3.186}$$

This can be seen by noting that the first term in (3.181) does not contribute with c and only TT fusion gives powers of c. For $k=2s+1$, c^sh_J order only comes from the OPE between all different $T(z_i)$'s, which in total gives c^s:

$$\langle J_aJ_bT(z_1)\cdots T(z_{2s+1})\rangle\supset(c/2)^s\sum_{k=1}^{2s+1}\sum_{\substack{\{p,q\}\\p_i,q_i\neq k}}\prod_i\frac{1}{z_{p_iq_i}^4}\langle J_aJ_bT(z_k)\rangle\sim O(c^sh_J)\tag{3.187}$$

where $\{p,q\}$ are all different choices of pairs of indices from 1 to $2s+1$ except k. Transformation to w plane, due to (3.168) we have

$$\begin{aligned}\langle J_a J_b T(w_1)\cdots T(w_{2s+1})\rangle &= \mathbb{J}_a^{h_J}\mathbb{J}_b^{h_J}\left(\prod_{i=1}^{2s+1} J_{z_i}^2\right)\left\langle J_a J_b \prod_{i=1}^{2s+1}\left(T(z_i)-\frac{h_J z_{ab}^2}{z_{ia}^2 z_{ib}^2}\right)\right\rangle \\ &\supset \mathbb{J}_a^{h_J}\mathbb{J}_b^{h_J}\left(\prod_{i=1}^{2s+1} J_{z_i}^2\right)(c/2)^s\sum_{k=1}^{2s+1}\sum_{\substack{\{p,q\}\\ p_i,q_i\neq k}}\prod_i \frac{1}{z_{p_iq_i}^4}\left\langle J_a J_b\left(T(z_k)-\frac{h_J z_{ab}^2}{z_{ka}^2 z_{kb}^2}\right)\right\rangle \\ &= 0\cdot O(c^s h_J) \end{aligned} \tag{3.188}$$

This shows that, up to terms suppressed by $1/c$, the insertion of P_{T^k} reduces to just insertion of vacuum $|0\rangle\langle 0_w|$.

In $h_J \sim c \to \infty$ limit, the leading order of all P_{T^k} insertions are h_J^k/c^k terms. One can also see all these terms vanishes in w plane. That is the argument in [27]. The reason why their method also applies to our weaker limit $O(1)\sim h_{\mathcal{O}} \ll h_J \ll c$ is that we are using the same expansion of h_J/c and $1/c$ in w plane, in which only terms suppressed by $1/c$ survive due to the conformal transformation.

3.C.2 Application to W

Using the conformal transformation, four point function reads

$$\begin{aligned}\langle J_a J_b \mathcal{O}_1\mathcal{O}_2\rangle_z &= \mathbb{J}_a^{-h_J}\mathbb{J}_b^{-h_J}\mathbb{J}_1^{-h_{\mathcal{O}}}\mathbb{J}_2^{-h_{\mathcal{O}}}\langle J_a J_b\mathcal{O}_1\mathcal{O}_2\rangle_w \\ &\approx \mathbb{J}_a^{-h_J}\mathbb{J}_b^{-h_J}\mathbb{J}_1^{-h_{\mathcal{O}}}\mathbb{J}_2^{-h_{\mathcal{O}}}\langle J_a J_b\rangle_w\langle 0_w|\mathcal{O}_1\mathcal{O}_2\rangle_w \\ &= \langle J_a J_b\rangle_z \mathbb{J}_1^{-h_{\mathcal{O}}}\mathbb{J}_2^{-h_{\mathcal{O}}}\frac{1}{w_{12}^{2h_{\mathcal{O}}}}\end{aligned} \tag{3.189}$$

Plugin the coordinate transformation, we find that

$$\mathcal{V}(u)\equiv\frac{\langle J_a J_b\mathcal{O}_1\mathcal{O}_2\rangle_z}{\langle J_a J_b\rangle_z\langle\mathcal{O}_1\mathcal{O}_2\rangle_z}=\left(\frac{z_{12}^2}{\mathbb{J}_1\mathbb{J}_2 w_{12}^2}\right)^{h_{\mathcal{O}}}=\left(\frac{\alpha^2u^2(1-u)^{\alpha-1}}{(1-(1-u)^\alpha)^2}\right)^{h_{\mathcal{O}}},\qquad u=\frac{z_{12}z_{ab}}{z_{1a}z_{2b}} \tag{3.190}$$

which has branch cut of u from 1 to $+\infty$.

We are interested in cases with even number $\mathcal{O}$ insertion. In leading order, this can be calculated as

$$\frac{\langle J_a J_b\mathcal{O}_1\cdots\mathcal{O}_{2n}\rangle_z}{\langle J_a J_b\rangle_z}=\frac{\mathbb{J}_a^{-h_J}\mathbb{J}_b^{-h_J}}{\langle J_a J_b\rangle_z}\left(\prod_{i=1}^{2n}\mathbb{J}_i^{-h_{\mathcal{O}}}\right)\langle J_a J_b\mathcal{O}_1\cdots\mathcal{O}_{2n}\rangle_w$$

$$
\begin{aligned}
&\approx \left(\prod_{i=1}^{2n} \mathbb{J}_i^{-h_{\mathcal{O}}}\right) \langle 0_w | \mathcal{O}_1 \cdots \mathcal{O}_{2n} \rangle_w \\
&\approx \left(\prod_{i=1}^{2n} \mathbb{J}_i^{-h_{\mathcal{O}}}\right) \sum_{\{(s_{2i}, s_{2i+1})\}} \prod_{i=1}^{n} \langle 0_w | \mathcal{O}_{s_{2i}} \mathcal{O}_{s_{2i+1}} \rangle_w \\
&= \sum_{\{(s_{2i}, s_{2i+1})\}} \prod_{i=1}^{n} \left[\left(\frac{z_{s_{2i}, s_{2i+1}}^2}{\mathbb{J}_{s_{2i}} \mathbb{J}_{s_{2i+1}} w_{s_{2i}, s_{2i+1}}^2} \right)^{h_{\mathcal{O}}} \langle \mathcal{O}_{s_{2i}} \mathcal{O}_{s_{2i+1}} \rangle_z \right] \\
&= \sum_{\{(s_{2i}, s_{2i+1})\}} \prod_{i=1}^{n} \left[\mathcal{V}(u_{s,i}) \langle \mathcal{O}_{s_{2i}} \mathcal{O}_{s_{2i+1}} \rangle_z \right], \qquad u_{s,i} \equiv \frac{z_{s_{2i}, s_{2i+1}} z_{ab}}{z_{s_{2i},a} z_{s_{2i+1},b}}
\end{aligned} \tag{3.191}
$$

where $\{(s_{2i}, s_{2i+1})\}$ is the collection of contractions between s_{2i}-th and s_{2i+1}-th operators. In the second line we ignored higher orders of $1/c$, and in third line we used large $\mathcal{N}$ (large c) ansatz to factorize all $\mathcal{O}$'s in two point functions. Associated with antiholomorphic part, (3.191) becomes (3.81).

3.C.3 Explicit expression of A

Here we give an explicit derivation of (3.86) from (3.84) for $t_s = t$ and $x_s = x$. The discussion of this subsection has some parallel to that of [64] for OTOCs in a large c CFT.

From (3.79), $\mathcal{V}(u)$ is real for $u < 1$ and has a branch cut along $u \in (1, \infty)$. With $t_s = t, x_s = x$ we have

$$
u_1 = \frac{4 e^{\frac{2\pi}{\beta} y_+}}{(e^{i\epsilon_1} - e^{\frac{2\pi}{\beta} y_+ + i\epsilon_J})(e^{\frac{2\pi}{\beta} y_+ + i\tilde{\epsilon}_J} - e^{i\tilde{\epsilon}_1})}, \quad \bar{u}_1 = \frac{4 e^{\frac{2\pi}{\beta} y_-}}{(e^{-i\epsilon_1} - e^{\frac{2\pi}{\beta} y_- - i\epsilon_J})(e^{\frac{2\pi}{\beta} y_- - i\tilde{\epsilon}_J} - e^{-i\tilde{\epsilon}_1})} \tag{3.192}
$$

where we have introduced

$$
y_+ = x - x_1 + t, \qquad y_- = x - x_1 - t \ . \tag{3.193}
$$

Recall that $\mathcal{V}^+$ is defined with ordering $\epsilon_1 < \epsilon_J < \tilde{\epsilon}_J < \tilde{\epsilon}_1$, while $\mathcal{V}^-$ with ordering $\epsilon_J < \epsilon_1 < \tilde{\epsilon}_J < \tilde{\epsilon}_1$. Let us look at the behavior of $A(u_1, \bar{u}_1)$ as we increase t from 0 while keeping $x - x_1$ fixed (assuming $x - x_1$ is not exactly zero). For sufficiently small t, regardless of the sign of $x - x_1$, $(0, x_1)$ and (t, x) are spacelike separated, with $u_1, \bar{u}_1 < 0$. In this case ϵ's do not matter, and thus $\mathcal{V}^+ = \mathcal{V}^-$, leading to $A = 0$. This of course can be deduced from (3.83) without doing any calculations as the commutator of spacelike separated operators must vanish.

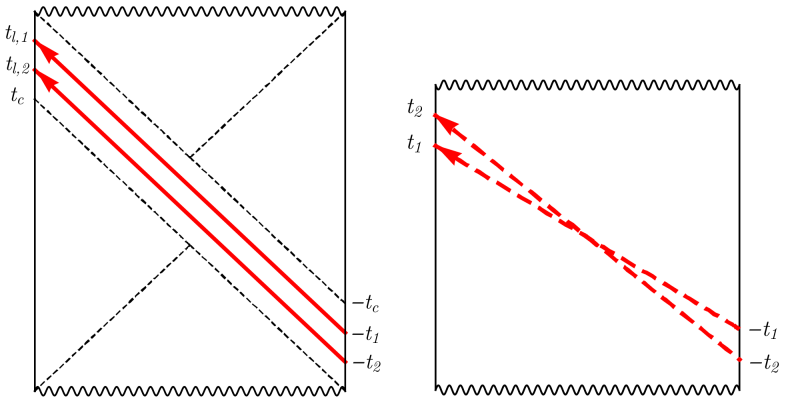

(a) (b)

Figure 3.10: The relation between emission time and arrival time in two different regimes. (a) is the semi-classical regime, in which the earlier a signal (smaller $-t_s$) is sent, the earlier (smaller t_l) the arrival of the signal at the other boundary. In particular, as $-t_s \to -\infty$, $t_l(t_s) \to t_c$ which is the earliest possible arrival time, and as $-t_s \to -t_c$, $t_l(t_s) \to +\infty$. (b) describes the situation of (3.135) and the CFT results of Sec. 3.4, where the arrival time t is the negative of emission time $-t_s$.

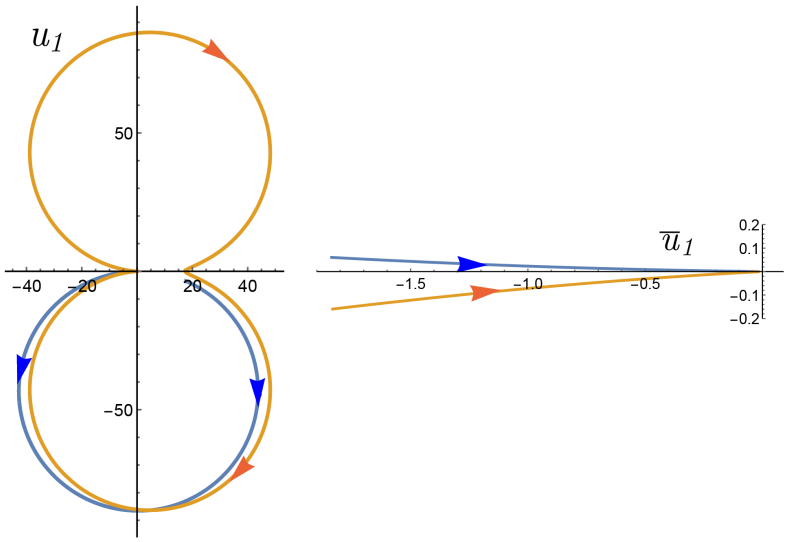

(a) (b)

Figure 3.11: Plots of u_1 (plot (a)) and $\bar{u}_1$ (plot (b)) as a function of t. Blue and yellow are for $\mathcal{V}^+$ and $\mathcal{V}^-$ respectively. One can see that u_1 stays on first sheet for $\mathcal{V}^+(u_1)$, but moves to second sheet for $\mathcal{V}^-(u_1)$; $\bar{u}_1$ stays on first sheet for both $\mathcal{V}^\pm(\bar{u}_1)$.

With sufficiently large t, $(0, x_1)$ and (t, x) become timelike separated. Consider, e.g. $x - x_1 < 0$, for which u_1 starts being negative at $t = 0$ and is again negative for large t, but in between u_1 undergoes nontrivial motions in the complex plane as the lightcone $y_+ = 0$ is crossed. For $\mathcal{V}^{(+)}$, one finds that u_1 remains on the first sheet throughout the process, while for $\mathcal{V}^{(-)}$, u_1 crosses the branch cut from upper half u-plane and moves to the second sheet. In contrast, $\bar{u}_1$ always remains real and negative. See Fig. 3.11. We thus find that for sufficiently large t,

$$A(u_1, \bar{u}_1) = (\mathcal{V}_1(u_1) - \mathcal{V}_2(u_1))\mathcal{V}_1(\bar{u}_1), \quad x - x_1 < 0 \tag{3.194}$$

where $\mathcal{V}_1(u)$ ($\mathcal{V}_2(u)$) denotes the value along the negative real axis on the first (second) sheet,

$$\mathcal{V}_1(u) = \left(\frac{\alpha(-u)}{\sqrt{1-u}} \frac{1}{-(1-u)^{-\alpha/2} + (1-u)^{\alpha/2}}\right)^{2h_\mathcal{O}}, \tag{3.195}$$

$$\mathcal{V}_2(u) = \left(\frac{\alpha(-u)}{\sqrt{1-u}} \frac{1}{(1-u)^{-\alpha/2} e^{i\pi\alpha} - (1-u)^{\alpha/2} e^{-i\pi\alpha}}\right)^{2h_\mathcal{O}} . \tag{3.196}$$

Similarly for $x_s - x_1 > 0$ we find that, u_1 always remains real, negative, but $\bar{u}_1$ moves nontrivially in the complex plane as the light cone is crossed. Again one finds that $\mathcal{V}^{(+)}$ remains on the first sheet, while $\mathcal{V}^{(-)}$ moves to the second sheet from above. We thus find

$$A(u_1, \bar{u}_1) = (\mathcal{V}_1(\bar{u}_1) - \mathcal{V}_2(\bar{u}_1))\mathcal{V}_1(u_1), \quad x - x_1 > 0 \, . \tag{3.197}$$

One consistent check is that (3.194) and (3.197) agree when $x = x_1$. We can write (3.194) and (3.197) in a unified way as

$$A(u_1, \bar{u}_1) = (\mathcal{V}_1(u_1) - \mathcal{V}_2(u_1))\mathcal{V}_1(\bar{u}_1) \tag{3.198}$$

with now u_1 and $\bar{u}_1$ defined as

$$u_1 \equiv -\frac{4e^{\frac{2\pi}{\beta}(t-|x-x_1|)}}{(1-e^{\frac{2\pi}{\beta}(t-|x-x_1|)})^2}, \qquad \bar{u}_1 \equiv -\frac{4e^{\frac{2\pi}{\beta}(t+|x-x_1|)}}{(1-e^{\frac{2\pi}{\beta}(t+|x-x_1|)})^2} \, . \tag{3.199}$$

3.D Full k-dependence in multiple operator species

In this appendix, we will use the following notation:

$$W = \sum_{n=0}^{\infty} \frac{(-ig)^n}{n!} \sum_{\{\alpha_i\}} W_n, \quad W_n = \frac{1}{k^n} \left\langle [\mathcal{O}_{\alpha_n}, [\mathcal{O}_{\alpha_{n-1}}, \cdots [\mathcal{O}_{\alpha_1}, J] \cdots] \; \tilde{J} \tilde{\mathcal{O}}_{\alpha_n} \cdots \tilde{\mathcal{O}}_{\alpha_1} \right\rangle_\beta \tag{3.200}$$

where we suppressed all spacetime coordinates. In order to calculate W in the case of multiple operator species, we need to note that there are three types of contractions,

$$G\delta_{\alpha_i\alpha_j} \equiv \left\langle \mathcal{O}_{\alpha_i}\tilde{\mathcal{O}}_{\alpha_j}\right\rangle, \quad H\delta_{\alpha_i\alpha_j} \equiv \left\langle \mathcal{O}_{\alpha_i}\mathcal{O}_{\alpha_j}\right\rangle, \quad \tilde{H}\delta_{\alpha_i\alpha_j} \equiv \left\langle \tilde{\mathcal{O}}_{\alpha_i}\tilde{\mathcal{O}}_{\alpha_j}\right\rangle \tag{3.201}$$

where we used the fact that all locations of $\mathcal{O}$ and $\tilde{\mathcal{O}}$ are the same and at origin.

Since (3.81) is factorized as product of 4-pt functions encoded in $\mathcal{V}(u_i)\mathcal{V}(\bar{u}_i)$, to calculate W_n we only need to worry about the relative ordering of the four operators related to each u_i and $\bar{u}_i$. For G type contraction, there are two different orderings: $\langle 1ab\tilde{1}\rangle$ and $\langle a1b\tilde{1}\rangle$, which are $\mathcal{V}_1(u)\mathcal{V}_1(\bar{u})$ and $\mathcal{V}_2(u)\mathcal{V}_1(\bar{u})$ respectively. For H type contraction, there are four different orderings: $\langle 12ab\rangle$, $\langle 1a2b\rangle$, $\langle 2a1b\rangle$ and $\langle a21b\rangle$ which are $\mathcal{V}_1(\mu)\mathcal{V}_1(\bar{\mu})$, $\mathcal{V}_{-1}(\mu)\mathcal{V}_1(\bar{\mu})$, $\mathcal{V}_2(-\mu)\mathcal{V}_1(-\bar{\mu})$ and $\mathcal{V}_1(-\mu)\mathcal{V}_1(-\bar{\mu})$ respectively (see Fig. 3.12). For $\tilde{H}$ type contraction, there is only one ordering: $\langle ab\tilde{2}\tilde{1}\rangle$, which is $\mathcal{V}_1(\mu)\mathcal{V}_1(\bar{\mu})$. Here the subscript i of $\mathcal{V}_i$ means the value on i-th sheet given by (3.87), (3.88) and

$$\mathcal{V}_{-1}(u) = \left(\frac{\alpha(-u)}{\sqrt{1-u}}\frac{1}{(1-u)^{-\alpha/2}e^{-i\pi\alpha}-(1-u)^{\alpha/2}e^{i\pi\alpha}}\right)^{2h_{\mathcal{O}}} \tag{3.202}$$

In all above statements, the cross ratios are $u = u_1$ in (3.199) with $x_1 = 0$ and

$$\mu = \frac{2i\sin\frac{\pi\epsilon}{\beta}}{\sinh\frac{2\pi}{\beta}(t-|x|)+2i\sin\frac{\pi\epsilon}{\beta}}, \quad \bar{\mu} = \frac{2i\sin\frac{\pi\epsilon}{\beta}}{\sinh\frac{2\pi}{\beta}(t+|x|)+2i\sin\frac{\pi\epsilon}{\beta}}, \quad 0<\epsilon<\beta \tag{3.203}$$

where ϵ is the difference of ϵ-prescription in the time ordering of $\mathcal{O}_1$ and $\mathcal{O}_2$ and it now plays a role as UV regulator [22].

[22] In order to evaluate the Lorentzian correlation function in (3.81) one has to assign ϵ_i for each $\mathcal{O}_i$ before

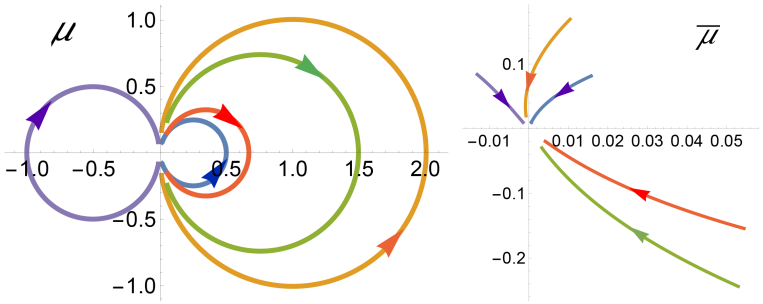

Figure 3.12: The plot of μ and $\bar{\mu}$. The blue, yellow, green, red and purple are for $\langle 12ab\rangle$, $\langle 1a2b\rangle$, $\langle 2a1b\rangle$, $\langle a21b\rangle$ and $\langle ab\tilde{2}\tilde{1}\rangle$ respectively.

For any given choice of contractions, the number of H contraction must be the same as $\tilde{H}$. To be more precise, with q contractions of H, then number of $\tilde{H}$ is q and the number of G is $n-2q$. In such a contraction, the scaling of (3.81) is $H^q\tilde{H}^qG^{n-2q}$. If we track all commutators in W_n, we will find that the contribution from this contraction is

$$\begin{aligned} W_n/\langle J_aJ_b\rangle \supset & C_qH^q\left[(\mathcal{V}_1(\mu)-\mathcal{V}_{-1}(\mu))\mathcal{V}_1(\bar{\mu})+(\mathcal{V}_1(-\mu)-\mathcal{V}_2(-\mu))\mathcal{V}_1(-\bar{\mu})\right]^q \\ & \times\tilde{H}^q\left[\mathcal{V}_1(\mu)\mathcal{V}_1(\bar{\mu})\right]^qG^{n-2q}\left[(\mathcal{V}_1(u)-\mathcal{V}_2(u))\mathcal{V}_1(\bar{u})\right]^{n-2q} \end{aligned} \tag{3.204}$$

where C_q is a constant. A consistent check is that in (3.204) there are in total $4^q\cdot 2^{n-2q}=2^n$ terms, which is the same number of terms in the expansion of commutators (3.74). In general, C_q depends on how we choose the q contractions. However, the structure of conformal blocks does not depend on the detail of the q contraction choices. This implies a simple counting rule for W_n: we only need to track the contractions of H, $\tilde{H}$ and G, then replace all $H\tilde{H}$ as H_0^2 and G as G_0, where we define

$$H_0^2=H\tilde{H}\left[(\mathcal{V}_1(\mu)-\mathcal{V}_{-1}(\mu))\mathcal{V}_1(\bar{\mu})+(\mathcal{V}_1(-\mu)-\mathcal{V}_2(-\mu))\mathcal{V}_1(-\bar{\mu})\right]\mathcal{V}_1(\mu)\mathcal{V}_1(\bar{\mu}) \tag{3.205}$$

$$G_0=G(\mathcal{V}_1(u)-\mathcal{V}_2(u))\mathcal{V}_1(\bar{u}) \tag{3.206}$$

Hence, evaluation of W_n boils down to the problem of calculating C_q for various contractions. In the following, since $H=\tilde{H}$ by definition, we will not distinguish them and only use H.

To count C_q is somewhat tricky. Due to the factor $1/k^n$ in W_n, any $\mathcal{O}_\alpha$ contracting with its dual $\tilde{\mathcal{O}}_\alpha$ contributes with $\sum_\alpha\delta_{\alpha\alpha}/k=1$, but contracting with any other operators contributes with only $1/k$. Keeping this in mind, we will use the following procedure:

1. For n pairs of $\mathcal{O}_{\alpha_s}$ and $\tilde{\mathcal{O}}_{\alpha_s}$, we define the sum of all possible contractions as S_n. Starting from $\mathcal{O}_{\alpha_1}$, there are two types of contraction: i) contracting $\tilde{\mathcal{O}}_{\alpha_1}$ gives G; ii) $n-1$ choices of contracting with $\mathcal{O}_{\alpha_i}$ with $i\neq 1$ in total give $(n-1)H/k$; iii) $n-1$ contracting with $\tilde{\mathcal{O}}_{\alpha_i}$ with $i\neq 1$ in total give $(n-1)G/k$. For i), we call it as completing a chain. Then redo step 1 with the next $\mathcal{O}$, say $\mathcal{O}_{\alpha_2}$. For ii), do step 2. For iii), do step 3.

2. For ii) in step 1, continue with its counterpart $\tilde{\mathcal{O}}_{\alpha_i}$. We define the sum of all possible contractions in such case, namely $n-2$ pairs of $\mathcal{O}_{\alpha_s}$ and $\tilde{\mathcal{O}}_{\alpha_s}$ and two $\tilde{\mathcal{O}}$'s (namely $\tilde{\mathcal{O}}_{\alpha_1}$ and $\tilde{\mathcal{O}}_{\alpha_i}$), as T_{n-2}. We have three choices: i) contracting with $\tilde{\mathcal{O}}_{\alpha_1}$ completes a chain and gives H; ii) $n-2$ choices of contracting with $\mathcal{O}_{\alpha_j}$ with $j\neq 1,i$ in total give $(n-2)G/k$; iii) $n-2$ contracting with $\tilde{\mathcal{O}}_{\alpha_j}$ with $j\neq 1,i$ in total give $(n-2)H/k$.

---

continuation. Since all the $\mathcal{O}$'s commute, the relative values of their ϵ's do not matter. Therefore we can assign ϵ ordering for each pairing such that ϵ for each Virasoro block is the same. Physically it is natural to take ϵ of order $O(\beta)$, and in the main body of this paper, we will choose $\epsilon=\beta/2$ for definiteness.

3. For iii) in step 1, continue with its counterpart $\mathcal{O}_{\alpha_i}$. We define the sum of all possible contractions in such case, namely $n-2$ pairs of $\mathcal{O}_{\alpha_k}$ and $\tilde{\mathcal{O}}_{\alpha_k}$ plus one pair of $\mathcal{O}_{\alpha_1}$ and $\tilde{\mathcal{O}}_{\alpha_i}$ with different indicies, as U_{n-2}. We have three choices: i) contracting with $\tilde{\mathcal{O}}_{\alpha_1}$ completes a chain and gives G; ii) $n-2$ choices of contracting with $\mathcal{O}_{\alpha_j}$ with $j \neq 1, i$ in total give $(n-2)H/k$; iii) $n-2$ contracting with $\tilde{\mathcal{O}}_{\alpha_j}$ with $j \neq 1, i$ in total give $(n-2)G/k$.

4. In step 1, completing a chain becomes S_{n-1}. In step 2, i) becomes S_{n-2}, ii) becomes T_{n-3}, and iii) becomes U_{n-3}. In step 3, i) becomes S_{n-2}, ii) becomes T_{n-3}, and iii) becomes U_{n-3}. For any $S_\#$ cases, do step 1, for any $T_\#$ cases, do step 2, and for any $U_\#$ cases, do step 3. This process ends when we finish all contractions.

By above constructive procedure, we have the following induction relations:

$$S_n = GS_{n-1} + (n-1)G/kU_{n-2} + (n-1)H/kT_{n-2} \tag{3.207}$$
$$U_n = GS_n + nG/kU_{n-1} + nH/kT_{n-1} \tag{3.208}$$
$$T_n = HS_n + nG/kT_{n-1} + nH/kU_{n-1} \tag{3.209}$$

Comparing (3.207) with (3.208), we find $S_n = U_{n-1}$. Plug this back and cancel T_n. The induction relation of S_n turns out to be

$$S_{n+2} = G\left(1 + \frac{2(n+1)}{k}\right) S_{n+1} + (H^2 - G^2)\frac{n+1}{k}\left(1 + \frac{n}{k}\right) S_n \tag{3.210}$$

To solve this induction relation, define $\gamma = H^2/G^2 - 1$ and $S_n \to G^n S_n$. (3.210) becomes

$$S_{n+2} = \left(1 + \frac{2(n+1)}{k}\right) S_{n+1} + \frac{n+1}{k}\left(1 + \frac{n}{k}\right)\gamma S_n \tag{3.211}$$

We can check first a few terms explicitly starting with $S_1 = 1$ and $S_0 = 1$, which suggests that S_n should be a polynomial like

$$S_n = \sum_{i=0}^{[n/2]} a_i(n)\gamma^i \tag{3.212}$$

Taking this ansatz, the induction splits into even and odd cases of n. Plug this into (3.211) and compare the coefficients of γ^i. For $n = 2p$,

$$a_i(2p+2) = \frac{4p+k+2}{k} a_i(2p+1) + \frac{(2p+1)(2p+k)}{k^2} a_{i-1}(2p),\ i = 1, \cdots, p \tag{3.213}$$

$$a_{p+1}(2p+2) = \frac{(2p+1)(2p+k)}{k^2} a_p(2p) \tag{3.214}$$

$$a_0(2p+2) = \frac{4p+k+2}{k} a_0(2p+1) \tag{3.215}$$

For $n = 2p-1$,

$$a_i(2p+1) = \frac{4p+k}{k} a_i(2p) + \frac{2p(2p+k-1)}{k^2} a_{i-1}(2p-1),\ i = 1, \cdots, p \tag{3.216}$$

$$a_0(2p+1) = \frac{4p+k}{k} a_0(2p) \tag{3.217}$$

Solving (3.214) gives

$$a_p(2p) = \frac{(2p-1)!!(2p+k-2)!!}{k^{2p-1}k!!} \tag{3.218}$$

Solving (3.215) and (3.217) gives

$$a_0(n) = \frac{(2n+k-2)!!}{k^{n-1}k!!} \tag{3.219}$$

Multiply (3.216) with $\frac{4p+k+2}{k}$ and sum with (3.213). We get

$$\begin{aligned} a_i(2p+2) =& \frac{(4p+k+2)(4p+k)}{k^2} a_i(2p) + \frac{2p(2p+k-1)(4p+k+2)}{k^3} a_{i-1}(2p-1) \\ &+ \frac{(2p+1)(2p+k)}{k^2} a_{i-1}(2p) \end{aligned} \tag{3.220}$$

Let us check a few i's to see if any rule exists. Setting $i = 1$ and using (3.219) leads to

$$a_1(2p+2) = \frac{(4p+k+2)(4p+k)}{k^2} a_1(2p) + \frac{(4p+k-4)!!}{k^{2p-1}k!!} \cdot \frac{(4p+k)(8p^2+4kp+k-2)}{k^2} \tag{3.221}$$

Taking the ansatz

$$a_1(2p) = \frac{(4p+k-4)!!}{k^{2p-1}k!!} \bar{a}_1(2p) \tag{3.222}$$

the induction is simplified as

$$(4p+k-2)\bar{a}_1(2p+2) = (k+4p+2)\bar{a}_1(2p) + (8p^2+4kp+k-2) \tag{3.223}$$

This is very easy to solve if we assume $\bar{a}_1(2p)$ is a qudratic polynomial of p. Using the initial condition $\bar{a}_1(2) = 1$ from (3.218), we solve it as $\bar{a}_1(2p) = p(2p-1)$ and

$$a_1(2p) = \frac{(4p+k-4)!!}{k^{2p-1}k!!} p(2p-1) \tag{3.224}$$

With (3.216), we also get

$$a_1(2p+1) = \frac{(4p+k-2)!!}{k^{2p}k!!}p(2p+1) \tag{3.225}$$

We can follow the induction relation again to solve $a_2(2p)$ and $a_2(2p+1)$. It turns out that

$$a_2(2p) = \frac{(4p+k-6)!!}{k^{2p-1}k!!}\cdot\frac{p(p-1)}{2}\cdot(2p-1)(2p-3) \tag{3.226}$$

$$a_2(2p+1) = \frac{(4p+k-4)!!}{k^{2p}k!!}\cdot\frac{p(p-1)}{2}\cdot(2p+1)(2p-1) \tag{3.227}$$

It is very tempting to guess the following general formula

$$a_i(2p) = \frac{(4p+k-2i-2)!!}{k^{2p-1}k!!}\cdot\frac{p!}{(p-i)!i!}\cdot\frac{(2p-1)!!}{(2p-2i-1)!!} \tag{3.228}$$

$$a_i(2p+1) = \frac{(4p+k-2i)!!}{k^{2p}k!!}\cdot\frac{p!}{(p-i)!i!}\cdot\frac{(2p+1)!!}{(2p-2i+1)!!} \tag{3.229}$$

One can easily check that this ansatz solves the induction relations (3.213)-(3.217). Substitute the solution to (3.212), and we get

$$\begin{aligned} S_n &= \frac{k^{1-n}(2n+k-2)!!}{k!!}{}_2F_1(\frac{1}{2}-\frac{n}{2},-\frac{n}{2},1-\frac{k}{2}-n,-\gamma) \\ &= \frac{k^{1-n}(2n+k-2)!!}{k!!}(1+\gamma)^{n/2}{}_2F_1(-n,1-k-n,1-\frac{k}{2}-n,\frac{\sqrt{1+\gamma}-1}{2\sqrt{1+\gamma}}) \\ &= (k)_n\left(\frac{1+\sqrt{1+\gamma}}{k}\right)^n{}_2F_1(-n,\frac{k}{2},k,\frac{2\sqrt{1+\gamma}}{\sqrt{1+\gamma}+1}) \end{aligned} \tag{3.230}$$

where in the second line we used identity [63]

$${}_2F_1(a,a+\frac{1}{2},c,z) = (1-z)^{-a}{}_2F_1(2a,2c-2a-1,c,\frac{\sqrt{1-z}-1}{2\sqrt{1-z}}) \tag{3.231}$$

and in the third line we used the reduction formula

$${}_2F_1(-n,b,c,z) = \frac{(b)_n}{(c)_n}(1-z)^n{}_2F_1(-n,c-b,1-b-n,\frac{1}{1-z}) \tag{3.232}$$

Indeed, given (3.230), (3.211) is exactly the contiguous relation of hypergeometric function

$$(c-a){}_2F_1(a-1,b,c;z)+(2a-c+(b-a)z){}_2F_1(a,b,c;z)+a(z-1){}_2F_1(a+1,b,c;z) = 0 \tag{3.233}$$

for $a=-n-1$, $b=k/2$, $c=k$ and $z=\frac{2\sqrt{1+\gamma}}{\sqrt{1+\gamma}+1}$.

Note that $W_n = G^n S_n$ with replacement $H^2 \to H_0^2$ and $G \to G_0$. It is ready to calculate W [23]

$$W/\left\langle J\tilde{J}\right\rangle = \sum_{n=0}^{\infty}\frac{1}{n!}(-ig)^n G_0^n S_n = \left(1+\frac{ig(G_0+H_0)}{k}\right)^{-k/2}\left(1+\frac{ig(G_0-H_0)}{k}\right)^{-k/2} \tag{3.234}$$

where we used the fact

$$\sum_{n=0}^{\infty}\frac{(c-a)_n}{n!}t^n {}_2F_1(a-n,b,c,x) = \frac{(1-t)^{a-c}}{(1-x)^b}{}_2F_1(c-a,b,c,\frac{x}{(1-x)(t-1)}) \tag{3.235}$$

3.E Robustness of regenesis

For the deformed thermofield double state $\gamma^L(t_0,x_0)\left|\Psi\right\rangle$, we will calculate $G^{LR}(t,t_s)$ in this appendix to see how the regenesis is affected.

The left and right two point function in this deformed state is

$$W_\gamma \equiv \frac{\left\langle\Psi\right|\gamma^L(t_0)e^{-igV}J^L(t)e^{igV}J^R(-t_s)\gamma^L(t_0)\left|\Psi\right\rangle}{\left\langle\Psi\right|\gamma^L(t_0)\gamma^L(t_0)\left|\Psi\right\rangle} \tag{3.236}$$

where the spatial coordinates are suppressed. Similar to (3.69), using BCH formula, it becomes

$$W_\gamma = \sum_{n=0}^{\infty}\frac{(-ig)^n}{n!L^n}\int_{-\frac{L}{2}}^{\frac{L}{2}}\left(\prod_{k=1}^{n}dx_k\right)W_{\gamma,n} \tag{3.237}$$

with

$$W_{\gamma,n} = \frac{\left\langle\gamma[\mathcal{O}_n,[\mathcal{O}_{n-1},\cdots[\mathcal{O}_1,J]\cdots]\gamma\tilde{J}\tilde{\mathcal{O}}_n\cdots\tilde{\mathcal{O}}_1\right\rangle_\beta}{\left\langle\gamma\gamma\right\rangle_\beta} \tag{3.238}$$

where each term in the commutator is

$$w_{\gamma,n} \equiv \frac{\left\langle\gamma_A\gamma_B J_a J_b\mathcal{O}_1\cdots\mathcal{O}_{2n}\right\rangle}{\left\langle\gamma_A\gamma_B\right\rangle} \tag{3.239}$$

in which the coordinate of γ is z_A and z_B.

[23] The convergence of series requires $|g(G_0\pm H_0)/k|<1$. For large $k\to\infty$ any g is allowed, but in $k=1$ g is bounded above. However, we will treat W as an analytic function of t and t_s. Note that in small t,t_s case, G_0 and H_0 are close to zero, which releases the upper bound of g.

Assuming $c \gg h_\gamma \gg h_J$, we could first do a conformal transformation with respect to γ^L by introducing a branch cut from z_A to z_B

$$1-v=\left(1-\frac{z_{AB}z}{z_B(z_A-z)}\right)^{\eta},\ \eta=\sqrt{1-24\frac{h_\gamma}{c}} \tag{3.240}$$

with a Jacobian

$$\widehat{\mathbb{J}}(z)\equiv\frac{\partial z}{\partial v}=\frac{(z-z_A)(z-z_B)}{\eta z_{AB}}\left[\frac{z_A(z-z_B)}{z_B(z-z_A)}\right]^{-\eta} \tag{3.241}$$

Similar to (3.191), (3.239) becomes

$$\begin{aligned} w_{\gamma,n}&=\frac{\widehat{\mathbb{J}}_a^{-h_\gamma}\widehat{\mathbb{J}}_b^{-h_\gamma}}{\langle\gamma_A\gamma_B\rangle_z}\left(\widehat{\mathbb{J}}_a^{-h_J}\widehat{\mathbb{J}}_b^{-h_J}\prod_{i=1}^{2n}\widehat{\mathbb{J}}_i^{-h_\mathcal{O}}\right)\langle\gamma_A\gamma_B J_aJ_b\mathcal{O}_1\cdots\mathcal{O}_{2n}\rangle_v \\ &\approx\left(\widehat{\mathbb{J}}_a^{-h_J}\widehat{\mathbb{J}}_b^{-h_J}\prod_{i=1}^{2n}\widehat{\mathbb{J}}_i^{-h_\mathcal{O}}\right)\langle 0_v|J_aJ_b\mathcal{O}_1\cdots\mathcal{O}_{2n}\rangle_v \end{aligned} \tag{3.242}$$

For the expectation value in v plane $\langle 0_v|J_aJ_b\mathcal{O}_1\cdots\mathcal{O}_{2n}\rangle_v$, since $\langle 0_v|$ behaves exactly as ordinary vacuum state, we can apply the same technique to simply it. Previous result (3.191) applies with a simple coordinate replacement $z\to v$. After some manipulation, it turns out that

$$w_{\gamma,n}\approx\langle J_aJ_b\rangle_z\,\mathcal{U}_\eta(u_J)\sum_{\{(s_{2i},s_{2i+1})\}}\prod_{i=1}^{n}\left[\mathcal{V}_\eta(u_{s,i})\mathcal{V}_\alpha(r_{s,i})\left\langle\mathcal{O}_{s_{2i}}\mathcal{O}_{s_{2i+1}}\right\rangle_z\right] \tag{3.243}$$

where

$$\mathcal{U}_\eta(u)=\left(\frac{\eta^2u^2(1-u)^{\eta-1}}{(1-(1-u)^\eta)^2}\right)^{h_J},\quad \mathcal{V}_\eta(u)=\left(\frac{\eta^2u^2(1-u)^{\eta-1}}{(1-(1-u)^\eta)^2}\right)^{h_\mathcal{O}} \tag{3.244}$$

and

$$u_J\equiv\frac{z_{ab}z_{AB}}{z_{aA}z_{bB}},\quad u_{s,i}\equiv\frac{z_{s_{2i},s_{2i+1}}z_{AB}}{z_{s_{2i},A}z_{s_{2i+1},B}},\quad r_{s,i}\equiv\frac{v_{s_{2i},s_{2i+1}}v_{ab}}{v_{s_{2i},a}v_{s_{2i+1},b}} \tag{3.245}$$

where the new variable $v=v(z)$ is given by (3.240). The antiholomorphic part is parallel with above discussion.

It is clear that from (3.238), the relative ordering among γ, J and $\tilde{J}$ is always fixed as $\left\langle\gamma_AJ\gamma_B\tilde{J}\right\rangle$, and that among γ, $\mathcal{O}$ and $\tilde{\mathcal{O}}$ is also fixed as $\left\langle\gamma_A\mathcal{O}_i\gamma_B\tilde{\mathcal{O}}_i\right\rangle$. The commutators in (3.238) will only be affected by the relative ordering among $\mathcal{O}$, J and $\tilde{J}$, and this leads (3.238) to

$$W_{\gamma,n}=\langle J_aJ_b\rangle\,\mathcal{U}_\eta(u_{ab})\mathcal{U}_\eta(\bar{u}_{ab})\sum_{\text{all pairings}}\prod_{i=1}^{n}\left[\mathcal{V}_\eta(u_i)\mathcal{V}_\eta(\bar{u}_i)A_\alpha(r_i,\bar{r}_i)\left\langle\mathcal{O}_{i1}\mathcal{O}_{i2}\right\rangle\right] \tag{3.246}$$

where A_α is the difference of two orderings $\left\langle \mathcal{O}J\tilde{J}\tilde{\mathcal{O}}\right\rangle$ and $\left\langle J\mathcal{O}\tilde{J}\tilde{\mathcal{O}}\right\rangle$

$$A_\alpha(r_i,\bar{r}_i)\equiv \mathcal{V}^+_\alpha(r_i)\mathcal{V}^+_\alpha(\bar{r}_i)-\mathcal{V}^-_\alpha(r_i)\mathcal{V}^-_\alpha(\bar{r}_i) \tag{3.247}$$

It follows that for large k and large L cases, we have

$$\frac{W_\gamma}{\langle J_aJ_b\rangle}=\mathcal{U}_\eta(u_J)\mathcal{U}_\eta(\bar{u}_J)\times\begin{cases}\exp\left(-igG\mathcal{V}_\eta(u_0)\mathcal{V}_\eta(\bar{u}_0)A_\alpha(r_0,\bar{r}_0)\right) & \text{large } k\\ \exp\left(-\frac{igG}{L}\int_{-L/2}^{L/2}dx_1\mathcal{V}_\eta(u_1)\mathcal{V}_\eta(\bar{u}_1)A_\alpha(r_1,\bar{r}_1)\right) & \text{large } L\end{cases} \tag{3.248}$$

where subscript 0 means taking $x_1=0$. In these formula, $\mathcal{V}_\eta$ can be absorbed into the definition of coefficient g (at least in large k case), and the prefactor $\mathcal{U}_\eta$ controls the overall traversability. In the main body of this paper, we use a simpler notation $\mathcal{J}(t,t_0)\equiv\mathcal{U}_\eta(u_J)\mathcal{U}_\eta(\bar{u}_J)$ and $\mathcal{G}(t,t_0;x_1)\equiv\mathcal{V}_\eta(u_1)\mathcal{V}_\eta(\bar{u}_1)$.

To be more precise, let us study the value of these conformal blocks in ϵ-prescription. For $\mathcal{U}_\eta$ and $\mathcal{V}_\eta$, we assign $\epsilon_A<\{\epsilon_J,\epsilon_1\}<\epsilon_B$ and any positive small value for $\tilde{\epsilon}_J$ and $\tilde{\epsilon}_1$ in

$$u_J=-\frac{e^{\frac{2\pi}{\beta}(t_0+x_0)}(e^{\frac{2\pi}{\beta}(x+t)+i\epsilon_J}+e^{\frac{2\pi}{\beta}(x_s+t_s)+i\tilde{\epsilon}_J})(e^{i\epsilon_A}-e^{i\epsilon_B})}{(e^{\frac{2\pi}{\beta}(x+t)+i\epsilon_J}-e^{\frac{2\pi}{\beta}(x_0+t_0)+i\epsilon_A})(e^{\frac{2\pi}{\beta}(x_s+t_s)+i\tilde{\epsilon}_J}+e^{\frac{2\pi}{\beta}(x_0+t_0)+i\epsilon_B})} \tag{3.249}$$

$$\bar{u}_J=-\frac{e^{\frac{2\pi}{\beta}(x_0-t_0)}(e^{\frac{2\pi}{\beta}(x-t)-i\epsilon_J}+e^{\frac{2\pi}{\beta}(x_s-t_s)-i\tilde{\epsilon}_J})(e^{-i\epsilon_A}-e^{-i\epsilon_B})}{(e^{\frac{2\pi}{\beta}(x-t)-i\epsilon_J}-e^{\frac{2\pi}{\beta}(x_0-t_0)-i\epsilon_A})(e^{\frac{2\pi}{\beta}(x_s-t_s)-i\tilde{\epsilon}_J}+e^{\frac{2\pi}{\beta}(x_0-t_0)-i\epsilon_B})} \tag{3.250}$$

Similar for u_1 and $\bar{u}_1$ by setting $x=x_s=x_1$ and $t=t_s=0$ with corresponding ϵ. In general, we need to take all ϵ's to zero at the end of calculation, which seemingly leads to trivial u_J and $\bar{u}_J$. However, we could smear it for some small range in time for γ^L that equivalently sets ϵ_{AB} small but finite. For $t_s-t_0-|x_s-x_0|,\ t-t_0-|x-x_0|\gg\beta$, it is clear from (3.249) and (3.250) that

$$u_J\to -i(e^{-\frac{2\pi}{\beta}(x+t)}+e^{-\frac{2\pi}{\beta}(x_s+t_s)})e^{\frac{2\pi}{\beta}(t_0+x_0)}\epsilon_{AB},\ \bar{u}_J\to -i(e^{\frac{2\pi}{\beta}(x-t)}+e^{\frac{2\pi}{\beta}(x_s-t_s)})e^{\frac{2\pi}{\beta}(t_0-x_0)}\epsilon_{AB} \tag{3.251}$$

Similarly for $t_0-t_s-|x_s-x_0|,\ t_0-t-|x-x_0|\gg\beta$, we have

$$u_J\to i(e^{\frac{2\pi}{\beta}(x+t)}+e^{\frac{2\pi}{\beta}(x_s+t_s)})e^{-\frac{2\pi}{\beta}(t_0+x_0)}\epsilon_{AB},\quad \bar{u}_J\to i(e^{\frac{2\pi}{\beta}(t-x)}+e^{\frac{2\pi}{\beta}(t_s-x_s)})e^{\frac{2\pi}{\beta}(x_0-t_0)}\epsilon_{AB} \tag{3.252}$$

This shows that for finite ϵ_{AB}, u_J and $\bar{u}_J$ are suppressed by $|t_0-t_s|$ and $|t_0-t|$ exponentially.

Set $t=t_s$ and $x=x_s$, and check the contour of u_J and $\bar{u}_J$. For simplicity we will take $x_0-x>0$ from now on. We find that u_J is on -1-th sheet when $t-t_0>x_0-x$, and on first sheet when $t-t_0<x_0-x$. On the other hand, $\bar{u}_J$ is on second sheet when $t_0-t>x_0-x$,

and on first sheet when $t_0 - t < x_0 - x$. The value of $\mathcal{U}_\eta$ on either sheet is given by

$$\mathcal{U}_{\eta,-1}(u) = \left(\frac{\eta(-u)}{\sqrt{1-u}}\frac{1}{(1-u)^{-\eta/2}e^{-i\pi\eta} - (1-u)^{\eta/2}e^{i\pi\eta}}\right)^{2h_J} \tag{3.253}$$

$$\mathcal{U}_{\eta,1}(u) = \left(\frac{\eta(-u)}{\sqrt{1-u}}\frac{1}{-(1-u)^{-\eta/2} + (1-u)^{\eta/2}}\right)^{2h_J} \tag{3.254}$$

$$\mathcal{U}_{\eta,2}(u) = \left(\frac{\eta(-u)}{\sqrt{1-u}}\frac{1}{(1-u)^{-\eta/2}e^{i\pi\eta} - (1-u)^{\eta/2}e^{-i\pi\eta}}\right)^{2h_J} \tag{3.255}$$

Taking large c but $cu_J, c\bar{u}_J$ fixed limit and using (3.251) and (3.252), we see that

$$\mathcal{U}_\eta(u_J)\mathcal{U}_\eta(\bar{u}_J) \to \begin{cases} \left(1 - \frac{2h_\gamma}{\epsilon_{AB}}Q_J\right)^{-2h_J}, & \text{for } |t_0 - t| - |x_0 - x| \gg \beta \\ 1, & \text{for } |x_0 - x| - |t_0 - t| \gg \beta \end{cases} \tag{3.256}$$

where

$$Q_J = e^{\frac{2\pi}{\beta}(|t-t_0|-t_*-|x_0-x|)} \tag{3.257}$$

Similar results applies to u_1 and $\bar{u}_1$ in $\mathcal{V}_\eta$, which in the same limit gives

$$\mathcal{V}_\eta(u_1)\mathcal{V}_\eta(\bar{u}_1) \to \begin{cases} \left(1 - \frac{2h_\gamma}{\epsilon_{AB}}Q_1\right)^{-2h_\mathcal{O}}, & \text{for } |t_0| - |x_0 - x_1| \gg \beta \\ 1, & \text{for } |x_0 - x_1| - |t_0| \gg \beta \end{cases} \tag{3.258}$$

where

$$Q_1 = e^{\frac{2\pi}{\beta}(|t_0|-t_*-|x_0-x_1|)} \tag{3.259}$$

Since $\epsilon_{AB} < 0$, this shows that (3.256) and (3.258) are monotonically decreasing real function of t.

For the contour of r_1 and $\bar{r}_1$, one should first track the contour of various z coordinates in v plane. In the following we will only consider $x_1 < x < x_0$ [24]. Since the $z \to v(z)$ map has singularity at z_A, we set the ordering of ϵ's to be $\epsilon_A < \epsilon_1 < \epsilon_J < \epsilon_B$ and $\tilde{\epsilon}_J < \tilde{\epsilon}_1$ for $\mathcal{V}^+_\alpha$, and switch the ordering between ϵ_J and ϵ_1 for $\mathcal{V}^-_\alpha$. Start with $t = t_0 = 0$ and send t and t_0 to various value. In this process, for both orderings, we find that $v(z_a)$ and $v(z_1)$ moves to -1-th sheet when $t - t_0 > x_0 - x$ and $-t_0 > x_0 - x_1$ respectively, and $v(\bar{z}_a)$ and $v(\bar{z}_1)$ moves to second sheet when $t_0 - t > x_0 - x$ and $t_0 > x_0 - x_1$ respectively, in which

$$v_{-1} = 1 - e^{2\pi i\eta}\left(1 - \frac{z_{AB}z}{z_B(z_A - z)}\right)^\eta, \quad v_2 = 1 - e^{-2\pi i\eta}\left(1 - \frac{z_{AB}z}{z_B(z_A - z)}\right)^\eta \tag{3.260}$$

[24] For the case x_0 is in between x_1 and x (e.g. $x_1 < x_0 < x$), one will get trivial A_α that is not continuous in x_0 to the case $x_1 < x < x_0$. This means that our s-channel approximation does not hold in such a case.

while $v(z_b)$, $v(z_{\tilde{1}})$ and their antiholomorphic parts are all on the first sheet.

Take these values of v in r plane, we find that for $\mathcal{V}^+$ both r_1 and $\bar{r}_1$ stay in the first sheet, whereas for $\mathcal{V}^-$ r_1 stays in first sheet but $\bar{r}_1$ moves to second sheet when $t > x - x_1$ just like ordinary case. This leads to

$$A_\alpha(r_1, \bar{r}_1) = \mathcal{V}_{\alpha,1}(r_1)(\mathcal{V}_{\alpha,1}(\bar{r}_1) - \mathcal{V}_{\alpha,2}(\bar{r}_1)), \quad \text{for } t > x - x_1 \tag{3.261}$$

Taking large c and e^t/c fixed limit for $|t_0| \ll t_*$ and $|t - t_0| \ll t_*$ case, one can show that

$$A_\alpha \sim 1 - (1 + iQ)^{-2h_\mathcal{O}} \tag{3.262}$$

where Q is the same as (3.115). For general range of t_0, the calculation of A_α becomes tricky and we are not completely sure how to calculate it reliably in the s-channel approximation. Physically, we should expect $|A_\alpha|$ is bounded as a $O(1)$ function.

References

[1] O. Aharony, M. Berkooz, and B. Katz. Non-local effects of multi-trace deformations in the ads/cft correspondence. *Journal of High Energy Physics*, 2005(10):097, 2005.

[2] D. Amati, M. Ciafaloni, and G. Veneziano. Effective action and all order gravitational eikonal at Planckian energies. *Nucl. Phys.*, B403:707–724, 1993.

[3] R. E. Arias, M. Botta Cantcheff, and G. A. Silva. Lorentzian AdS, Wormholes and Holography. *Phys. Rev.*, D83:066015, 2011.

[4] D. Bak, C. Kim, and S.-H. Yi. Bulk view of teleportation and traversable wormholes. *JHEP*, 08:140, 2018.

[5] M. Banados, M. Henneaux, C. Teitelboim, and J. Zanelli. Geometry of the 2+ 1 black hole. *Physical Review D*, 48(4):1506, 1993.

[6] M. Banados, C. Teitelboim, and J. Zanelli. Black hole in three-dimensional spacetime. *Physical Review Letters*, 69(13):1849, 1992.

[7] N. Bao, A. Chatwin-Davies, J. Pollack, and G. N. Remmen. Traversable Wormholes as Quantum Channels: Exploring CFT Entanglement Structure and Channel Capacity in Holography. 2018.

[8] C. Barcelo and M. Visser. Traversable wormholes from massless conformally coupled scalar fields. *Phys. Lett.*, B466:127–134, 1999.

[9] T. Barrella, X. Dong, S. A. Hartnoll, and V. L. Martin. Holographic entanglement beyond classical gravity. *JHEP*, 09:109, 2013.

[10] M. Berkooz, A. Sever, and A. Shomer. Double-trace'deformations, boundary conditions and spacetime singularities. *Journal of High Energy Physics*, 2002(05):034, 2002.

[11] B. Bhawal and S. Kar. Lorentzian wormholes in Einstein-Gauss-Bonnet theory. *Phys. Rev.*, D46:2464–2468, 1992.

[12] M. Blake, H. Lee, and H. Liu. A quantum hydrodynamical description for scrambling and many-body chaos. 2017.

[13] R. Bousso. A Covariant entropy conjecture. *JHEP*, 07:004, 1999.

[14] R. Bousso, Z. Fisher, S. Leichenauer, and A. C. Wall. Quantum focusing conjecture. *Phys. Rev.*, D93(6):064044, 2016.

[15] P. Breitenlohner and D. Z. Freedman. Stability in gauged extended supergravity. *Annals of Physics*, 144(2):249–281, 1982.

[16] W. Bunting, Z. Fu, and D. Marolf. A coarse-grained generalized second law for holographic conformal field theories. *Class. Quant. Grav.*, 33(5):055008, 2016.

[17] E. Caceres, A. S. Misobuchi, and M.-L. Xiao. Rotating traversable wormholes in AdS. 2018.

[18] X. O. Camanho, J. D. Edelstein, J. Maldacena, and A. Zhiboedov. Causality Constraints on Corrections to the Graviton Three-Point Coupling. *JHEP*, 02:020, 2016.

[19] S. Carlip. The (2+ 1)-dimensional black hole. *Classical and Quantum Gravity*, 12(12):2853, 1995.

[20] J. Cotler and K. Jensen. A theory of reparameterizations for AdS_3 gravity. 2018.

[21] X. Dong, D. Harlow, and A. C. Wall. Reconstruction of Bulk Operators within the Entanglement Wedge in Gauge-Gravity Duality. *Phys. Rev. Lett.*, 117(2):021601, 2016.

[22] X. Dong and A. Lewkowycz. Entropy, extremality, euclidean variations, and the equations of motion. *arXiv preprint arXiv:1705.08453*, 2017.

[23] N. Engelhardt and A. C. Wall. Quantum Extremal Surfaces: Holographic Entanglement Entropy beyond the Classical Regime. *JHEP*, 01:073, 2015.

[24] T. Faulkner, R. G. Leigh, O. Parrikar, and H. Wang. Modular Hamiltonians for Deformed Half-Spaces and the Averaged Null Energy Condition. 2016.

[25] T. Faulkner, A. Lewkowycz, and J. Maldacena. Quantum corrections to holographic entanglement entropy. *JHEP*, 11:074, 2013.

[26] A. L. Fitzpatrick, J. Kaplan, and M. T. Walters. Universality of Long-Distance AdS Physics from the CFT Bootstrap. *JHEP*, 08:145, 2014.

[27] A. L. Fitzpatrick, J. Kaplan, and M. T. Walters. Virasoro conformal blocks and thermality from classical background fields. *Journal of High Energy Physics*, 2015(11):200, 2015.

[28] A. L. Fitzpatrick, J. Kaplan, M. T. Walters, and J. Wang. Eikonalization of Conformal Blocks. *JHEP*, 09:019, 2015.

[29] E. E. Flanagan, D. Marolf, and R. M. Wald. Proof of classical versions of the bousso entropy bound and of the generalized second law. *Physical Review D*, 62(8):084035, 2000.

[30] Z. Fu, B. Grado-White, and D. Marolf. A perturbative perspective on self-supporting wormholes. 2018.

[31] P. Gao, D. L. Jafferis, and A. Wall. Traversable Wormholes via a Double Trace Deformation. *JHEP*, 12:151, 2017.

[32] N. Graham and K. D. Olum. Achronal averaged null energy condition. *Phys. Rev.*, D76:064001, 2007.

[33] M. Gttner, J. G. Bohnet, A. Safavi-Naini, M. L. Wall, J. J. Bollinger, and A. M. Rey. Measuring out-of-time-order correlations and multiple quantum spectra in a trapped ion quantum magnet. *Nature Phys.*, 13:781, 2017.

[34] R. Haag, N. M. Hugenholtz, and M. Winnink. On the equilibrium states in quantum statistical mechanics. *Communications in Mathematical Physics*, 5(3):215–236, 1967.

[35] F. M. Haehl and M. Rozali. Effective Field Theory for Chaotic CFTs. 2018.

[36] P. Hayden and J. Preskill. Black holes as mirrors: Quantum information in random subsystems. *JHEP*, 09:120, 2007.

[37] P. Hayden and J. Preskill. Black holes as mirrors: Quantum information in random subsystems. *JHEP*, 09:120, 2007.

[38] D. Hochberg and M. Visser. Null energy condition in dynamic wormholes. *Physical review letters*, 81(4):746, 1998.

[39] D. M. Hofman, D. Li, D. Meltzer, D. Poland, and F. Rejon-Barrera. A Proof of the Conformal Collider Bounds. *JHEP*, 06:111, 2016.

[40] D. M. Hofman and J. Maldacena. Conformal collider physics: Energy and charge correlations. *JHEP*, 05:012, 2008.

[41] V. E. Hubeny, M. Rangamani, and T. Takayanagi. A Covariant holographic entanglement entropy proposal. *JHEP*, 07:062, 2007.

[42] I. Ichinose and Y. Satoh. Entropies of scalar fields on three-dimensional black holes. *Nucl. Phys.*, B447:340–372, 1995.

[43] W. Israel. Thermo-field dynamics of black holes. *Physics Letters A*, 57(2):107–110, 1976.

[44] W. R. Kelly and A. C. Wall. Holographic proof of the averaged null energy condition. *Phys. Rev.*, D90(10):106003, 2014. [Erratum: Phys. Rev.D91,no.6,069902(2015)].

[45] J. Koeller and S. Leichenauer. Holographic Proof of the Quantum Null Energy Condition. *Phys. Rev.*, D94(2):024026, 2016.

[46] E.-A. Kontou and K. D. Olum. Averaged null energy condition in a classical curved background. *Phys. Rev.*, D87(6):064009, 2013.

[47] E.-A. Kontou and K. D. Olum. Proof of the averaged null energy condition in a classical curved spacetime using a null-projected quantum inequality. *Phys. Rev.*, D92:124009, 2015.

[48] L. S. Levitov, A. V. Shytov, and A. Y. Yakovets. Quantum Breaking of Elastic String. *Physical Review Letters*, 75:370–373, July 1995.

[49] J. Maldacena, A. Milekhin, and F. Popov. Traversable wormholes in four dimensions. 2018.

[50] J. Maldacena and X.-L. Qi. Eternal traversable wormhole. 2018.

[51] J. Maldacena, S. H. Shenker, and D. Stanford. A bound on chaos. *JHEP*, 08:106, 2016.

[52] J. Maldacena, D. Stanford, and Z. Yang. Diving into traversable wormholes. *Fortsch. Phys.*, 65(5):1700034, 2017.

[53] J. Maldacena and L. Susskind. Cool horizons for entangled black holes. *Fortschritte der Physik*, 61(9):781–811, 2013.

[54] J. Maldacena and L. Susskind. Cool horizons for entangled black holes. *Fortsch. Phys.*, 61:781–811, 2013.

[55] J. M. Maldacena. Eternal black holes in anti-de Sitter. *JHEP*, 04:021, 2003.

[56] D. Marolf and A. C. Wall. Eternal black holes and superselection in ads/cft. *Classical and Quantum Gravity*, 30(2):025001, 2012.

[57] M. S. Morris and K. S. Thorne. Wormholes in spacetime and their use for interstellar travel: A tool for teaching general relativity. *Am. J. Phys*, 56(5):395–412, 1988.

[58] M. S. Morris, K. S. Thorne, and U. Yurtsever. Wormholes, time machines, and the weak energy condition. *Physical Review Letters*, 61(13):1446, 1988.

[59] A. Nahum, S. Vijay, and J. Haah. Operator Spreading in Random Unitary Circuits. *Phys. Rev.*, X8(2):021014, 2018.

[60] T. Numasawa, N. Shiba, T. Takayanagi, and K. Watanabe. Epr pairs, local projections and quantum teleportation in holography. *arXiv preprint arXiv:1604.01772*, 2016.

[61] K. Papadodimas and S. Raju. An Infalling Observer in AdS/CFT. *JHEP*, 10:212, 2013.

[62] L. Parker and D. Toms. *Quantum field theory in curved spacetime: quantized fields and gravity*. Cambridge University Press, 2009.

[63] A. Prudnikov, Y. A. Brychkov, and O. Marichev. *Integrals and Series, Volume 3: More Special Functions*. Gordon and Breach, New York, 1992.

[64] D. A. Roberts and D. Stanford. Two-dimensional conformal field theory and the butterfly effect. *Phys. Rev. Lett.*, 115(13):131603, 2015.

[65] S. Ryu and T. Takayanagi. Holographic derivation of entanglement entropy from AdS/CFT. *Phys. Rev. Lett.*, 96:181602, 2006.

[66] M. J. Schlosser. Multiple hypergeometric series: Appell series and beyond. In *Computer Algebra in Quantum Field Theory*, pages 305–324. Springer, 2013.

[67] S. H. Shenker and D. Stanford. Black holes and the butterfly effect. *arXiv preprint arXiv:1306.0622*, 2013.

[68] S. H. Shenker and D. Stanford. Black holes and the butterfly effect. *JHEP*, 03:067, 2014.

[69] S. N. Solodukhin. Restoring unitarity in BTZ black hole. *Phys. Rev.*, D71:064006, 2005.

[70] R. F. Streater and A. S. Wightman. *PCT, spin and statistics, and all that*. Princeton University Press, 2016.

[71] A. Strominger and D. M. Thompson. A Quantum Bousso bound. *Phys. Rev.*, D70:044007, 2004.

[72] L. Susskind. Copenhagen vs Everett, Teleportation, and ER=EPR. *Fortsch. Phys.*, 64(6-7):551–564, 2016.

[73] L. Susskind. Er= epr, ghz, and the consistency of quantum measurements. *Fortschritte der Physik*, 64(1):72–83, 2016.

[74] L. Susskind. ER=EPR, GHZ, and the consistency of quantum measurements. *Fortsch. Phys.*, 64:72–83, 2016.

[75] L. Susskind and Y. Zhao. Teleportation through the wormhole. *Phys. Rev.*, D98(4):046016, 2018.

[76] Y. Takahasi and H. Umezawa. Thermo field dynamics. *Collect. Phenom.*, 2:55–80, 1975. [,303(1974)].

[77] M. Thibeault, C. Simeone, and E. F. Eiroa. Thin-shell wormholes in Einstein-Maxwell theory with a Gauss-Bonnet term. *Gen. Rel. Grav.*, 38:1593–1608, 2006.

[78] W. G. Unruh. Notes on black-hole evaporation. *Physical Review D*, 14(4):870, 1976.

[79] M. Visser. Lorentzian wormholes. *From Einstein to Hawking, 412 pp.. AIP Press*, 1, 1996.

[80] M. Visser, S. Kar, and N. Dadhich. Traversable wormholes with arbitrarily small energy condition violations. *Physical review letters*, 90(20):201102, 2003.

[81] A. C. Wall. Ten Proofs of the Generalized Second Law. *JHEP*, 06:021, 2009.

[82] A. C. Wall. Proving the Achronal Averaged Null Energy Condition from the Generalized Second Law. *Phys. Rev.*, D81:024038, 2010.

[83] A. C. Wall. Proof of the generalized second law for rapidly changing fields and arbitrary horizon slices. *Physical Review D*, 85(10):104049, 2012.

[84] A. C. Wall. The generalized second law implies a quantum singularity theorem. *Classical and Quantum Gravity*, 30(16):165003, 2013.

[85] E. Witten. Multi-trace operators, boundary conditions, and ads/cft correspondence. *arXiv preprint hep-th/0112258*, 2001.

[86] B. Yoshida and A. Kitaev. Efficient decoding for the Hayden-Preskill protocol. 2017.